On the Mechanism of the Large-Scale Seasonally Varying Upwelling in the Region of the Tropical Tropopause

by

Elena Yulaeva

A dissertation submitted in partial fulfillment
of the requirements for the degree of

Doctor of Philosophy

University of Washington

1997

Approved by---------- (Chairperson of Supervisory Committee)

Program Authorized
to Offer Degree Atmospheric Sciences

Date April 11, 1997

Doctoral Dissertation

In presenting this dissertation in partial fulfillment of the requirements for the Doctoral Degree at the University of Washington, I agree that the Library shall make its copies freely available for inspection. I further agree that extensive coping of this dissertation is allowable only for scholarly purposes, consistent with "fair use" as prescribed in the U.S. Copyright Law. Requests for copying or reproduction of this dissertation may be referred to University Microfilms, 1490 Eisenhower Place, P.O. Box 975, Ann Arbor, MI 48106, to whom the author has granted "the right to reproduce and sell (a) copies of the manuscript in microform and/or (b) printed copies of the manuscript made from microform."

Signature E. Ovalle

Date 04-11-97

University of Washington

Abstract

On the Mechanism of the Large-Scale Seasonally Varying Upwelling in the Region of the Tropical Tropopause

by Elena Yulaeva

Chairperson of Supervisory Committee
Professor James R. Holton
Department of Atmospheric Sciences

This work investigates the physical mechanisms that determine the large-scale upwelling through the tropical tropopause, one of the principal components of stratosphere-troposphere mass exchange. The global-scale mean meridional circulation in the lower stratosphere and the upward branch of the tropospheric Hadley circulation which form the two interrelated parts of atmospheric dynamics in the region of the tropical tropopause are considered together. The comparative roles of two main mechanisms: non-local extratropical wave-induced zonal forcing and local radiative and (tropospheric) cumulus heating in controlling the mean meridional circulation in the tropical stratosphere and troposphere are investigated. The study includes objective analysis of observational data and numerical simulation of the upwelling with a specially designed two-dimensional, zonally symmetric spectral model based on the transformed Eulerian mean equations. The analysis of the NCAR/NCEP Reanalysis data reveals the seasonally varying circulation patterns in the upper troposphere and in the lower

stratosphere. The observed mean meridional circulation in the lower stratosphere can be viewed as a superposition of two components: an equatorially symmetric component forced by the monsoon part of the diabatic heating, and an equatorially asymmetric component forced by the seasonally varying wave-induced zonal forcing in the stratosphere. At any given time, the mean meridional mass stream function in the upper troposphere can be considered as a combination of two elements: a circulation related to the oceanic ITCZ and a circulation related to the diabatic heating in the continental monsoons.

The experiments with the model are designed to elucidate two aspects of the climatological-mean annual march. The first aspect concerns the annual cycle in the temperature of the tropical tropopause, which is considered to be a manifestation of the annual march in the upwelling in the region of the tropical tropopause, with a minimum (in upwelling) in July-August and a maximum in January-February. The modeling results prove that the seasonal variability of the upward mass flux through the tropical tropopause is controlled by eddy induced zonal forcing in the stratosphere. The second aspect concerns the marked asymmetry between the Northern Hemisphere tropospheric zonal wind fields in the transition seasons, with the westerly jetstream located at higher latitudes in October-November than during April-May. The experiments with the model suggest that the difference in the cumulus heating associated with a northward migration of the ITCZ from May to October appears to be the main mechanism responsible for this asymmetry.

TABLE OF CONTENTS

List of Figures

List of Tables

ACKNOWLEDGMENTS

I would like to thank my "star team" of advisors at the Department of Atmospheric Sciences, University of Washington, Professors James R. Holton and John M. Wallace. Their encouragement and support throughout this work, and the amount of time and energy they devoted to this study, made this dissertation possible. Their insightful ideas and constructive comments, and the willingness to go together with me through numerous versions of the dissertation over the last two years, are much appreciated. Professors Conway Leovy, David Battisti, Edward Sarachik, my committee members, provided unique and valuable insights in both the dissertation topic and the specifics of scientific life in American universities. I want to thank all the JISAO people for their help and encouragement. Thanks also to Margaret Black Lab, for her unique contribution into my work. Special thanks go to Kathryn Stout who made my connection from Michigan, and this dissertation, possible. I am very thankful to Ingrid Quertermous for the emotional support.

To a certain extent, this dissertation has grown out of my research background and experience in Moscow, Russia, which was formed at Moscow Physical-Technical Institute, and later at the Russian Academy of Sciences. Valentin Dymnikov, from the Department of Numerical Methods, Russian Academy of Sciences, has been a constant inspiration and a generous source of deep and interesting ideas. I am deeply indebted to this school.

I also want to thank my parents for their unconditional love and for enormous amount of time they spent with my son Ivan giving me plenty of time to work on my research. My son was also very understanding and supportive.

I am also indebted to the kicking of my yet unborn son which established some physiological deadlines for my dissertation defense. I want also to thank my husband, who was the first reader and editor. Without his understanding and support this dissertation would have been competed two years ago.

Chapter 1 Introduction

The exchange of mass and chemical constituents between the stratosphere and the troposphere is one of the central research topics in modern climatological studies. This research is inspired by the need to assess the impact of human activities on the atmosphere. The transport of chemical species between the troposphere and stratosphere can alter the chemical and, hence, the radiative and dynamical balances of the atmosphere. For instance, chemical tracers transported from the troposphere into the stratosphere may be responsible for the depletion of stratospheric ozone *(WMO, 1995)*. The downward transport of chemical species into the troposphere represents the main removal mechanism for many of stratospheric constituents. Besides, it may also alter the tropospheric radiative-dynamical budget (*Ramaswamy et al., 1992*).

Hoskins et al. [1985] argued that the dynamics of the troposphere and the stratosphere cannot be completely separated. However, differences in chemical and dynamical processes, as well as in the characteristic time scales of the vertical transport (a few hours in the troposphere due to moist convection versus a few months in the stratosphere) give credence to the distinct treatment of the stratosphere and troposphere. Thus, understanding of the exchange of mass and chemical constituents between the stratosphere and troposphere (hereafter referred to as stratosphere-troposphere exchange, or STE) becomes crucial for modeling atmospheric dynamics and predicting global climate changes.

The layer separating the troposphere from the stratosphere is called the tropopause. Conventionally, the tropopause is marked by a prominent change or a reversal in the sign of the atmospheric temperature lapse rate. The definition states

that the tropopause is the lowest level at which the temperature lapse rate decreases to 2K/km or less and the lapse rate averaged between this level and any level within the next 2 km does not exceed 2K/km.

Until recently, nearly all the studies of the STE were based on regional empirical observations *(Reed and Danielsen; 1959, Reiter et al., 1969; Kritz et al., 1991).* The emphasis was mostly on the synoptic and small-scale mechanisms of exchange. However, the understanding of STE is incomplete without a dynamical, radiative and chemical description of the global atmosphere *(Holton et al., 1995).*

Fig. 1.1 from *Holton et al., [1995]* summarizes the dynamical processes involved in the global-scale picture of general circulation and mass transport. The bold line indicates the position of the tropopause. The transport across the tropopause could occur in two totally different ways: first, as an adiabatic transport along isentropes, and second, as a diabatic transport across isentropes. In the regions where the isentropes intersect the tropopause (the dark shaded region in the picture), much of the STE is due to adiabatic eddy motions (the wiggly arrows in Fig.1.1). These motions lead to large latitudinal displacements of the tropopause, followed by irreversible mixing on small scales. *Holton et al., [1995]* have suggested that this shaded region be referred to as "lowermost extratropical stratosphere". It is the only region of the stratosphere for which the exchange of chemical constituents with the troposphere can occur along the isentropes. This kind of transport requires consideration of the synoptic and small-scale processes *(WMO, 1986).*

On the contrary, in the regions where isentropic surfaces lie entirely within the stratosphere or troposphere, the STE is accomplished by a slow ascent or descent across isentropic surfaces, which can be described within the framework of the large-

scale circulation.

As discussed by *Holton et al., [1995]*, this distinction between the regions with different dynamical processes places STE in the framework of the general circulation, and suggests that the global-scale mass exchange across the lower-stratospheric isentropes can be used as a measure of the global STE on seasonal and longer timescales.

The results of *Rosenlof and Holton [1993]* for the rate of mass transfer across the 100-hPa surface showed that the monthly mean upwelling in mass transport is limited to the equatorial region between 15°N and 15°S. This statement, together with the fact, that the tropical tropopause nearly coincides with the 380°K surface, suggest that the upward mass transport across the tropical tropopause a useful measure of the global STE.

In order to describe this upward mass transport in the tropics it is essential to clarify the complex mechanism of the global-scale dynamics in the region of the tropical tropopause.

According to *Holton et al., [1995]* , the adiabatic deformations of the tropopause shape in the tropics by small-scale processes are of little significance to transport. What is more significant is the diabatic transport across the tropical tropopause that may be associated with the large-scale diabatic ascent.

There are two competitive large-scale mechanisms that determine the upwelling in the region of the tropical tropopause at the seasonal time scales: the global-scale mean meridional circulation in the lower stratosphere and the upward branch of the tropospheric Hadley circulation.

In their recent review on the stratosphere - troposphere exchange, *Holton et al.,*

[1995] stress the view that the mean meridional circulation in the tropical lower stratosphere is non-locally controlled by the wave-induced forcing in extratropics. Planetary and small-scale waves, generated in troposphere, propagate into the middle atmosphere where they dissipate and break, producing a westward zonal force. This forcing drives a 'suction pump' mechanism. The direction of the circulation induced by this suction pump is determined by two constraints in the rotating atmosphere: conservation of the Ertel's Potential Vorticity, and mass continuity. The adjustment time of this induced circulation is determined by the velocities of the fastest waves (acoustic and small-scale gravity waves) and is much shorter than all the other dynamical time-scales.

In the extratropics, the wave-induced forcing pushes the air persistently westward, so that an air parcel has to move poleward there to conserve its potential vorticity, and then has to descend at higher latitudes. Mass continuity requires that the air in the tropics be pulled upward. Following *Haynes et al. [1991]*, this effect can be called "downward and sideways " control of the circulation in the lower stratosphere.

A review of the theory of "downward and sideways" control (*Holton et al., 1995]*) of the meridional circulation is given in Chapter 2. Within this approach, analytical difficulties arise primarily in the tropics, where nonlinearity plays a significant role in establishing a steady circulation. At any particular time it is necessary to simultaneously determine the mean meridional circulation and the angular momentum distribution. Besides, the pure 'downward' control principle is inapplicable in those regions in the tropics where the angular momentum contours are closed *(Rosenlof, 1994)*. Thus, one has to turn to numerical simulations of the

dynamics in the region of the tropical tropopause .

A different perspective on the meridional circulation in the tropical lower stratosphere considers this circulation to be a thermally-induced Hadley circulation. This approach was investigated by *Dunkerton [1989, 1990]*. The radiative heating, antisymmetric about the equator, that is characteristic of the middle and upper stratosphere during solstice seasons, would produce a single Hadley cell with ascent in the "summer" hemisphere, and descent in the "winter" hemisphere. Dunkerton argued, however, that the strength of this cell depends upon non-local eddy-induced zonal forcing. Thus, he suggested treating the mean meridional circulation in the lower stratosphere as a combination of the Hadley circulation and a residual circulation, remotely induced by extratropical eddy forcing.

The closeness of the circulation to either the first or the second regime is determined by the relative values of internal dynamical and radiative dissipation times, as well as by the time period of the oscillation forcing (*Garcia, 1987*). Therefore, an adequate understanding of the mean meridional circulation in the lower stratosphere requires not only an accurate specification of eddy zonal forcing but also precise radiation computations coupled with the dynamics.

This view of the tropical mean meridional circulation as a superposition of a locally induced Hadley circulation and a remotely induced eddy forced circulation, can also be generalized to the tropospheric tropical circulation.

The monthly mean observations of *Oort and Rasmuson [1970]* demonstrated that the Hadley circulation actually consists of a single cell extending from the summer hemisphere far into the winter hemisphere. The second cell barely exists in the summer hemisphere. The empirical evidence is at variance with the widelyheld notion

of a nearly symmetric Hadley circulation, as obtained from both analysis of annual mean data and results of axially symmetric models with specific heating symmetric about the equator (*Schneider, 1977; Held and Hou, 1980)*. The observed Hadley circulation can be interpreted from the perspectives of two different theories.

The first theory assumes that the meridional circulation in the tropics is completely determined by local radiative and cumulus heating. The shape and intensity of the circulation are very sensitive to the location of the center of heating off the equator (*Lindzen and Hou, 1988; Plumb and Hou, 1992)*. This theory considers moist convection to play the role of an external heating in an otherwise dry atmosphere. This manifestation of cumulus convection is described in the framework of the Conditional Instability of the Second Kind (CISK) theory of cumulus convection (*Charney and Eliassen, 1964*). However, there are a lot of discrepancies between the underlying assumption of CISK and the observations (*Xu and Emanuel, 1989*).

The second theory states that the tropical meridional circulation is non-locally induced by the extratropical eddy zonal forcing (as in the tropical lower stratosphere). The strength of this induced meridional circulation is increased by the coupling with the cumulus convection as described within the framework of the Statistical-Equilibrium theory (*Arakawa and Schubert, 1974; Emanuel et al., 1994)*. The Statistical - Equilibrium principle assumes that the cumulus convection affects the temperature profile rather than the net heating in the convecting region. Thus, as discussed in *Emanuel et al., [1994]*, the large-scale ascent "feels" an effective, positive static stability that is about an order of magnitude less than the dry static stability.

As the above discussion shows, the available theoretical and empirical studies of the mechanism of the stratosphere - troposphere mass exchange lack consistency in the critical region of the tropical tropopause. Thus, the primary goal of this work is to clarify how the large-scale dynamical processes described above work together to determine the seasonally varying circulation in the region of the tropical tropopause.

The work consists of ten chapters. Chapter 2 reviews the theory of the non-local control of the mean meridional circulation within the framework of the Transformed Eulerian Mean (TEM) equations. Chapter 3 focuses on an examination of empirical data on the atmospheric dynamics in the region of the tropical tropopause. Analysis and qualitative explanation of the observed mean meridional circulations in both stratosphere and troposphere are presented within the framework of the non-local control theory, followed by a description of zonal forcing induced by Rossby waves. A 2D TEM model which has been developed and used for studying the complex dynamical processes in the region of the tropical tropopause is described in Chapter 4. Chapter 5 deals with the results of a model simulation of the meridional circulations in the stratosphere, while in Chapter 6 we describe the Hadley circulation produced by the model. The mechanism for coupling the remotely-induced tropospheric Hadley circulation with cumulus convection is presented in Chapter7. A brief description of the radiative code is given in Chapter 8. The results of the simulation of the dynamical processes in the region of the tropical tropopause with a model that includes both the stratosphere and the troposphere are discussed in Chapter 9. Finally, a summary and conclusions are given in Chapter 10.

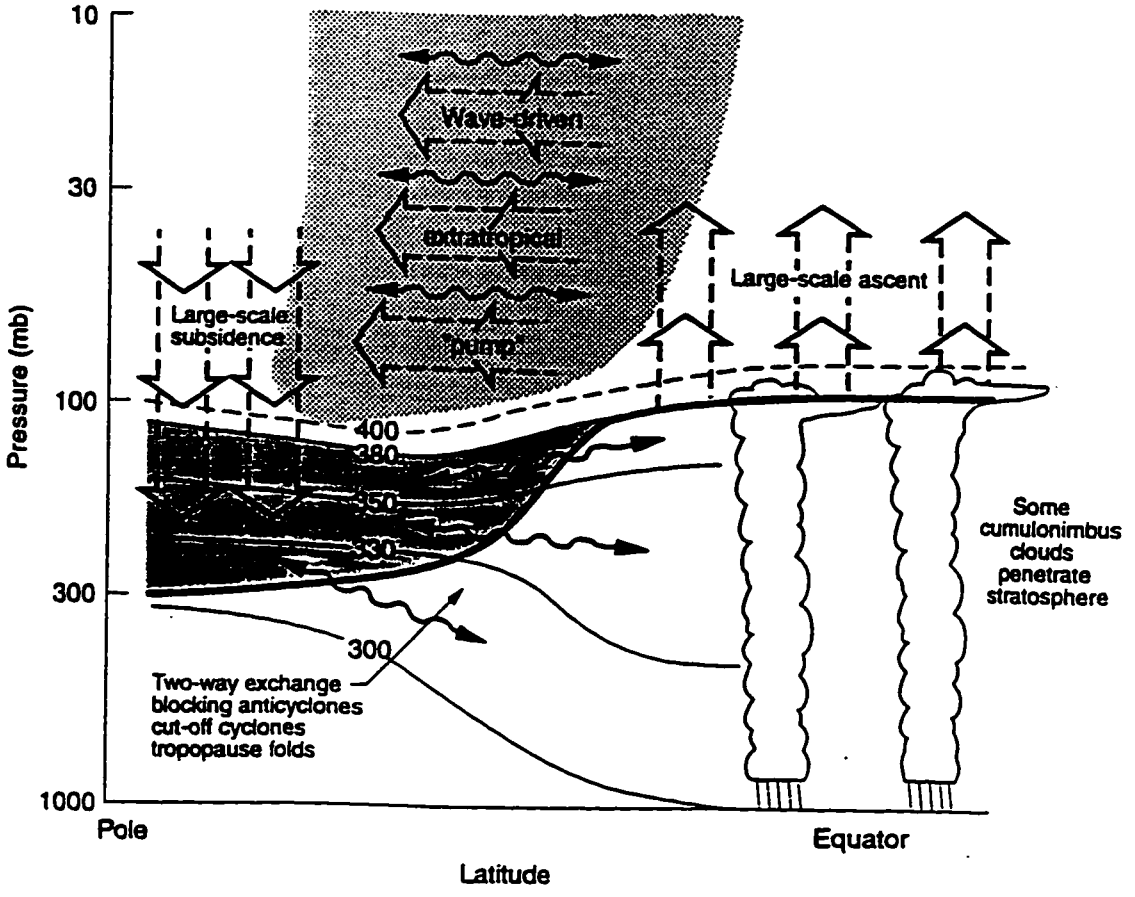

Figure 1.1: Dynamical aspects of stratosphere-troposphere exchange. From Holton et.al.,1995. The tropopause is shown by the thick line. Thin lines are isentropic surfaces labeled in K. The heavily shaded region is the "lowermost stratosphere". The region above the 380K surface is the "overworld". Light shading in the "overworld" denotes wave-induced forcing (the extratropical "pump"). The wavy double headed horizontal arrows denote the meridional transport by eddy motions. The broad vertical arrows show the transport by the global-scale Lagrangian mean circulation.

Chapter 2 Non-local Control of the Meridional Circulation

It is now widely recognized that the global-scale dynamics of the atmosphere is inherently non-local. Probably, the best currently available qualitative model revealing this non-local character is the "suction pump" concept of circulation in the middle atmosphere described by *Holton et al. [1995]*. This mechanism is applicable to any dynamical fluid in which fast waves are allowed.

As pointed out by *Holton et al. [1995]*, the underlying idea of the "suction pump" mechanism is contained in it's name. When you switch on a domestic vacuum cleaner, the air almost immediately begins moving towards the suction pump. The delay time between turning on the vacuum cleaner and the establishment of the flow towards the suction tube is determined by the time of propagation of fast (in comparison with all other processes of interest) acoustic waves. Therefore, the process is fundamentally non-local, and the pressure gradient force at a particular place can not be considered the cause of the circulation.

Global-scale dynamical processes in the real atmosphere are analogous to those described above: the eddy motions in the extratropical stratosphere and troposphere drive a global-scale "suction pump" which draws air into the tropical stratosphere and pushes it poleward and downward (*Holton et al., 1995*). The established global circulation is always uni-directional for the following reasons. First, the eddy-induced force with magnitude varying seasonally and interanually, is almost always retrograde of the earth's rotation (i.e. westward). Second, the direction of the circulation itself is determined by the constraint on the conservation of the Ertel's potential vorticity following the motion in adiabatic frictionless flow in a rotating atmosphere. The

magnitude of the planetary part of the absolute vorticity increases poleward. Thus, the westward acceleration due to eddy-induced forcing in middle latitudes makes an imaginary ring of air move poleward and then downward. Mass continuity requires a corresponding upward mass flux in lower latitudes.

This chapter presents an analytical and empirical foundation for the formalism of the "suction pump" mechanism in the real atmosphere, with emphasis on the tropics.

The structural description of the circulation in the tropical stratosphere derived from 2D diagnostic models is followed by a discussion of the analytical model based on a mathematical description of the non-local effect of the lateral body forcing upon the zonally symmetric circulation. This approach was reviewed in *Holton et al., [1995].* and is based on the original work of *Haynes et al., [1991].* The symmetric model was generalized to the case of the zonally averaged atmospheric flow. This provided a physical interpretation of the wave-driven forcing and the characteristic scales of the response.

There are several alternative ways in which the distinction between the zonal mean and eddy parts can be made. As discussed in *Holton [1974],* different averaging schemes result in different patterns of mean circulation. From all the possible types we have chosen to work within Transformed Eulerian Mean (TEM) framework. The reasons for this choice are described below.

2.1 Transformed Eulerian-Mean Framework

In the long run, we are interested in the description of the transport of tracers, and thus would prefer to use the generalized Lagrangian-mean (GLM) formalism. The GLM approach "involves taking averages following fluid parcels rather than averaging

over a set of coordinates fixed in space" *(Andrews et al, 1987, p.133)*. However, it is extremely hard to use this formalism with real data.

Another commonly used type of averaging, the conventional Eulerian-mean (EM) measured in isentropic coordinates, provides a good approximation of the advective transport of tracers (*Tung 1982*). Besides, as was mentioned in Chapter 1, the use of isentropic coordinates allows for clear separation between the transports along isentropes (adiabatic transport by the eddies) and across isentropes (the diabatic transport by large-scale dynamics). However, again, it is inconvenient to work in an isentropic coordinate system, especially when the problem requires analysis or model implementation of data on pressure surfaces.

These constraints motivated *Andrews and McIntyre [1976, 1978]* to propose the TEM framework as an alternative to the available techniques. *Andrews and McIntyre* noted that the main drawback of the EM description of the meridional circulation in pressure coordinates is that in the thermodynamic equation there tends to be a strong cancellation between the eddy heat flux convergence and the adiabatic cooling, while the diabatic heating is just a small residual. However, from a physical point of view, the motion of air parcels across isentropic surfaces must be accompanied by changes in their potential temperature in the process of diabatic heating/cooling. Therefore, the part of the vertical velocity associated with the diabatic heating/cooling is, essentially, the velocity that determines the mean vertical circulation. *Andrews and McIntyre* called this variable the residual mean vertical velocity. Essentially, it represents the part of the Eulerian-mean vertical velocity for which the adiabatic cooling is not entirely cancelled by the horizontal eddy heat flux.

Formulating a model in terms of the residual Eulerian circulation has two

principal advantages. The first is that, insofar as the assumption of the steady state and conservative waves holds, the planetary wave motion has no effect on the mean meridional circulation or on the distribution of most chemical constituents (the non-acceleration theorem). Hence, the TEM formalism avoids the problem of cancellation between the Eulerian eddy and the mean circulation effects. The second advantage is that the residual circulation provides a description of atmospheric motions that is in much better accord with both physical intuition and the actual motion of air parcels. *Dunkerton [1978]* showed that for linear steady conservative planetary waves the residual circulation is equivalent to the circulation obtained with the Lagrangian-mean theory.

However, it is important to realize that the residual circulation and the Lagrangian mean circulation are not always equivalent. Whenever wave disturbances are growing or decaying rapidly the two circulations will be different. As was pointed out by *McIntyre, [1987]*, this problem cannot be solved simply by adopting the Lagrangian-mean formalism. In fact, the Lagrangian averaging procedure becomes impractical to apply when waves grow to large amplitude. In contrast, the residual vertical and meridional velocities are always definable, so that we can always obtain the residual circulation. As was discussed by *Rosenlof [1995]*, the TEM residual circulation is a reasonable proxy for the net Lagrangian motion even when the conditions of no transience and dissipation are slightly violated.

The TEM equations are obtained from the EM equations by defining the residual meridional velocity :

$$\bar{v}^* = \bar{v} - \frac{1}{\rho}\frac{\partial}{\partial z}\frac{\rho\overline{v'T'}}{N^2}\frac{R}{H} \qquad (2.1a)$$

and the residual vertical velocity:

$$\overline{w}^* = \overline{w} + \frac{1}{a\cos\varphi}\frac{\partial}{\partial\varphi}\left[\cos\varphi\overline{v'T'}\right]\frac{R}{HN^2} \qquad (2.1b)$$

where $\overline{X} = \frac{1}{2\pi}\int_0^{2\pi} X(\lambda)d\lambda$ and $X' = X - \overline{X}$

The use of notation here is conventional and is explained in detail below (2.6).

After substitution of $\overline{v}$ and $\overline{w}$ into the ordinary EM equations one obtains the TEM equations in the form:

$$\frac{\partial\overline{u}}{\partial t} - f\overline{v}^* = \overline{G} \qquad (2.2)$$

$$f\overline{u} = -\frac{1}{a}\frac{\partial\overline{\Phi}}{\partial\varphi} \qquad (2.3)$$

$$\frac{\partial\overline{\Phi}}{\partial z} = \frac{R\overline{T}}{H} \qquad (2.4)$$

$$\frac{1}{a\cos\varphi}\frac{\partial}{\partial\varphi}\left(\overline{v}^*\cos\varphi\right) + \frac{1}{\rho}\frac{\partial}{\partial z}\left(\rho\overline{w}^*\right) = 0 \qquad (2.5)$$

$$\frac{\partial\overline{T}}{\partial t} + \overline{w}^*\frac{N^2H}{R} = \overline{Q} \qquad (2.6)$$

where: φ is the latitude,

$z = -H\log\left(\frac{P}{P_0}\right)$ - the log-pressure height,

Ω - the angular velocity of the earth,

R - the gas constant for dry air,

a - the radius of the Earth,

$\rho = \rho_0 \exp(-z/H)$ - the basic state density,

$N^2 = \frac{R}{H}\left(\frac{dT_0}{dz} + \frac{\kappa T_0}{H}\right)$ - the static stability,

$\bar{u}$ - the zonal mean velocity, $\bar{v}^*$ - the residual meridional velocity,

$\bar{w}^*$ - the residual vertical velocity,

$\bar{T}$ - the zonally averaged temperature,

$H = RT_0/g$ - the equivalent atmospheric depth,

$\overline{\Phi}$ - geopotential,

$\overline{Q} = \overline{Q_s} + \overline{Q_l}$ the total diabatic heating which is the sum of short and long wave heating,

$\overline{G}$ - the Eliassen-Palm (E-P) flux divergence.

We have written down the linear quasi-geostrophic version of TEM equations solely for the purpose of making clearer the qualitative description, which follows.

Equation (2.2) is the zonal momentum equation. It states that the zonal forcing exerted by resolved eddies, is balanced by three terms: the mean zonal flow acceleration, the Coriolis acceleration due to the residual mean motion, and the Rayleigh friction that by itself is just a parameterization of unresolved eddies. The other equations have the following meanings: equation (2.3) is the thermal wind equation; (2.4) is the hydrostatic approximation; (2.5) is the mass continuity equation. Equation (2.6) is the thermodynamic energy equation in which the net diabatic heating is balanced by the sum of adiabatic warming/cooling due to vertical motions and the temperature tendency.

We now distinguish between the short wave part of the diabatic heating which, to a first order of approximation, can be considered independent of temperature, and the long wave part. The latter depends upon the temperature distribution which, in turn,

is coupled with the wind. Therefore, this part of the diabatic heating can be considered as an internal mechanism for relaxation to radiative equilibrium rather than an external forcing. For our set of equations we will express this longwave heating as a Newtonian cooling with radiative relaxation time α_r^{-1} (on the order of 20 days). Thus, $\overline{Q_l} = -\alpha_r \overline{T}$. Equations 2.2 - 2.6 together describe the zonally averaged circulation in the atmosphere, thus providing an analytical framework for our study.

Next section discusses the use of diagnostic models based on the TEM equations to infer the main features of the mean meridional circulation in the tropical stratosphere from the observed thermodynamical fields.

2.2 Structure and Circulation of the Stratosphere Derived from 2D Diagnostic Models.

The lack of vertical velocity measurements on a global basis makes it difficult to directly observe the mean meridional circulation. Usually, some kind of diagnostic model is used for inferring the mean meridional circulation *(Murgatroyd and Singleton, 1961; Solomon et al., 1986; Yang et al., 1990)*. There are two different types of diagnostic models that can be used for our purposes. The first is based on radiative transfer schemes, and calculates the diabatic/residual circulation using the thermodynamic energy equation:

$$\overline{w_d} = \frac{\overline{Q} - \frac{\partial \overline{\theta}}{\partial t} - \frac{\overline{v_d}}{a}\frac{\partial \overline{\theta}}{\partial \varphi}}{\frac{\partial \overline{\theta}}{\partial z}} \qquad (2.7)$$

In (2.7), $\overline{Q} = \overline{Q_0} - \frac{1}{\rho_0}\frac{\partial}{\partial z}\left[\rho_0\left(\frac{\overline{v'\theta'\theta_\varphi}}{a\overline{\theta}_z} + \overline{w'\theta'}\right)\right]$ and, as was discussed in *Rosenlof [1995]*, the eddy flux divergence term is small and can be ignored in the quasi-geostrophic approximation. Thus, the meridional circulation can be calculated from the heating rates, either observed or computed with a radiation code based on the observed distributions of temperature and chemical species. For a detailed description of this method see *Solomon et al. [1986]*

Diagnostic models of the second type estimate the mean meridional circulation from the E-P flux divergence field, utilizing the downward control principle (*Rosenlof and Holton, 1993*). However, this principle is not entirely applicable in the tropics (see 2.3). Therefore, the "observed" mean meridional circulation presented in this chapter was actually obtained as the diabatic circulation derived from the temperature and heating rates fields within the framework of the first type of diagnostic model. These fields, which served as the input for the model, are described below.

The mean observed NMC temperature cross sections for all seasons are shown in Fig 2.1 (*Yang et al.,1990*). In the stratosphere, the mean infrared cooling is balanced primarily by radiative heating due to the absorption of solar ultraviolet by ozone and water vapor. As a result of this absorption, the mean temperature in the stratosphere increases with height to a maximum at the stratopause. The meridional temperature structures in the lower and in the upper stratosphere differ significantly. In the lower stratosphere there is a temperature minimum at the equator, and maxima at the summer pole and in midlatitudes of the winter hemisphere. Above about 30 mb, the temperature decreases uniformly from summer pole to winter pole in qualitative agreement with radiative equilibrium conditions. The radiative equilibrium temperature for the stratosphere in July is shown on Fig. 2.2 *(Andrews et al., 1987)*. By comparing

it with the one shown in Fig 2.1c, we note a strong departure of the lower stratospheric temperature from radiative equilibrium. As was already mentioned, these departures must be maintained by eddy transports. Thus, we cannot assume that the radiative heating and cooling patterns observed in the stratosphere cause the meridional circulation there. On the contrary, the observed thermal structure is a result of the eddies driving the flow away from a state of radiatively determined balance.

Using the above described temperature field and the observed distribution of the radiatively active gases as an input to radiative transfer calculations, one can easily obtain the corresponding heating rate distribution. Fig. 2.3. shows the heating rates for all seasons (*Yang et al., 1990*).

The diabatic circulation deduced from the heating rates, using the thermodynamic energy equation (2.7) and the continuity equation, is shown on Fig 2.4 (*Yang et al., 1990*). It consists of a two-cell diabatic circulation in the lower stratosphere, with rising motion in the equatorial region and sinking motion over both poles. The winter circulation is stronger and extends higher than the summer circulation. Above 25 km, the two-cell pattern changes to a pole-to-pole circulation, with upwelling in the summer hemisphere and subsidence in the winter hemisphere.

2.3 The Non-local Control Principle: Mathematical Formulation

A special case of what has come to be called the non-local control principle was first described by *Haynes et al [1991]*. They considered a zonally symmetric model of the middle atmosphere subjected to a prescribed steady force. This forcing was supposed to be a result of irreversible angular momentum transfer by Rossby and gravity waves due to their upward propagation and breaking. The results of *Haynes et*

al [1991] showed that, to the extent that the changes in mean circulation do not sufficiently alter the forcing, the extratropical diabatic mass flux across a given isentropic surface could be regarded as controlled exclusively by the distribution of this zonal forcing above this surface. *Haynes et al [1991]* called this the "downward control" principle.

This principle could be generalized as a "down and side-wards control" principle for the whole hemisphere when the assumptions of no transience and dissipation are relaxed. The "suction pump" mechanism of the global mean meridional circulation in the middle atmosphere, proposed by *Holton et al. [1995],* represents such a generalization.

Let us now assume that the short-wave heating and the zonal forcing are periodic with time with the frequency σ (*Garcia, 1987*) :

$$\begin{aligned} \overline{Q_s} &= Q_0 \exp(i\sigma t) \\ \overline{G} &= G_0 \exp(i\sigma t) \end{aligned} \tag{2.8a}$$

then

$$\overline{w}^* = \overline{w}_0^* \exp(i\sigma t) \tag{2.8b}$$

With the above assumptions we can now derive a single equation for vertical velocity (corresponding to equation (2.5) in *Holton et al., 1995*) :

$$\begin{aligned} &\frac{\partial}{\partial z}\left(\frac{1}{\rho}\frac{\partial \rho \overline{w}^*}{\partial z}\right) + \frac{i\sigma}{i\sigma+\alpha}\frac{N^2}{4\Omega^2 a^2 \cos\varphi}\frac{\partial}{\partial \varphi}\frac{\cos\varphi}{\sin^2\varphi}\frac{\partial \overline{w}^*}{\partial \varphi} = \\ &\frac{i\sigma}{i\sigma+\alpha}\frac{R/H}{4\Omega^2 a^2 \cos\varphi}\frac{\partial}{\partial \varphi}\frac{\cos\varphi}{\sin^2\varphi}\frac{\partial \overline{Q}}{\partial \varphi} + \frac{1}{2\Omega\cos\varphi}\frac{\partial}{\partial \varphi}\frac{\cos\varphi}{\sin\varphi}\frac{\partial \overline{G}}{\partial z} \end{aligned} \tag{2.9}$$

In general, the operator acting on $\overline{w}^*$ is elliptic. This means that a localized eddy

forcing or heating will cause a response that extends beyond the region of forcing. So, at any given point, $\overline{w}^*$ is affected by changes in eddy forcing and heating elsewhere and, therefore, is under non-local control.

Based on this equation, analytical predictions of the spatial structure of the response to a localized forcing for some extreme values of α,σ and their ratio α/σ were made by *Holton et al., [1995]*. The following summary repeats several of their main conclusions which have important consequences for our research.

The adiabatic limit ($\sigma/\alpha \to \infty$) (thoroughly studied by *Garcia [1987]* and *Plumb [1982]*) corresponds to dynamical processes with characteristic timescales of a few days (if the radiative relaxation time is around 20 days). Thus, this limit is not particularly relevant to our further discussion.

For dynamical timescales on the order of a month or longer, $\alpha > \sigma$. The characteristic scales for the response can be estimated by assuming that the two terms on the left-hand side of equation (2.9) approximately balance each other away from the forcing region. Thus,

$$\Delta z \approx \max\left[\left(\frac{\alpha}{\sigma}\right)^{1/2}\frac{2\Omega\sin\varphi}{N}a\Delta\varphi,\left(\frac{\alpha}{\sigma}\right)\left(\frac{2\Omega\sin\varphi}{N}\right)^2\frac{(a\Delta\varphi)^2}{H}\right] \qquad (2.10)$$

This means that for any given latitudinal scale we can analytically find the vertical scale of the response.

With an increase in the time scale of the forcing, the ratio σ/α decreases, and the latitudinal derivative term on the left-hand side of the equation (2.9) becomes smaller than the vertical derivative term. Therefore, for this case the assumption of a balance between these two terms requires a deepening of the response.

This last result is illustrated by Fig. 2.5 (a, b) (compare to Fig. 4 (a, b) from

Holton et al., 1995).This figure shows mass-flux stream lines of the response of our 2D model (described in Chapter 4) to forcing with periods of 30(a) and 360 (b) days, located at 60°N and 35km (dashed line). While the quantitative modeling outcome will be described in Chapter 5, on the qualitative level this picture reveals a deeper vertical penetration for 360 day forcing and a more latitudinally elongated response for 30 day forcing.

In the steady state limit($\sigma \to 0$) equation (2.9) becomes parabolic, and the non-local control in the nontropical region degenerates into the familiar downward control *(Haynes et al, 1991)*. This extreme case is presented in Fig. 2.6. It shows the mass-flux stream lines of the response to the steady zonal forcing located in middle latitudes. The dashed lines show the shape and strength of the zonal westward forcing. It should be noted that the streamfunction lines away from the forcing are lines of constant latitude. The streamfunction at any location is controlled by the distribution of wave-induced forcing. In our case, when the forcing is located in mid-latitudes, it does not influence the tropical regions.

The diabatic heating term in equation (2.9), would vanish under these conditions, so that the meridional circulation would be driven solely by eddies. In this case, any external heating must be balanced by an adjustment in the temperature field by the part of the heating that depends on temperature (i.e. by the longwave cooling).

In the steady-state limit, equation (2.9) yields an estimate of the time required for the response to reach a steady state after the zonal forcing is "turned on":

$$\sigma^{-1} \geq \alpha^{-1} \frac{N^2}{\left(2\Omega \sin\varphi a \Delta\varphi\right)^2} \min\left[\Delta z^2, H\Delta z\right] \qquad (2.11)$$

Thus, the adjustment time for the process is inversely proportional to the square of the latitude and to the characteristic horizontal length scale. This statement has two consequences that are very important for further discussion. First, the remote control principle is useful when applied to large spatial scales, for which the adjustment time is relatively short). On such scales the main underlying physical process can be described in the framework of the "suction pump" mechanism. Second, the adjustment time is very long in the tropics. Therefore, strictly speaking, in this region the steady downward control principle is inapplicable.

2.4 Non-local Control in the Tropics

As follows from the above discussion, a steady state conditions in the tropics cannot be treated in the framework of the linear equations. The reason is that in equation (2.9) the non-locally exerted zonal forcing will be balanced by the acceleration of the mean zonal wind. As was shown in *Holton et al., [1995]*, this equation can be used for estimating the extreme latitude at which the zonal forcing is still balanced by the Coriolis force associated with $\bar{v}^*$. The first two terms on the left-hand side should be of the same order. As a result *Holton et al., [1995]* obtained:

$$a\Delta\varphi = \left[\frac{\sigma}{\alpha}\frac{N^2a^2}{4\Omega^2}\min(\Delta z^2, H\Delta z\right]^{1/4} \qquad (2.12)$$

For typical values of $\alpha,\sigma,\Delta z$, the value of $\Delta\varphi$ from (2.12) equals 20° of latitude. This value represents an estimate of the effective location of the zonal forcing if it controls the quasi-steady observed circulation in the tropics (for instance, on the annual time scale).

The above limitation on the use of the downward control principle in the tropics

is a direct consequence of the linearization of the governing equations. Including nonlinear advection terms in the zonal momentum equation makes the analysis more complex, but extends its validity to the tropics.

In an attempt to include non-linearity in the mathematical formulation, *Haynes et al [1991]* derived the downward control principle by replacing equation (2.1) with a nonlinear zonal momentum equation in a steady state form

$$\frac{\partial(\psi,\overline{m})}{\partial(\varphi,z)} = \rho_0 a^2 \overline{G}\cos^2\varphi \qquad (2.13)$$

where: $\overline{m} \equiv a\cos\varphi(\overline{u} + a\Omega\cos\varphi)$, is the angular momentum per unit mass and ψ is the streamfunction defined as:

$\overline{v}^* = -\frac{1}{\rho\cos\varphi}\frac{\partial\psi\rho}{\partial z}$ and $\overline{w}^* = \frac{1}{a\cos\varphi}\frac{\partial\psi}{\partial\varphi}$.

Dividing (2.13) by $\overline{m}_\varphi = \frac{\partial(\overline{m},z)}{\partial(\varphi,z)}$, and integrating the resulting equation vertically (applying proper boundary conditions), *Haynes et al.* obtained the following solution for ψ:

$$\psi(\varphi,z) = \int_z^\infty \left\{\frac{\rho_0\overline{G}a^2\cos^2\varphi}{\overline{m}_\varphi}\right\}_{\varphi=\varphi(z')} dz' \qquad (2.14)$$

Using the definition of the residual stream function, (2.14) can be rewritten in the form of the equation for $\overline{w}^*$:

$$\overline{w}^* = -\frac{1}{a\rho_0\cos\varphi}\frac{\partial}{\partial\varphi}\left\{\int_z^\infty \left\{\frac{\rho_0\overline{G}a^2\cos^2\varphi}{\overline{m}_\varphi}\right\}_{\varphi=\varphi(z')} dz'\right\} \qquad (2.15)$$

In this equation, $\overline{w}^*$ is determined by both the zonal forcing and absolute angular momentum distribution. The latter can be divided into two components: the first

associated with the Earth's rotation, and the second with relative zonal motion.

The second component dominates in low latitudes. Thus, the relative angular momentum distribution plays a significant role in this region. However, as we already noted, a steady forcing would cause zonal wind acceleration in low latitudes. This, in turn, will change the angular momentum distribution. This complication makes the description of the meridional circulation in low latitudes fully nonlinear, since at any particular time we have to determine the meridional circulation and the angular momentum distribution simultaneously.

Another problem in using the non-local control principle for describing the mean meridional circulation in the tropics follows from the violation of Hide's theorem *(Hide, 1969)* This problem was discussed in several papers examining the Hadley circulation *(Schneider 1977; Lindzen 1990)*. If there is a local maximum or minimum of angular momentum in the interior of the atmosphere, then a closed constant angular momentum contour surrounding this point can be found. If the downgradient viscous fluxes of the angular momentum are negligible, a closed meridional circulation parallel to the angular momentum contours can exist (that is: $\frac{\partial(\varphi,m)}{\partial(\varphi,z)}=0$), independent of any additional zonal wave -induced forcing. *Rosenlof [1993]* showed that at the equator the angular momentum contours could indeed have interior extrema. Fig 2.7 presents the angular momentum contours computed from the gradient zonal wind based on 10 years of geopotential height UKMO data. Between 15°S and 15°N the contours of angular momentum do not extend continuously from the top to the bottom of the domain. Thus, a closed mean meridional circulation parallel to the momentum contours and independent of wave induced forcing can exist in this region

However, *Dunkerton [1991]* argued that even in this case the broad-scale

equatorial upwelling in the lower stratosphere could be realistically described only after an addition of a sufficient amount of extratropical zonal forcing. Besides, the phase of the annual march of the meridional circulation in the tropical stratosphere corresponds to the phase of the eddy-induced zonal forcing (*Rosenlof, 1995*). Hence there is evidence that, even in the low latitudes, the circulation is primarily controlled by the extratropical wave-driven 'pumping'.

The explanatory framework of the non local control principle, described in this chapter, constitutes the foundation for our further study of the dynamics in the region of the tropical tropopause, in both the interpretation of the observed atmospheric fields (Chapter 3), and in the 2-D modeling (Chapters 4 - 10).

The following chapter will describe the observed features of the meridional circulation in the region of low latitude tropopause. Both components of the meridional circulation in this region, tropospheric and stratospheric, will be examined and interpreted from the perspective of the non local control principle.

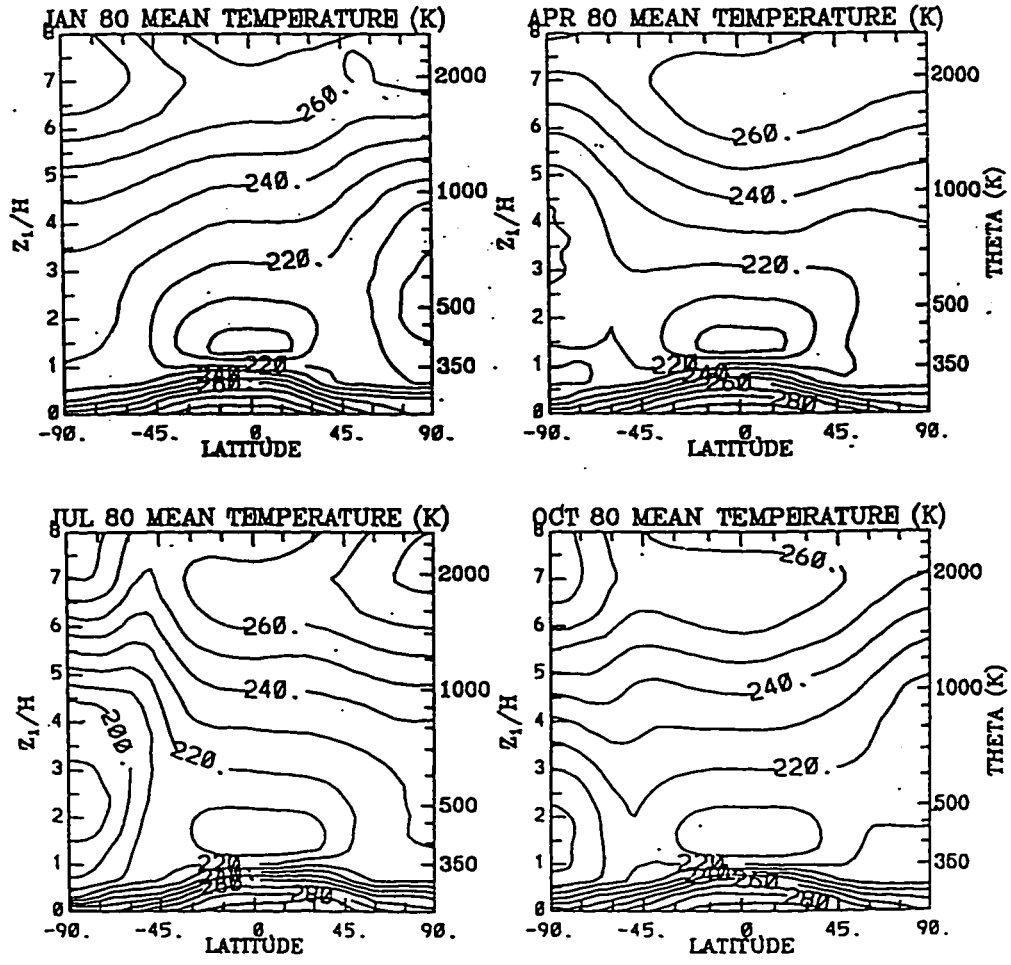

Figure 2.1: Observed NMC temperature (in degrees K) for 1980 as a function of latitude and potential temperature (from *Yang et al., 1990*).

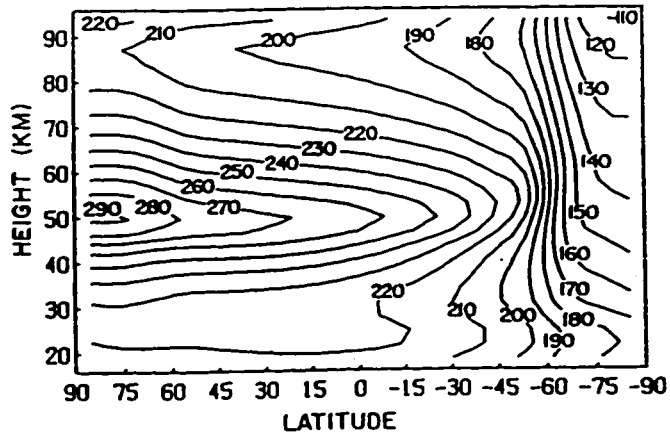

Figure 2.2: Radiative equilibrium temperature (in degrees K) for July (from *Andrews et al., 1987*).

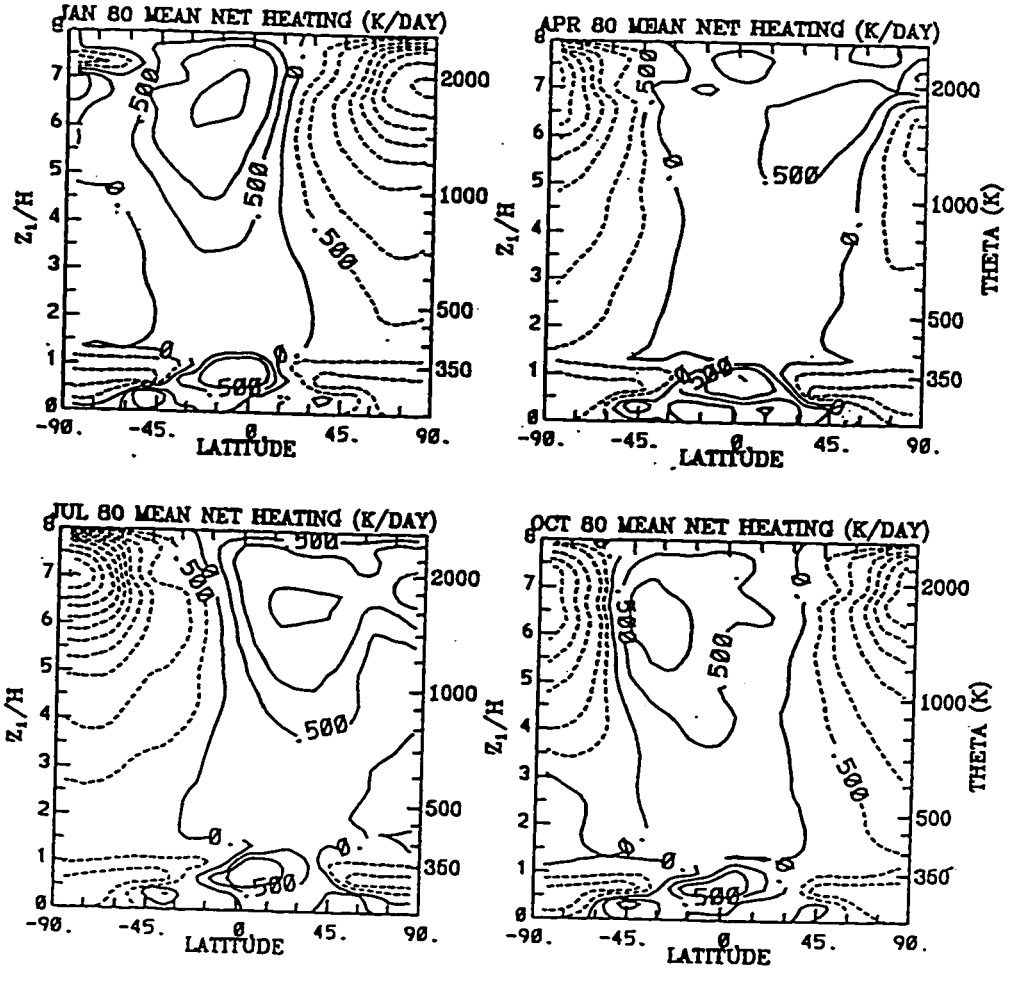

Figure 2.3: Calculated diabatic heating rate (K/day) as a function of latitude and potential temperature (from *Yang et al., 1990*).

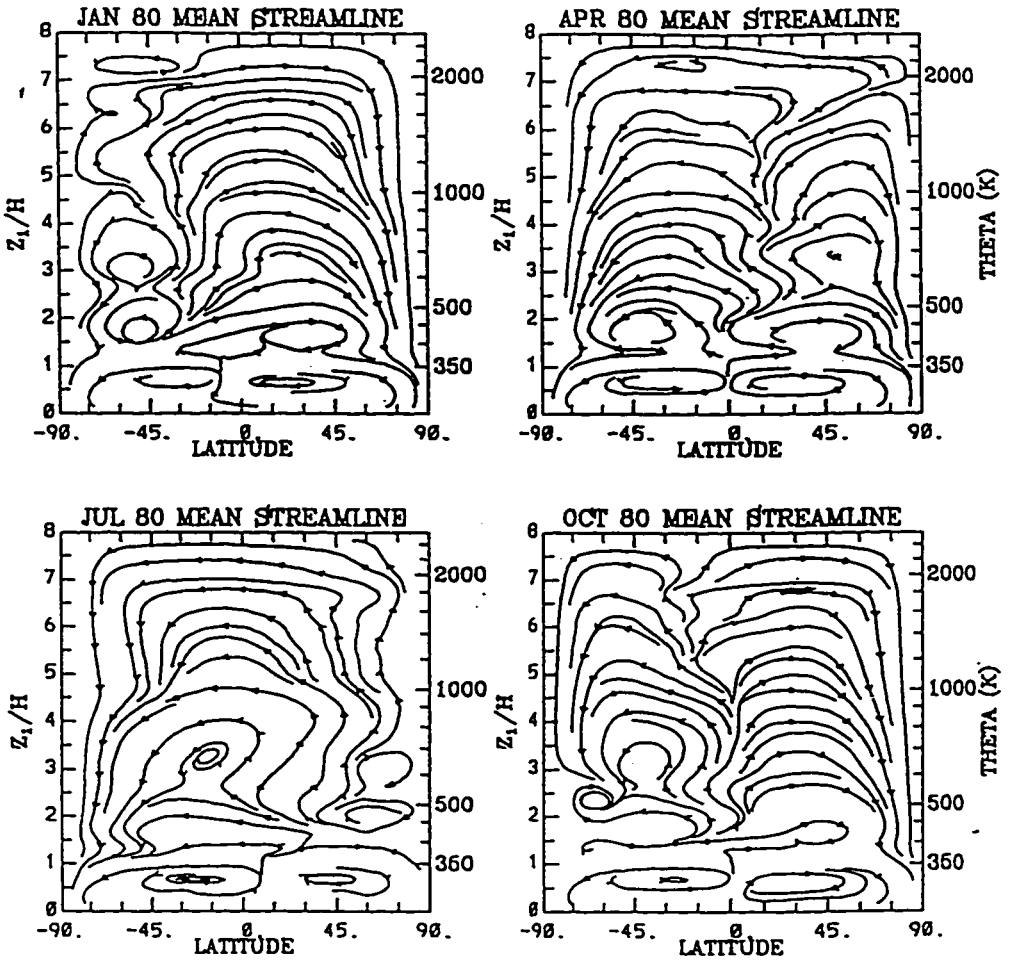

Figure 2.4: Streamlines for calculated diabatic heating as a function of latitude and potential temperature (from *Yang et al., 1990*).

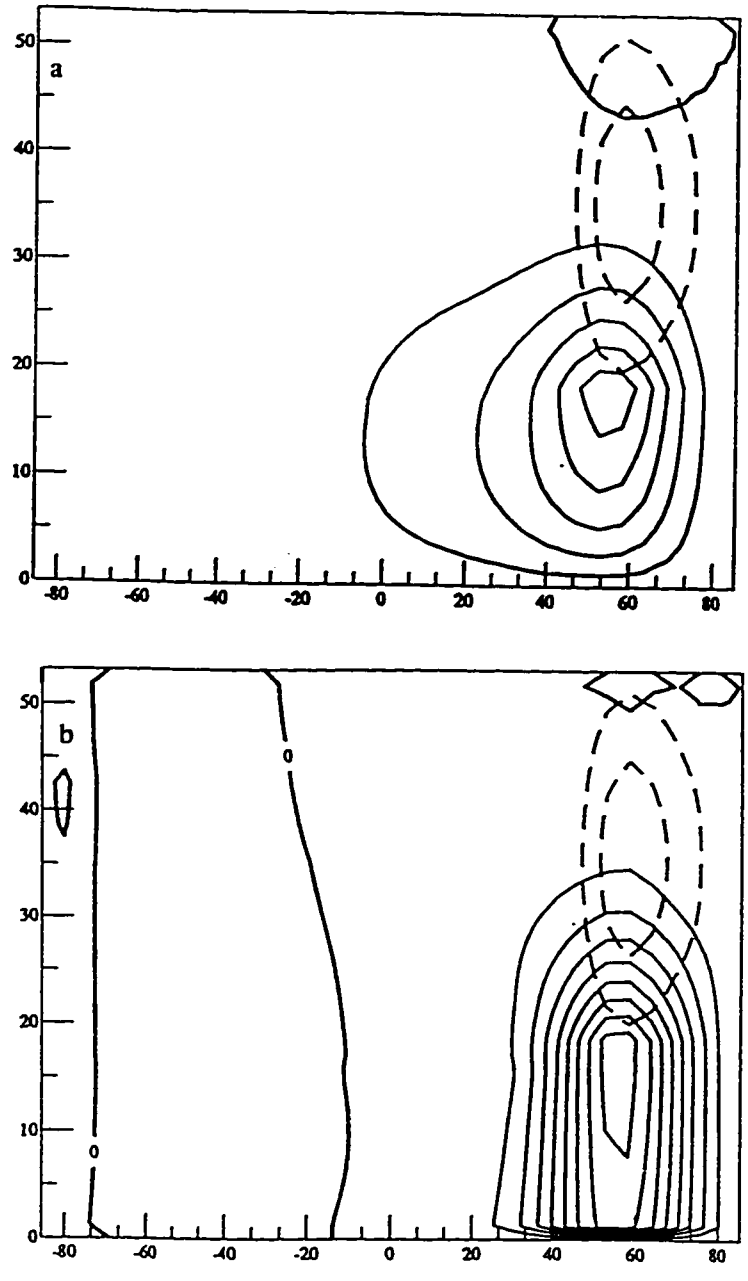

Figure 2.5: Numerical experiments (see chapter 5) on the response of the mean meridional circulation to a westward eddy-induced forcing located at 60°N and 35km (dashed contours). The solid contours are the streamlines, with the same contour interval in both panels. a) Shows the response to oscillatory forcing with a period of 30 days. b) Same as (a) but with the period of 360 days. The radiative damping time is 10 days in both cases. The numerical model (see chapter 4) includes nonlinear effects.

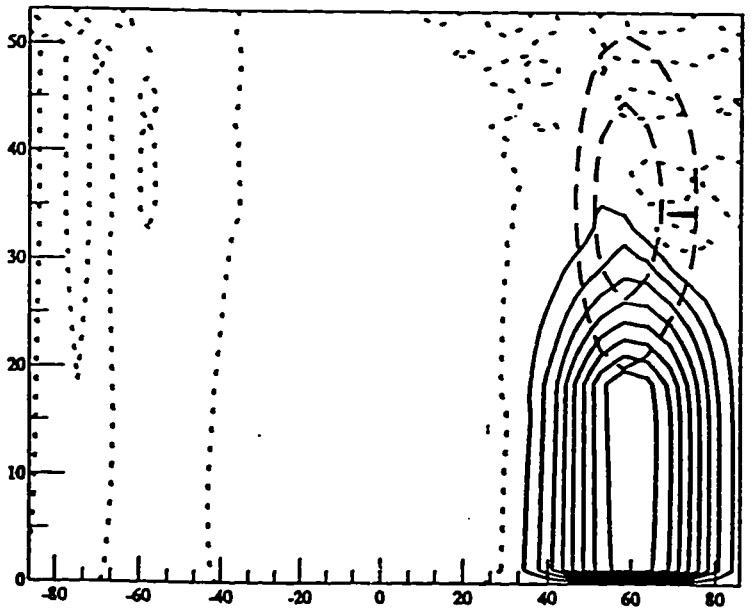

Figure 2.6: Same as Figure 2.5 but for a steady forcing.

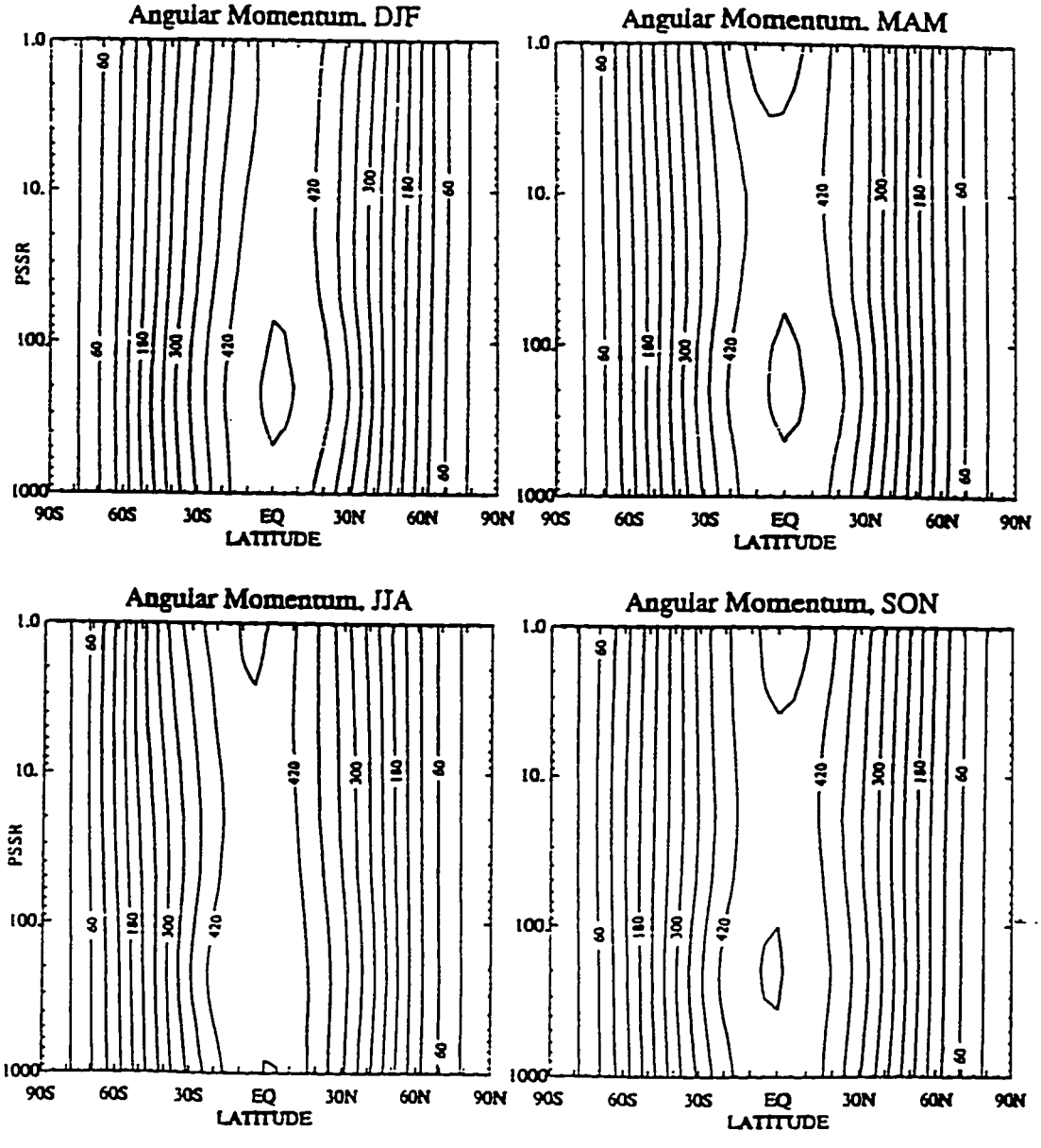

Figure 2.7:Angular momentum contours from *Rosenlof, [1994],* based on gradient zonal winds derived from 10 years of UKMO geopotential height data, in units 6.4×10^{6} m^{2}/sec.

Chapter 3 Empirical Analysis of the Large-Scale Dynamical Processes in the Tropics

The available observations of the structure and variability of the zonally averaged circulation in the tropics include radiosonde and satellite measurements of wind, temperature, pressure, precipitation, humidity and other meteorological variables. As was discussed in 2.2, we are interested in the dynamics on the seasonal time scale. Thus, in the rest of this work, if not stated otherwise, the characteristic time scales are assumed to be in the order of a few months.

This chapter is comprised of four parts. The first part shows that the observed annual cycle in the region of the tropical tropopause can be explained as a non-local response in the lower stratosphere to the seasonally varying extratropical eddy-induced forcing. Other dynamical processes that might cause the seasonal variations in this region are also discussed and compared with the eddy-induced circulation. It is concluded that the dynamics in this region are influenced by both the stratospheric and the tropospheric parts of the circulation. Therefore, the second part focuses on the processes in the troposphere. It describes the observed annual cycle of the Hadley circulation and the role of the remote eddy-induced forcing in maintaining this circulation. The third part describes the mean meridional circulation in the lower stratosphere deduced from the NCAR/NCEP reanalysis data. The last part of the chapter presents an empirical description of eddy-induced zonal forcing in the troposphere and stratosphere.

3.1 The Annual Cycle in the Tropical Lower-Stratosphere Temperatures and its Interpretation.

The annual temperature cycle in the tropical lower stratosphere was documented in the global temperature field by *Yulaeva et al. [1994]* based on a 13-year record from the microwave sounding unit (MSU) (flown aboard NOAA operational satellites), and obtained from the NASA Marshall Spaceflight Center, Huntsville. The characteristics and performance of this instrumentation are discussed in the series of papers by *Spencer and Christy [1990, 1993]*. The MSU-4 weighting function has a peak at about 100hPa and half-power points at about 150 and 40 hPa. It is ideally suited for analyzing the mean temperature of the lower stratosphere.

Fig.3.1 shows the annual march of climatological mean lower-stratospheric temperature obtained from monthly mean MSU-4 data for the period of 1979 - 1991. The top curve represents the temperature averaged over the region between 30°N and 30°S (referred to as the tropics in this section). The bottom curve presents the combined temperature field averaged over the regions poleward of 30° in the Northern and Southern hemispheres (the extratropics). The middle curve shows the globally averaged temperature. The amplitude of the annual cycle in the global mean temperature is about an order of magnitude smaller than that of the tropical mean. This difference in amplitudes can be explained as a result of a strong compensation between tropics and extratropics. Fig. 3.2 shows a scatterplot of month-to-month changes in temperature anomalies for the tropics versus extratropics, based on the same period of record. The correlation coefficient between the tropical and extratropical temperature changes is **-0.927** (if we exclude the months when the entire

lower stratosphere was warmed by the effect of volcanic eruptions).

A time-latitude section of the zonally averaged, climatological mean temperature perturbation about the annual mean value is plotted in Fig. 3.3. The temperature is weighted by the cosine of latitude in order to make it proportional to the perturbations in heat content per unit latitude. The annual cycle in the heat content in the tropics compensates for the large (factor of 2) difference in the amplitudes of the annual temperature cycle in the Northern and Southern Hemisphere polar stratosphere, thus leading to a very small annual cycle in global mean heat content shown in Fig. 3.1. The larger annual cycle in the Southern Hemisphere is a reflection of much lower wintertime temperatures there.

Yulaeva et al. [1994] suggested that these out-of-phase temperature variations between the tropics and extratropics are a signature of the annual cycle in the strength of the wave-driven, Lagrangian mean meridional circulation, which warms the high latitude winter stratosphere and cools the tropics. The rationale behind this conclusion is as follows.

Let's consider linearized version of the TEM thermodynamic energy equation (2.6) in which the radiative cooling is approximated in terms of linear relaxation at the rate κ toward a latitudinally dependent radiative equilibrium temperature T_0

$$\frac{\partial \overline{T}}{\partial t} + \kappa \overline{(T - T_0)} = \overline{w}^* \frac{N^2 H}{R} \tag{3.1}$$

Here, $\overline{w^*}$ is the residual zonal mean vertical velocity, defined as

$$\overline{w}^* = \overline{w} + \frac{R}{H} \frac{\partial \left(\overline{v'T'} / N^2 \right)}{\partial y} \tag{3.2}$$

We now suppose that some dynamical process drives a mean upward motion. Then, according to (3.1), the resulting adiabatic cooling must be balanced by either radiative relaxation, or local temperature changes, or both. For the characteristical vertical scale of the tropical annual cycle, the radiative time scale is about 30 days *(Fels 1982).* Therefore, on the seasonal timescale adiabatic cooling is balanced by radiative relaxation. Thus, an upward motion drives the temperature below the radiative equilibrium, and vice versa.

If (3.1) is multiplied by $\cos\varphi$ and integrated over latitude (assuming N to be constant), the adiabatic heating term vanishes by mass continuity. So we find that the variation of the global heat content must be due to variations in the radiative equilibrium temperature and/or in the radiative relaxation time scale. It follows that the annual cycle in the global heat content must be associated with diabatic forcing. As shown in Fig. 3.4, the peak-to-peak amplitude of the global mean annual cycle for the global mean lower-stratospheric temperature is only ~0.4°K, with the lowest temperatures during February, and the highest temperatures in August. It is nearly the opposite of what might have been expected in response to the annual variation in radiative drive owing to the variation in the sun-to-earth distance. The observed annual march in temperature follows the annual march in equatorial ozone (also shown on Fig. 3.4) with a lag of about 2 - 3 weeks. This lag, and the similarity in shape of the two curves, suggest that the observed annual march in the global mean temperature is caused by the annual march in the ozone concentration in the tropical lower stratosphere, where absorption of solar ultraviolet radiation by ozone is a major component of the heat budget.

The seasonal and latitudinal distribution of the ozone itself is the product of the

coupling between the photochemistry and the dynamical transport. *Yang et al [1991]* argue that the seasonal and latitudinal variations of the column density of the ozone are totally controlled by the dynamical transport by both advection and diffusion. Based on experimentation with their coupled 2D model in the isentropic coordinates, they showed that the qualitative features of the seasonal and latitudinal distribution of the column ozone are entirely determined by the advective part of the transport. However, the actual amplitudes can be affected by the diffusive part of the transport. Thus, the annual cycle in the tropical ozone is determined by the annual cycle in vertical advection in the tropics. Therefore, the seasonal variations in the global heat content are closely connected to the seasonal variations in the tropical upwelling.

An interpretation of the phase of the annual cycle in the zonal mean temperature of the lower stratosphere in the extratropics is simpler than for the global mean because it must be nearly in phase with the annual cycle in solar declination. However, the amplitude is smaller than the amplitude of the radiatively determined cycle *(Andrews et al, 1987)*. Owing to planetary wave activity, as well as to the upward extension of synoptic scale disturbances and gravity wave drag, there is a large Eliassen-Palm flux (E-P flux) divergence in the stratospheric winter hemisphere, as compared to summer hemisphere. This E-P flux divergence drives a residual meridional circulation characterized by subsidence in the extratropics. The downward motion maintains the winter temperature in the extratropics above the radiative equilibrium value. Due to mass continuity, this downward motion is balanced by a residual upwelling in the tropics and in the summer hemisphere. Thus in these regions the temperature is maintained below radiative equilibrium. The observed E-P flux divergence in the stratosphere during the Northern Hemisphere winter is much

stronger than during the Southern Hemisphere winter. Thus, the downwelling residual circulation at high latitudes is stronger during the Northern winter. It follows that the compensating upwelling in the tropical region must be stronger during the Northern winter, thus accounting for the phase of the observed annual cycle in the region of the tropical tropopause. This reasoning shows that the annual cycle in the dynamics in this region is driven by seasonal changes in the eddy-induced extratropical zonal forcing.

It remains to be shown that remote driving by winter stratosphere E-P flux divergence can account for the observed magnitude of the annual temperature cycle in the tropical lower stratosphere. *Holton [1990]* and *Rosenlof and Holton [1993]* have estimated the seasonal mean downward mass flux across the extratropical 100-mb surface from climatological E-P flux data. They found that the tropical upwelling required to balance the extratropical descent is twice as large in the Northern hemisphere winter season (DJF) as in the Southern hemisphere winter (JJA). According to *Holton [1990],* if this mass flux is assumed to occur uniformly in the belt from 20°S to 20°N , the mean vertical velocity across the tropical tropopause is about 2×10^{-4} m/s greater in DJF than in JJA. Assuming N^2 to be 3.3×10^{-4} s^{-2}, H=7 km, $\kappa=(1/30)$ day^{-1}, and neglecting the temperature tendency in the thermodynamic energy equation, we find that T(DJF)-T(JJA) ~ -4°K. This is approximately the same magnitude as the observed amplitude of the tropical temperature annual cycle at the 100 mb level. This simple analysis provides quantitative support for the hypothesis discussed above.

As shown in Chapter 2, the dynamics in the region of the tropical tropopause should also feel the influence of the tropospheric circulation. The next section focuses

on this complementary dynamical mechanism that can significantly contribute to the seasonal variability of the dynamics in the region of the tropical tropopause.

3.2 The Annual Cycle in the Tropospheric Mean Meridional Circulation.

3.2.1 Previous Observations

Reed and Vlcek [1969] were the first to suggest that the annual cycle in the upwelling through the tropical tropopause can be caused by the seasonal variability in the upward branch of the Hadley cell. They assumed that the Northern Hemisphere branch of the Hadley circulation has a pronounced annual cycle (with maximum amplitude in winter) as compared with much weaker annual cycle of the Southern Hemisphere branch. they argued that as a result, the equatorial upwelling in the troposphere should have an annual cycle with a maximum during the Northern Hemisphere winter. This upwelling penetrates into the lower stratosphere and produces the observed annual cycle through adiabatic cooling. Although for forcing with a latitudinal scale of about 1000 km (see eq. (2.10)) the estimated height of penetration of this upwelling into the stratosphere is only about 2 km, this mechanism can significantly contribute to the annual cycle of the upwelling in the region of the tropical tropopause. The questions that still remain open are what causes the seasonal variability in the upward branch of the Hadley cell, and whether this seasonal variability, in fact, contributes significantly to the observed annual cycle in the large-scale upwelling into the stratosphere.

Dickinson [1971b] argued that the minimum temperatures in the tropical lower stratosphere in January together with the maximum temperature in the middle latitudes in the winter stratosphere is caused by the annual march of the Hadley

circulation. His simulations showed that the seasonal difference in the mean meridional circulation in the troposphere is caused by variations in "both latent heat release and momentum fluxes".

Reid and Gage [1981] attributed the seasonal variation in the intensity of the upwelling in the ascending branch of the Hadley circulation to the annual cycle in sea surface temperature (SST) forced by variations in absorbed solar radiation. The tropical average ocean surface insolation exhibits maxima near the times of the equinoxes, and minima in July and December (see Fig. 3 in *Reid and Gage, 1981*). The insolation minimum is shallower in December than in July because of the annual cycle in the sun-earth distance. Using a simple coupled atmosphere-ocean model *Reid and Gage [1981]* numerically derived an annual cycle in the tropical SST. They argued that the amplitude and phase of the variation in the tropical average SST (with the maximum in April and the minimum in August) "represent delayed responses to the radiation maximum in March and the minimum in June" (*Reid and Gage, 1981, p. 1930*). The calculated variations in the SST field would cause the tropical tropopause height to have a maximum in April , and a minimum in August. However, observations show the maximum in February. This phase discrepancy suggests that the tropical upward motion is not directly controlled by the SST variations.

Fig. 3.5 *(Oort and Yienger, 1996)* shows the Eulerian monthly mean meridional circulation for each month as deduced from radiosonde observations. It is clearly seen that, except for April, the circulation is always dominated by a single cell extending from the hemisphere where radiative heating is maximum at this time, to the opposite hemisphere. Thus, the meridional circulation is almost always in a solstitial pattern, with maximum intensity during the Northern Hemisphere winter. The ideal average

equinoctial pattern symmetric about the equator is almost never realized.

Several recent attempts to explain these seasonal variations in the Hadley circulation reveal the existence of two conceptual views of the Hadley circulation.

The first view considers the Hadley circulation to be a zonally symmetric phenomenon that can be simulated with thermally forced, frictionally controlled, steady state models. This is essentially the view adopted by *Schneider and Lindzen [1977], Schneider [1978], Held and Hou [1980], Lindzen and Hou [1988].* They considered a circulation forced by an externally specified cumulus heating. *Lindzen and Hou [1988]* argued that Hadley transports are directed almost entirely into the winter hemisphere where they excite eddy instabilities. They also suggested that a smooth seasonal motion of the SST maximum back and forth across the equator is accompanied by far more abrupt changes in the Hadley circulation. The strength and pattern of the meridional circulation in their model was very sensitive to the latitudinal location of the SST maximum. Thus, the annual cycle in the upward branch of the Hadley circulation is mostly a reflection of hemispheric asymmetries in ITCZ locations.

The second view of the Hadley circulation *(Phillips, 1954, Williams, 1988, Satoh et al, 1994)* and the convection coupled with it, is that they constitute the zonally averaged features of the longitudinally varying atmosphere. Thus, they are non-locally controlled by the eddy-induced forcing. *Pfeffer [1992]* studied the changes in the meridional circulation during episodes of intensive baroclinic wave activity in the winter Northern Hemisphere. Though his analysis is done for dynamical processes with time scales of 5 days (i.e. in adiabatic limit), they lend further support to the notion that large convergence of the E-P flux in the middle troposphere in mid- and

high latitudes has an important influence on the meridional circulation in the tropical region of the troposphere.

3.2.2 The Zonally Averaged Circulation in the Troposphere as Derived from the Reanalysis Project Data

An important new source of dynamically consistent observations, that will be valuable for more intensive analysis of the nature and main characteristics of the zonally averaged circulation in the troposphere is provided within the framework of the Reanalysis Project *(Kalnay et al., 1996)*. This project is a product of cooperation between the National Center for Environmental Prediction (NCEP) and the National Center for Atmospheric Research (NCAR). Its main goal is to produce a consistent 40-year record of global atmospheric fields. All available measurements of atmospheric parameters on several pressure levels have been recovered and reanalyzed with state of the art data assimilation scheme. This procedure eliminates many of the inhomogeneties that are present in the previous operational analyses, thus providing a dataset more suitable for studies of interdecadal variability.

This study focuses on the thirteen years of monthly averaged observations of the structure and variations in the zonally averaged circulation available in the Reanalysis project data. These data have been analyzed together with the momentum fluxes from the NCAR Global Circulation Statistics Atlas *(Randel, 1992)* and with the observed precipitation data. The observed merged precipitation dataset for 1979 - 1992 was generated by Schemm based on the observed monthly total precipitation data from the world surface station climatology, and the estimated oceanic precipitation estimated from the MSU measurements *(Schemm et al., 1992)*.

As was discussed earlier in this chapter, the observed mean meridional circulation in the troposphere almost always consists of a single cell extending from the low latitudes in the summer hemisphere to the winter hemisphere. Fig. 3.6 shows (in log-pressure coordinates) a height-latitude section of the mass stream function for the meridional circulation deduced from the reanalyzed NCEP/NCAR data. In this picture, the circulation consists of two cells. Except for April and November, the winter hemisphere cell is stronger and broader than the summer hemisphere cell. We can also observe a gradual change in the circulation pattern over the seasons. During the Northern Hemisphere winter the strength of the circulation in this hemisphere increases, reaching its maximum in February. Then, it starts to weaken and at the same time the meridional circulation in the Southern Hemisphere starts to gain in strength. After an equinoctial pattern in April, the Southern Hemisphere cell exhibits a similar sequence of behavior to the Northern Hemisphere cell, reaching its maximum strength in August. The month to month variations in the meridional mass circulation derived from the reanalysis data and shown in Fig. 3.6 differs significantly from the previous "classical" picture of the Hadley circulation from *Oort and Rasmusson [1970].* It also somewhat different from the Hadley circulation determined from the radiosonde data (*Oort and Yienger, 1996).* Table 3.1 compares the main characteristics of the climatology of these two circulation patterns. It is clearly seen that there are differences, not only between the absolute values of the mass streamfunction but also in the time and the location of the maxima and minima in the Northern and Southern Hemispheres. Therefore, a thorough examination of the entire reanalysis zonally averaged data, might yield new insights into the mechanism of the seasonal variability of the Hadley circulation.

The behavior of several other meteorological variables is generally consistent with the observed march of the meridional mass circulation and is shown in Fig. 3.7 (latitude section of the zonally averaged precipitation), 3.8 (observed merged precipitation), 3.9 (time-latitude sections for the monthly mean zonally averaged climatological values) and 3.11 (time-latitude sections for the deviations from the annual mean of the monthly mean zonally averaged climatological values). The annual march in the zonally averaged meteorological variables shown in Fig. 3.6 - 3.11 can be summarized as follows.

- At each period of time, the circulation can be considered as a superposition of two elements: a circulation related to the oceanic ITCZ and a circulation related to the monsoons diabatic heating.
- A narrow spike observed at around 5-10° N in the the model and the observed merged precipitation, and in the omega vertical velocity (but not in the mass streamfunction) fields corresponds to the position of the ITCZ in the Pacific and Atlantic oceans *(Mitchell and Wallace, 1992).*
- This ITCZ feature is strongest in August-September (Fig. 3.9 b,d), and weakest in March-April, the time when weak Southern Hemisphere ITCZ sometimes appears in the eastern Pacific.
- The ITCZ migrates seasonally. It is closest to the equator in February-March, and farthest north in August-September (Figs. 3.9 b,d; 3.7; 3.8)
- The northward migration takes place smoothly, starting in March. The southward migration is much more abrupt and does not start until November (Figs. 3.9 b,d). The whole cycle very much resembles the phenomenon of a hysteresis loop. (This type of behavior in the climatological monthly mean OLR filed was earlier shown

by *Mitchell and Wallace,1992)*. As a result, the mean position of ITCZ is farther north in October-November, than in April-May.

- The comparison of Figs. 3.7 and 3.8, and panels (b) and (d) in Figs. 3.9, 3.11 reveals that the observed merged precipitation exhibits a narrower and more intense oceanic ITCZ feature, than the precipitation derived from the reanalysis. The discrepancy may be due to an overestimate of oceanic ITCZ rainfall in the MSU data (*R. Spencer, personal communication*), or to a failure of the model to simulate the intensity of the oceanic ITCZ *(Kalnay et al.,1996)*.
- The monsoon circulation is evident in all fields. However, it is best seen in the mass streamfunction field (Figs. 3.9a and 3.11a). The rainfall and omega vertical velocity fields exhibit odd symmetry about the equator (Fig. 3.11 b-d), while the streamfunction exhibits even symmetry and extends from 25°S to 25°N (Fig. 3.11a).
- The moonsoon mean meridional circulation is much stronger than the annually averaged mean meridional circulation (shown in Fig. 3.10a). The monsoon circulation is strongest in January and July, and is weakest around the transition times in April and October (Fig. 3.11).
- Northern Hemisphere monsoon persists about a month longer than the Southern Hemisphere monsoon (Fig. 3.11d)

3.2.3 The Zonal Wind

To further understand the seasonal variability of the meridional circulation, we will examine the zonal velocity field, an integral component of the zonally averaged circulation.

Fig. 3.12a presents the annual march in the zonal velocity field from the NCEP/NCAR reanalysis. For all seasons, the zonal wind at the equator in the lower troposphere and near the surface tends to be easterly. The midlatitude troposphere is characterized by westerly jets in both hemispheres. Westerly wind maxima of about 40 -50 m/s occur at around the 200 mb level. Further details are provided by Fig. 3.12b, which shows a latitude cross section of zonal wind at this level. As is clearly seen from this figure, the jet is stronger in the winter hemisphere where it is located at around 30°, as opposed to the summer, when it is shifted poleward to 45° - 50°. The jet is broader in the Southern Hemisphere, revealing two local maxima which are more pronounced during the spring and fall seasons. This double jet structure has been discussed in a number of works (i.e. *Yu and Hartman, 1993, Panetta, 1993*). The persistent existence of a second jet in the Southern Hemisphere, may indicate that the frequency of the rotation rate of the Earth belongs to the range of transition from the regime with one jet to a multiple jet regime.

The corresponding annual march in the eddy fluxes of zonal momentum is shown in Fig. 3.12c, and can be described as follows:

- the strongest poleward fluxes are found at around 200 mb level and at about the same latitude as the westerly wind maximum;
- the fluxest tend to be strongest during the wintertime;
- the annual march in the strength of the eddy fluxes of zonal momentum is stronger in the Northern Hemisphere

The relationship between the zonal wind velocity and the eddy zonal fluxes represents a 'chicken-egg' problem. The diagrams in Fig. 3.12 alone do not provide sufficient information for the determination, if the annual cycle of the zonal velocity is

caused by the zonal eddy forcing, or the seasonal variability of the eddies is maintained by the seasonal variability of the jet stream. We will investigate this problem later on in Chapter 5, using the 2D model simulations.

3.2.4 Fall vs Spring Transition

Another interesting aspect of the seasonal variability of the zonally averaged circulation that can provide some useful insights into the mechanisms of the general circulation, is the difference between the transition periods, i.e. the difference between the fall and the spring circulations.

The conventional meteorological spring season tends to be colder than the fall season due to the lag in the transition period for the tropospheric mean temperature field. In order to eliminate the asymmetry in the temperature distribution, we redefined the conventional fall and spring seasons (spring is considered to be the mean of April/May, and fall is the mean of October/November), so that the tropospheric mean temperature in spring is comparable to the tropospheric mean temperature in fall. In addition, during these months we observe the transition from the Northern Hemisphere monsoon precipitation pattern to the Southern Hemisphere monsoon (Fig. 3.11b), thus all the difference in the diabatic heating at this period is related to the oceanic ITCZ variability.

Fig. 3.13 shows meridional cross-sections of temperature, zonal velocity and meridional stream function for spring (left panels), fall (middle panels) and the difference between these two seasons (right panels). The temperature field in the lower troposphere (the upper row) is nearly symmetric about the equator in both spring and fall. Slightly higher temperatures are observed in mid-latitudes in the

middle troposphere of the Northern Hemisphere in April-May. The corresponding westerly jet (second row from the top) is closer to the equator in the Northern Hemisphere during April-May in agreement with results of *Fleming et al [1987].* In spring there is a less intense meridional circulation in tropics (third row).

The mean meridional circulation, shown in the lower panel, are relatively weak, and nearly symmetric in these seasons. However, a distinct difference pattern emerges, with more ascent around 10 -15°N and descent just south of the equator and near 30°N during April-May. The same features are apparent in the meridional profiles shown in Fig. 3.14, which also includes zonally averaged precipitation.

An important remaining question is whether the difference in diabatic heating between spring and fall is sufficient to cause the asymmetry in the zonally averaged circulation, or whether the difference in eddy forcing is an additional factor. This question will be examined in Chapter 9 during the discussion of the model simulation results.

The observations discussed in this section reveal a complex mechanism of the seasonally varying zonally averaged circulation in the upper troposphere. The next question to address is whether the behavior of the meridional circulation in the lower stratosphere is similar to its counterpart in the troposphere, or whether the processes in the lower stratosphere are totally different from the tropospheric processes.

3.3 Empirical Studies of the Annual Cycle of the Meridional Circulation in the Lower Stratosphere.

The features of the meridional circulation in the troposphere and in the lower stratosphere described in this chapter differ significantly from each other. Figure 3.15

shows the transition between the upper troposphere and the lower stratosphere circulation regimes. The mass stream functions (in deviations from the annual mean values) on panels (a) - (c) correspond to the 250 mb, 200 mb and 150 mb levels. The meridional stream function does not experience any significant qualitative changes upward from the 300 mb (Fig. 3.11a) to 150 mb levels. As was discussed in the section 3.2.2, the streamfunction in the tropics is dominated by the monsoon circulation, which exhibits even symmetry about the equator. However, already at the 100 mb level (panel d) the cell shifts northward from the equator. The circulation becomes stronger during the Northern Hemisphere winter, and the region of the corresponding upwelling in the Southern Hemisphere moves equatorward. This transition into the "stratospheric circulation" regime is even more evident at the next two panels (e-f), that show the streamfunction at 70 and 50 mb levels. The mean meridional circulation during the Northern Hemisphere winter is nearly twice as strong as during the Southern Hemisphere winter. The belt of intense upwelling is located near the equator, and the corresponding downwelling region is centered in mid latitudes of the winter hemisphere

In summary, the observed mean meridional circulation at 100 mb level can be viewed as a superposition of two components: the equatorially symmetric component forced by the monsoon part of the diabatic heating, and an equatorially asymmetric component forced by the seasonally varying wave-induced zonal forcing in the stratosphere.

The annual march of the eddy-induced zonal forcing can be represented by the diagrams shown in Fig. 3.16. The meridional eddy zonal momentum flux integrated upward from the 100 mb to 1 mb level (panel a) exhibits the monopole structure with

the maximum fluxes in the high latitudes in January-February in the Northern Hemisphere, and in September - October in the Southern Hemisphere. The amplitude of the zonal momentum eddy fluxes and their latitudinal gradient in the Northern Hemisphere is larger than in the Southern Hemisphere. The annual cycle of the zonal momentum eddy flux in the Northern Hemisphere is in phase with the seasonal cycle of downwelling in high latitudes in the Northern Hemisphere at this level. The annual march of the difference between the eddy zonal momentum flux at 65°N and 65°S (Fig. 3.16b) exhibits a pronounced maximum in February, with a secondary local maximum in November. However, the minimum in the strength of this measure of the eddy-induced zonal forcing occurs in April-May, two - three months earlier than the minimum in the tropical upwelling. Thus, judging from this simple calculations, it appears that there may be some discrepancies between the observed annual march of the eddy zonal momentum flux and the theoretically predicted wave-induced forcing. The last section of this chapter describes the more accurately calculated eddy-induced zonal forcing observed in the atmosphere.

3.4 Eddy-Induced Zonal Forcing.

The wave-induced forces in middle and high latitudes are believed to be mainly due to Rossby and gravity waves originating in the extratropical troposphere *(Edmon et al, 1980)*. An accurate calculation of the E-P flux divergence requires directly measured winds. This data do not exist for the atmosphere on a global basis. Therefore, an alternative balance wind estimation of some kind is necessary.

A possible method of estimating winds is based on the linear wind balance (*Rosenlof, 1994*). The resulting E-P flux divergence estimates in units m/s/day

computed for 1979 -1989 UKMO geopotential height data and averaged over each season are presented in Fig.3.17. In winter (DJF), maximum negative magnitudes of the E-P flux divergence are found between 60°N and 70° N in the middle and upper stratosphere. In summer (JJA) the maximum negative E-P flux divergence is observed also between 60°S and 70°S, but the magnitudes are significantly smaller than during the Northern Hemisphere winter (due to reduced wave activity). The two equinox seasons show very similar patterns in the troposphere. However in the stratosphere, more wave activity is observed in the Southern Hemisphere during its spring period (SON) than during the spring period (MAM) in the Northern Hemisphere. In all seasons the E-P flux divergence in tropical regions is very small and has a prevailing negative sign in the stratosphere.

It should be noted that the calculations discussed above did not include a gravity wave drag parameterization. The combined distribution of the zonal forcing for the momentum equation, which is the sum of the planetary scale wave E-P flux divergence and gravity wave drag, was derived indirectly by *Rosenlof [1994]*. Using the thermodynamic energy equation with observed temperature and with diabatic heating determined from a radiation model, she obtained the residual vertical velocity field. By substituting it into the continuity equation, she obtained the meridional residual velocity field, and was then able to deduce the E-P flux divergence based on the zonal momentum equation. Fig. 3.18 shows the total zonal forcing for the zonal mean momentum equation for January 1993 and July 1993. The zonal force is negative throughout most of the winter hemisphere. In the summer hemisphere small positive values are found near the stratopause. These data don't allow us to conclude whether the small regions of positive E-P flux divergence in high latitudes are just errors in the

calculation, or whether this is a manifestation of a real phenomenon. The maximum magnitude of the zonal forcing occurs between 30° and 60° in the winter hemisphere. Fig 3.19 shows the January - July difference in zonal forcing. During January the forcing in both hemispheres is stronger throughout most of the middle latitude stratosphere than in comparable latitudes during July. The difference in forcing between winter hemispheres is much larger than for summer hemispheres.

The comparison between figures 3.17 and 3.18 indicates that the gravity wave forcing is particularly important in Southern Hemisphere winter. The variations in the distribution of this forcing in the summer middle and upper stratosphere may be essential for causing the seasonal variations of the rising branch of stratospheric circulation *(Garcia and Boville, 1994)*. However, there are a lot of uncertainties in calculation of the gravity wave drag and, we will not consider this part of the zonal forcing in our qualitative discussion.

Fig. 3.20 shows the climatological mean E-P flux divergence for January and July in the units m/s/day from the Atlas of the Global circulation statistics derived from the 12 years of NMC operational geopotential height analysis *(Randel, 1992)*. The E-P flux patterns shown on this figure are quite similar to those produced by *Rosenlof [1994]*. Time spectral analysis of these data reveals that this zonal forcing has a very pronounced annual cycle with a maximum in winter.

The only qualitative discrepancy of this zonal forcing with the E-P flux divergence pattern calculated by *Edmon et al [1980]* and *Yang et al [1990]* is located at the surface. The zonal forcing patterns described in those two papers have a distinctive local divergence maximum at the surface in middle and high latitudes, while the NMC data do not show this maximum. However, the discrepancy at the surface is

apparently not related to the physical processes in the region of the tropical tropopause, the topic of our study, and we will not examine it further.

This chapter presented a description of the climatology of the observed global atmospheric zonally averaged circulation pattern, and the observed zonal forcing that may be responsible for it.

The next question to be addressed is whether model simulation experiments can help to explain the underlying complex physical mechanism.

Table 3.1: Comparison between NCAR/NCEP climatology of the Hadley circulation and the climatology of the Hadley circulation deduced from 26-yr set of daily global upper-air wind data (Oort and Yienger, 1996)

	Oort and Yienger *[1996]*	NCAR/NCEP reanalysis
NH max: month	Jan+February	January
NH max: $\times 10^{10}$ kg/s	22.9	16.8
NH max: height (mb)	462	400
NH max: latitude	8°N	10°N
SH max: month	July	August
SH max: $\times 10^{10}$ kg/s	19.3	17.6
SH max: height (mb)	594	400
SH max: latitude	7°S	5°S

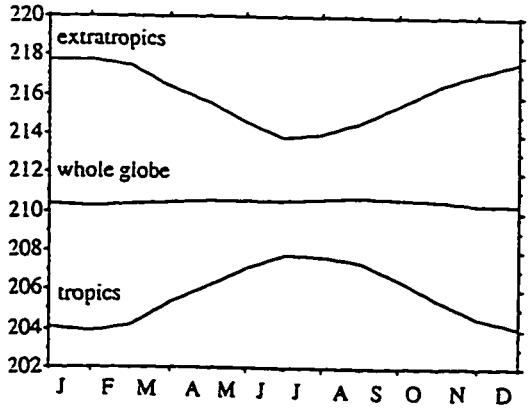

Figure 3.1: Climatological mean annual march of lower-stratospheric temperature based on MSU-4 data for the period 1979-1991, averaged over the tropics (30°S-30°N), the extratropics (poleward of 30°S and 30°N), and the entire globe.

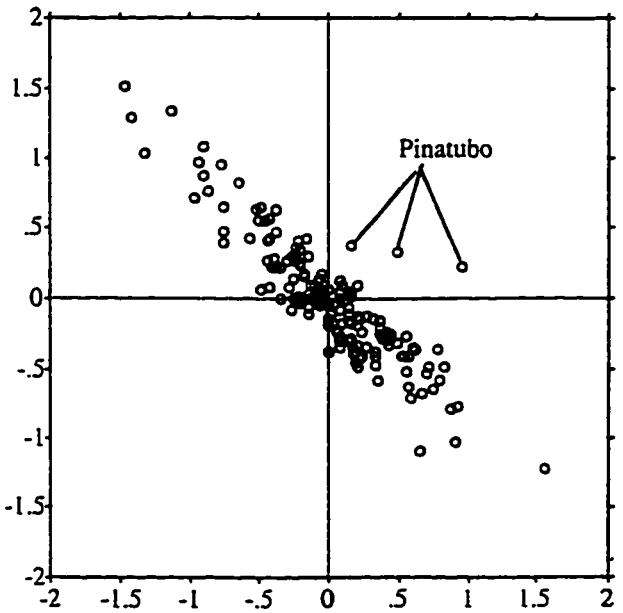

Figure 3.2: Scatterplot of T_n-T_{n-1}, where T_n is the mean temperature anomaly for the n-th month, based on the MSU-4 data for the period 1979-91. Each point represents a particular calendar year; the position on the abscissa represents the average value over the tropics, and the position on the ordinate represents an average over the extratropics (as defined in 3.1).

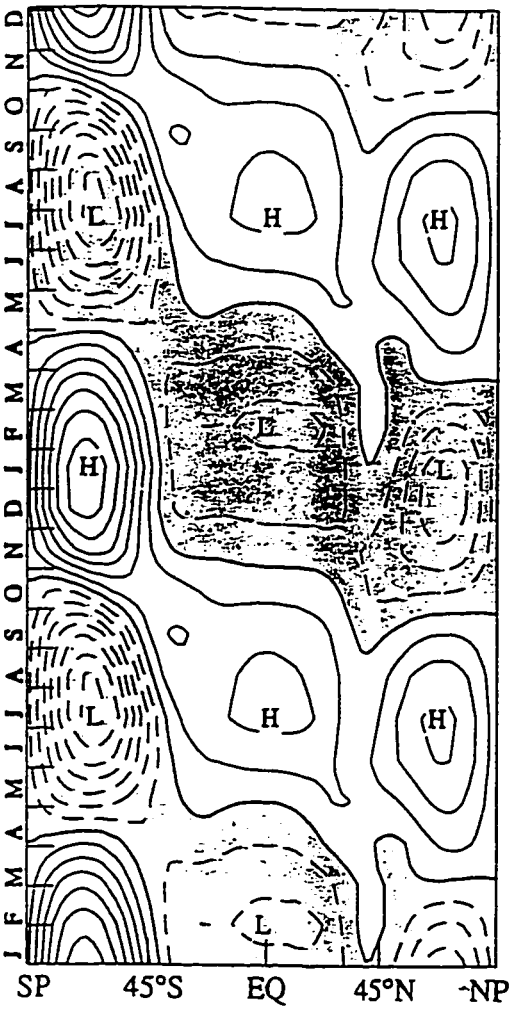

Figure 3.3: Time-latitude sections of climatological zonally averaged monthly mean temperature minus annual mean temperature at the same latitude, weighted by cosine of latitude, based on the MSU-4 data for the period 1979 - 1991. Contour interval: 1K; negative contours are dashed. Two complete cycles are shown.

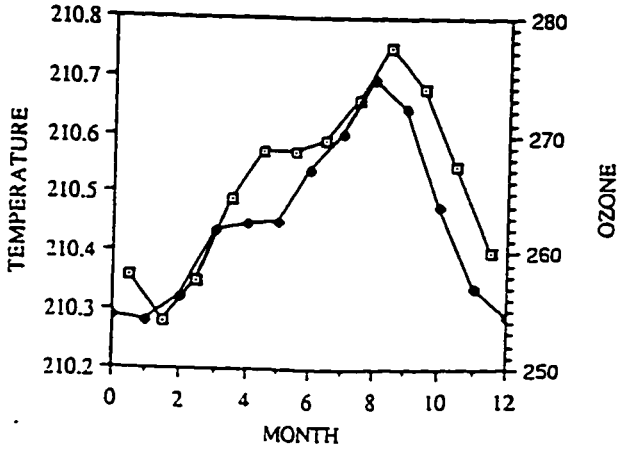

Figure 3.4: Annual march of global mean lower-stratospheric temperature from Fig. 3.1 shown on expanded scale (open squares), plotted with the annual time series for equatorial total ozone in Dobson units (solid diamonds) from *Shiotani [1992].*

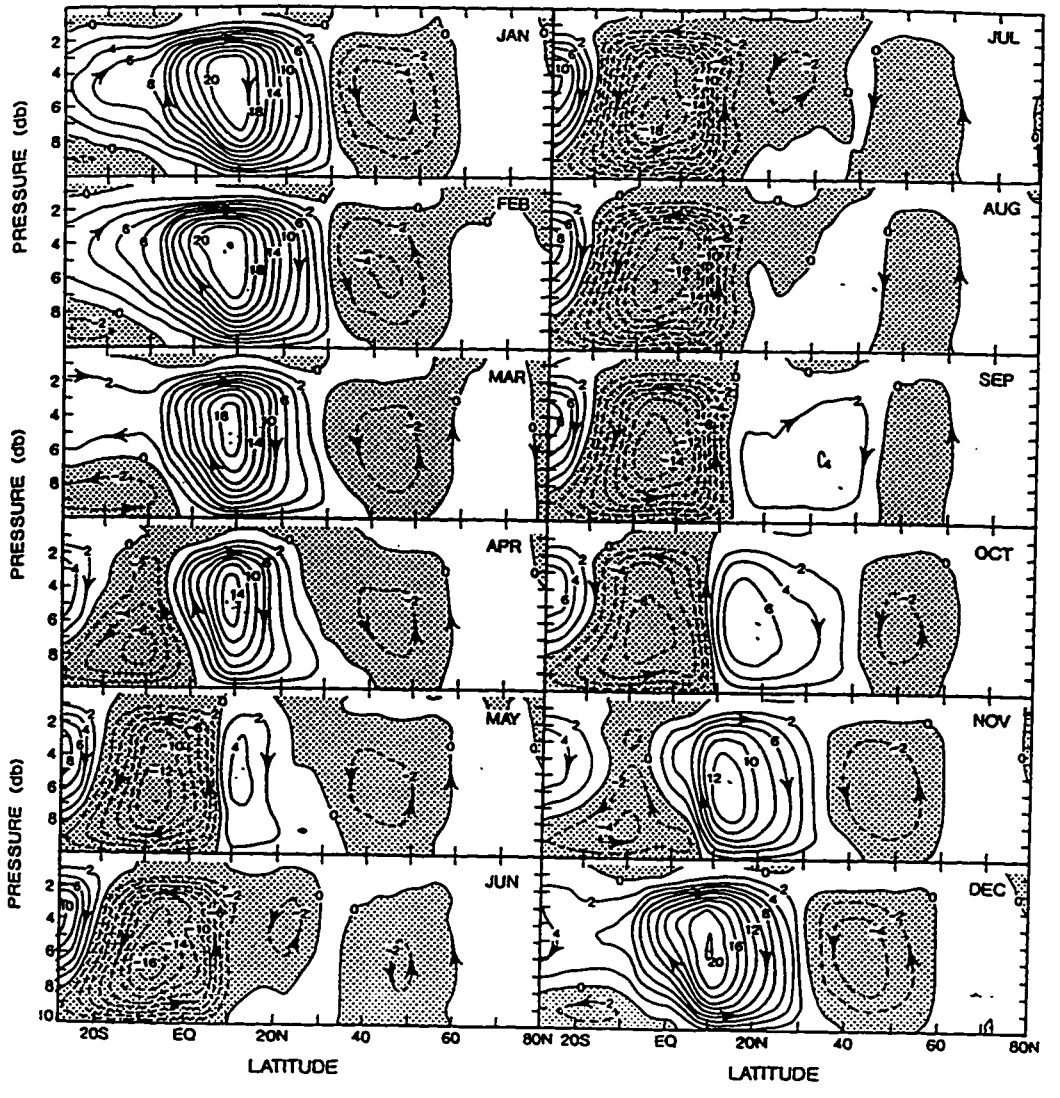

Figure 3.5: Streamlines of the Eulerian mean meridional circulation for each month. The isolines give the total transport of mass northward below the level considered. Units 10^{10} kg/s (from *Oort and Yienger, 1996*)

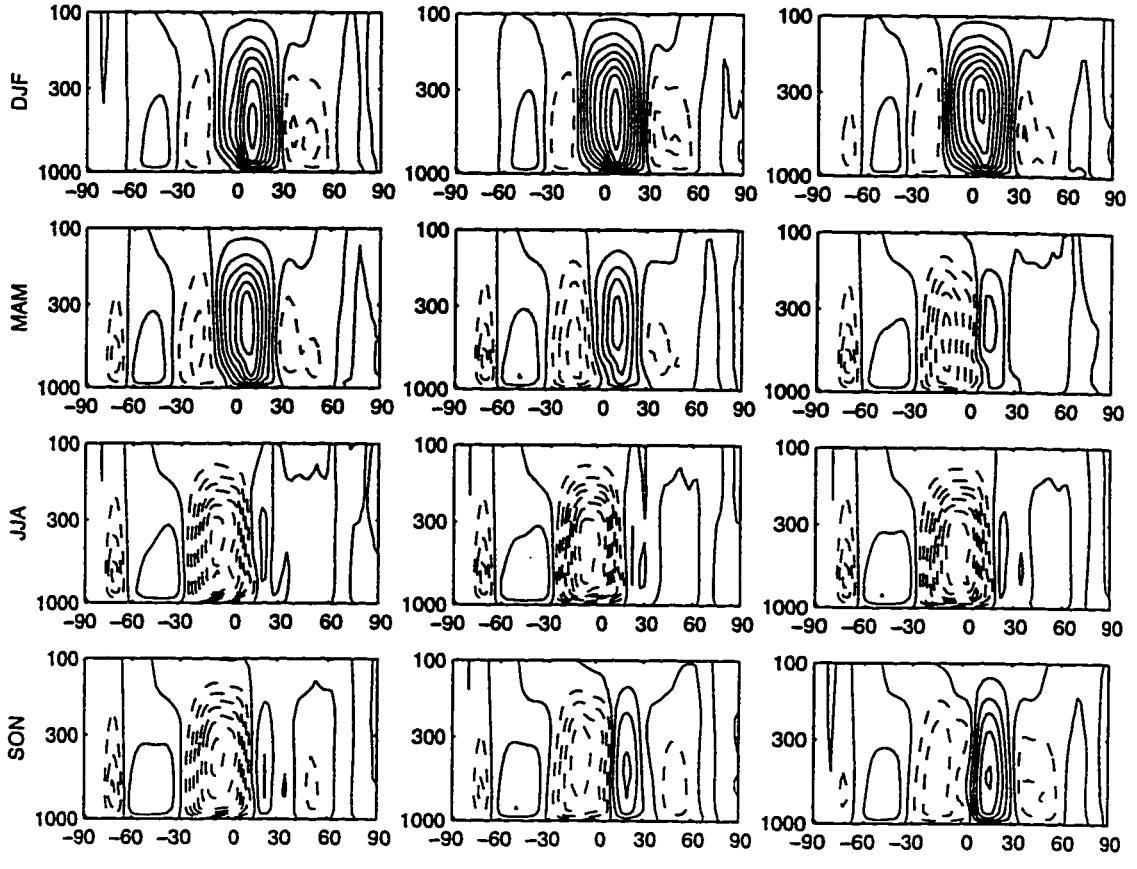

Figure 3.6: Monthly mean climatological streamfunction of the meridional circulation deduced from the reanalyzed NCEP/NCAR data for the years of 1982 - 1994. The height is a log-pressure coordinate. The left upper panel corresponds to December. Contour interval is 500 kg/s/m, dashed contours denote negative values.

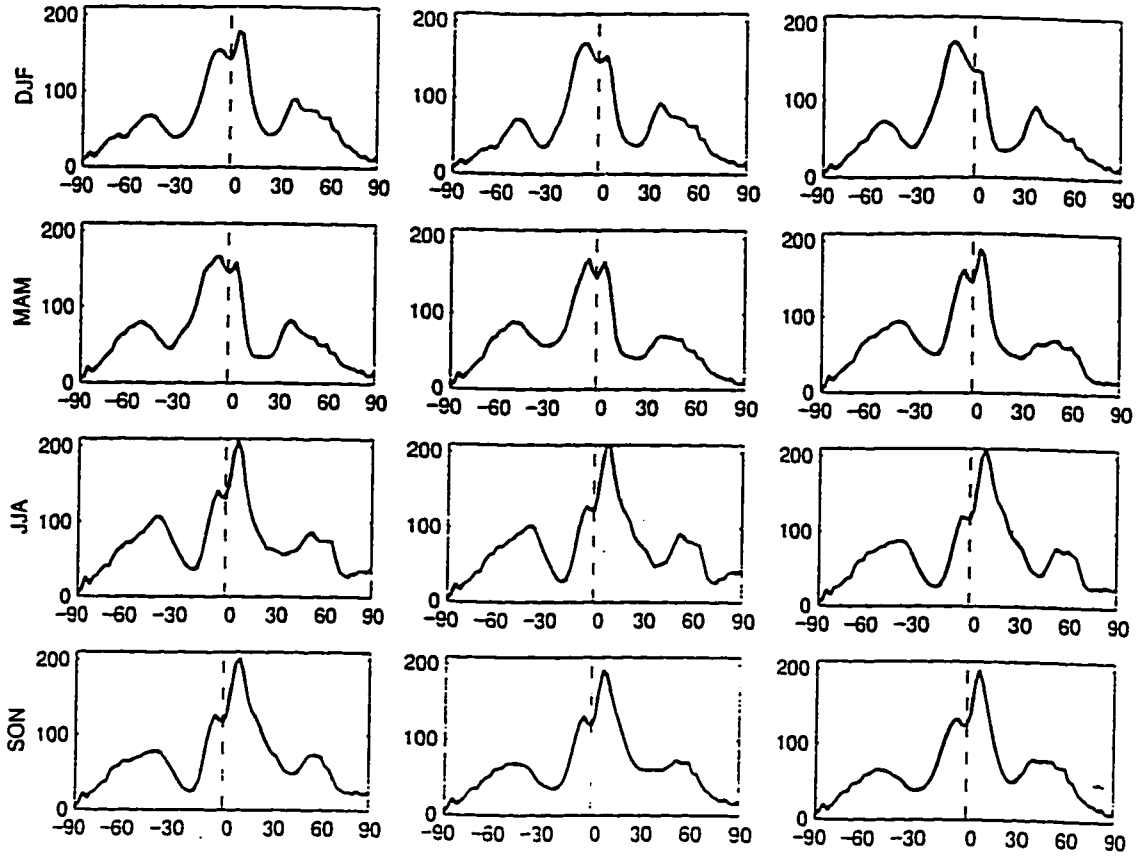

Figure 3.7: Same as Figure 3.6 but for the zonally averaged precipitation in mm/month derived from the same diagnostic model.

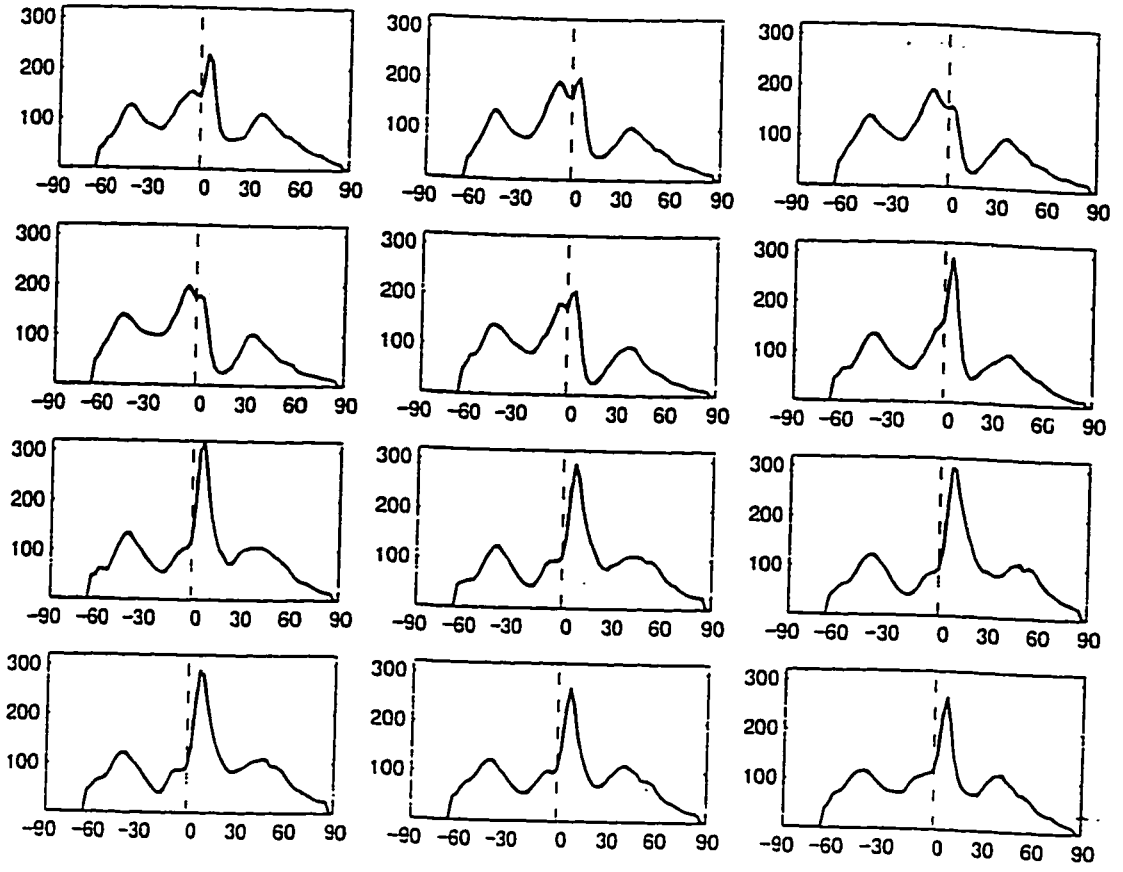

Figure 3.8: Same as in Figure 3.7 but for the merged precipitation (*Schlemm et al.,1992*)

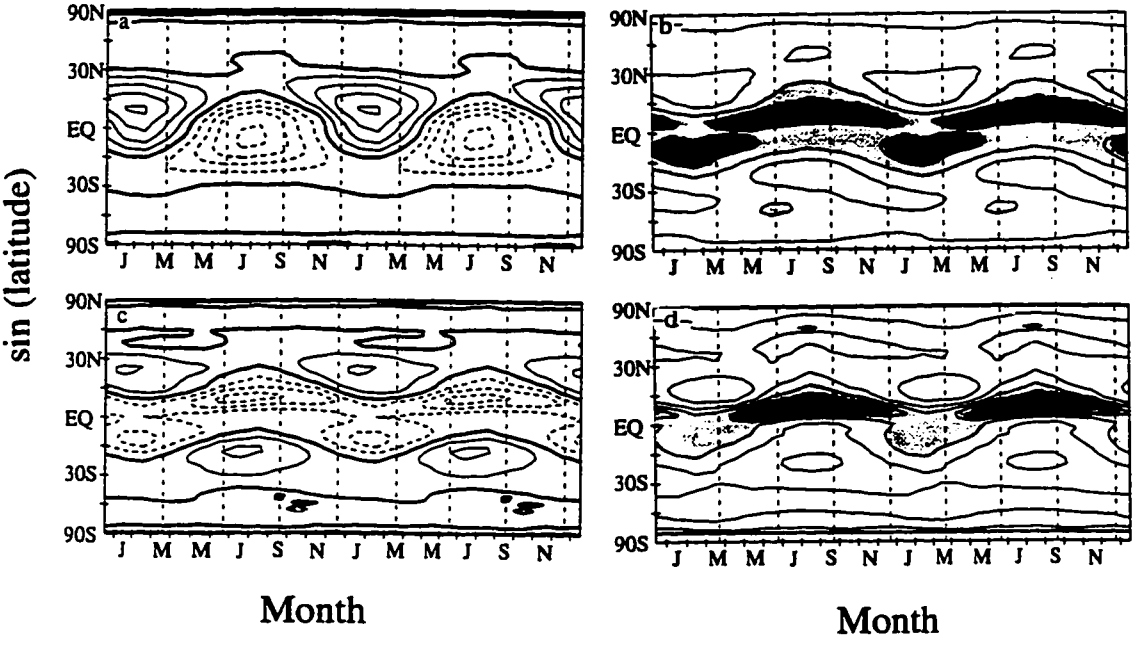

Figure 3.9: Time-latitude sections for some monthly mean zonally averaged climatological fields (NCEP/NCAR data). Negative values are shown with dashed lines.
(a) Mass stream function at 300 mb. Contour interval 1000 kg/s/m
(b) Precipitation, contour interval 50 mm/month. Thick line defines 100 mm/month contour. Regions where precipitation is greater than 100 mm/month are shaded.
(c) Omega at 300 mb, contour interval is 0.01 Pa/s
(d) Merged precipitation generated by Schemm based on the observed monthly total precipitation data from the world surface station climatology, and the estimated oceanic precipitation from the MSU measurements *(Schemm et al., 1992)*. Contour interval is 50 mm/month. Thick line defines 150 mm/month contour. Regions where precipitation is greater than 150 mm/month are shaded.

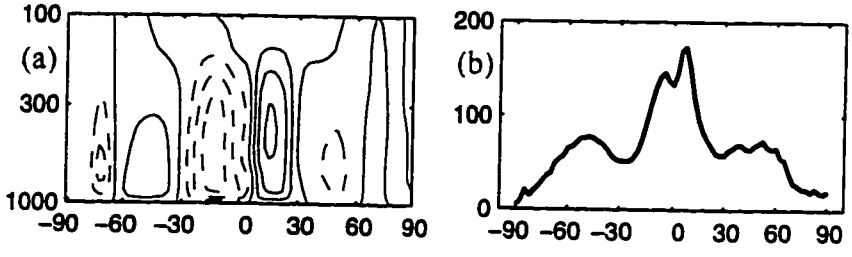

Figure 3.10: (a) Same as Figure 3.6, but for the annual mean streamfunction, contour interval is 500 kg/s/m, dashed contours denote negative values.
(b) Same as Figure 3.7, but for the annual mean monthly mean precipitation in mm/month.

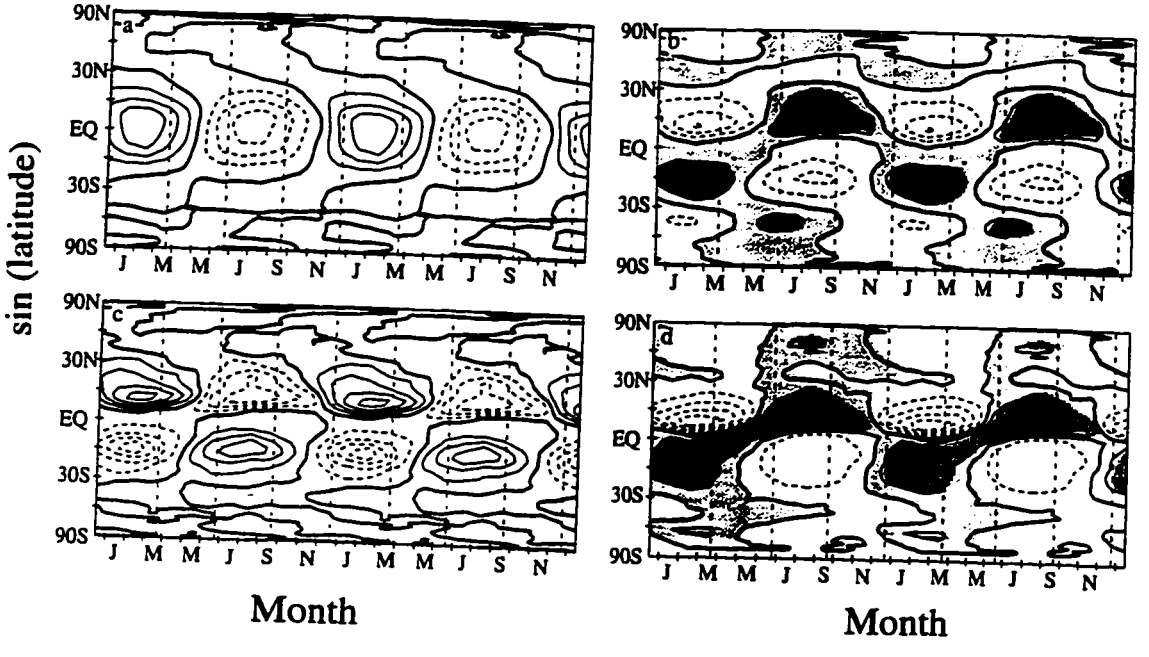

Figure 3.11: Same as Figure 3.9 but for the time-latitude sections for the deviations of the monthly mean zonally averaged climatological values from the annual means:
(a) Mass stream function at 300 mb. Contour interval: 1000 kg/s
(b) Precipitation, contour interval 25 mm/month
(c) Omega at 300 mb, contour interval is 0.005 Pa/s
Merged precipitation generated by Schemm *(Schemm et al., 1992).* Contour interval is 25 mm/month.

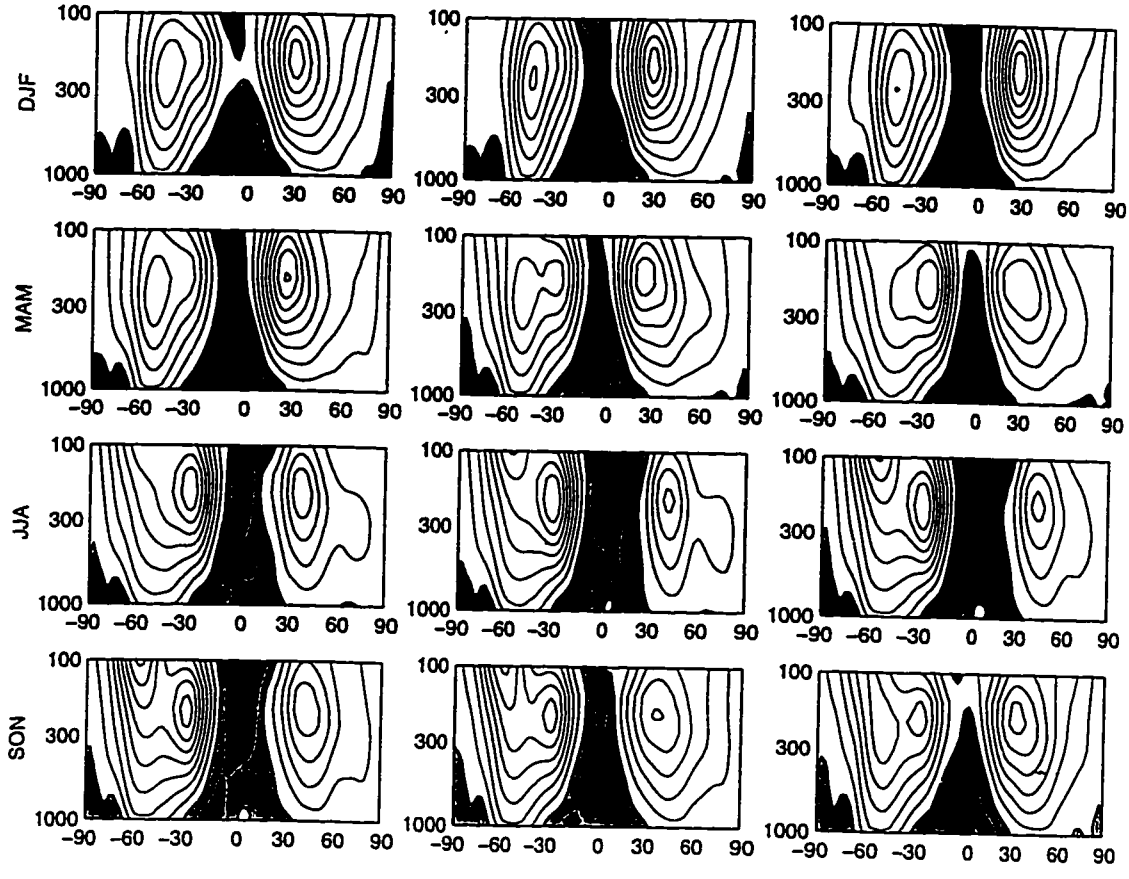

Figure 3.12: (a) Height-latitude section of the monthly mean climatological zonally averaged zonal velocity. Contour interval 5m/s, shading denotes easterly regions.

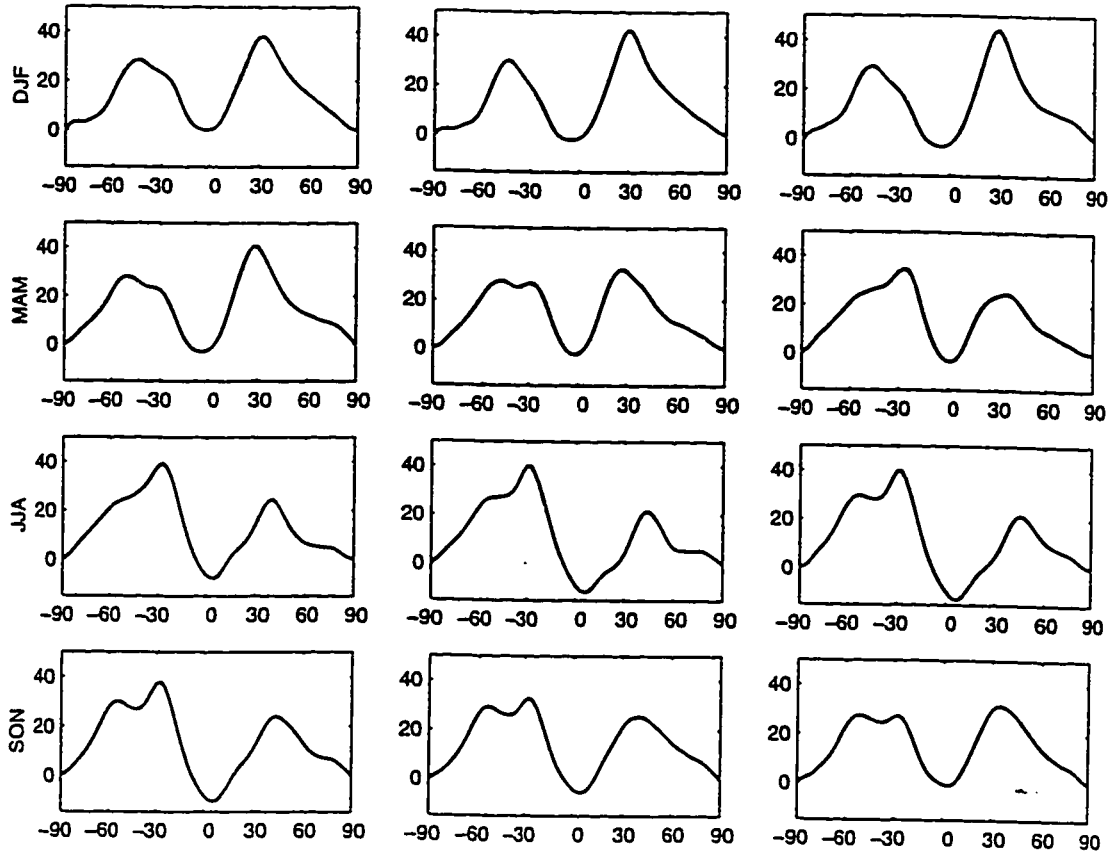

Figure 3.12 (continued) : (b) Latitude crossection of the zonal wind at 200 mb pressure level.

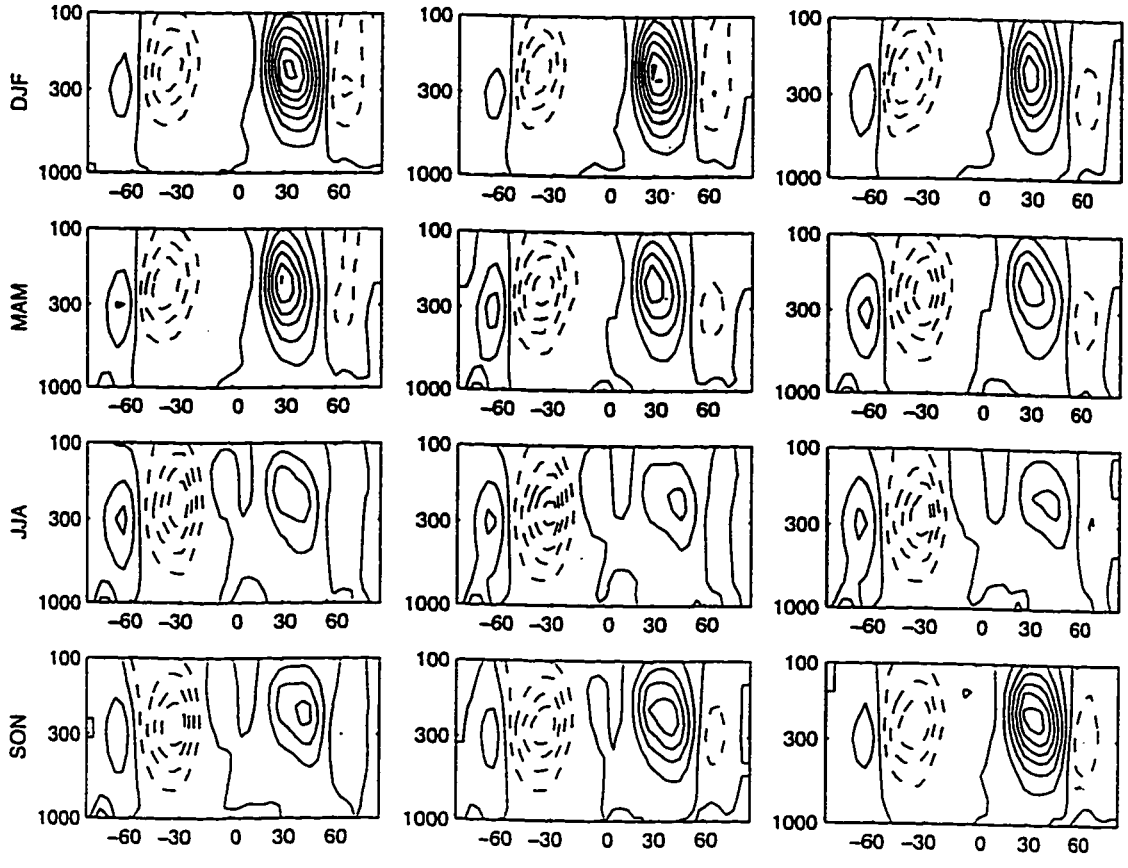

Figure 3.12 (continued) (c): Same as Figure 3.12a but for the climatological monthly mean eddy zonal momentum flux. Contour interval 10 m^2/s^2

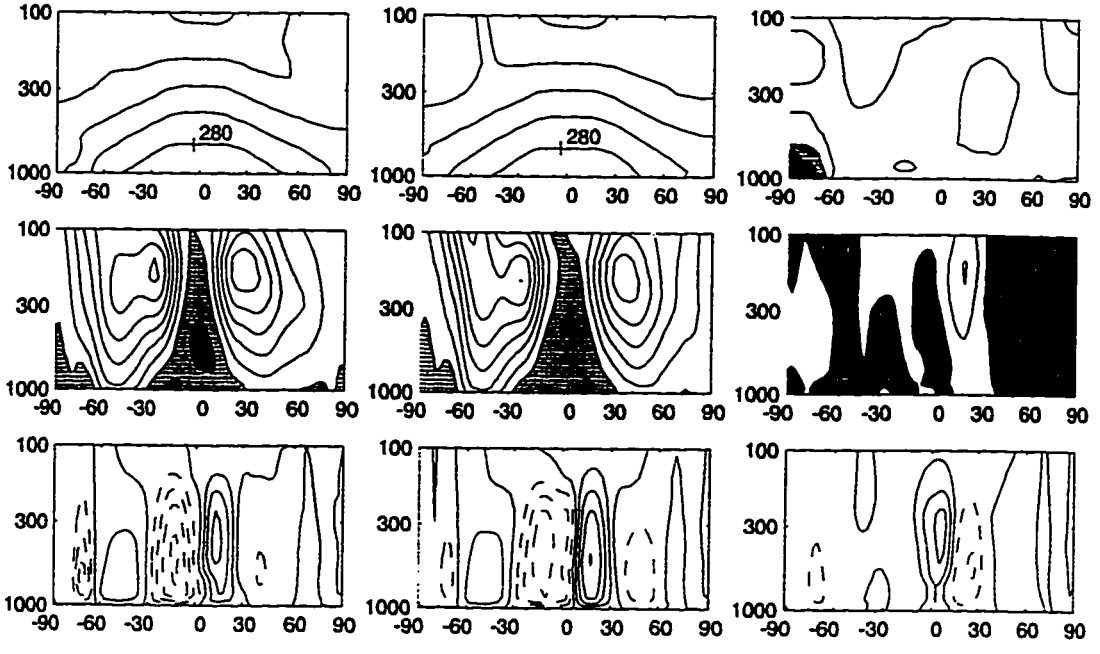

Figure 3.13: The high-latitude sections of some zonally averaged dynamical fields for spring (left panels), fall (middle panels) and the difference between spring and fall (right panels).

first row: temperature , contour interval 20°K;

second row: zonal velocity , contour interval 5m/s (2 m/s for the last right panel), regions of easterlies are shaded;

third row: meridional mass streamfunction, contour interval 500 kg/s

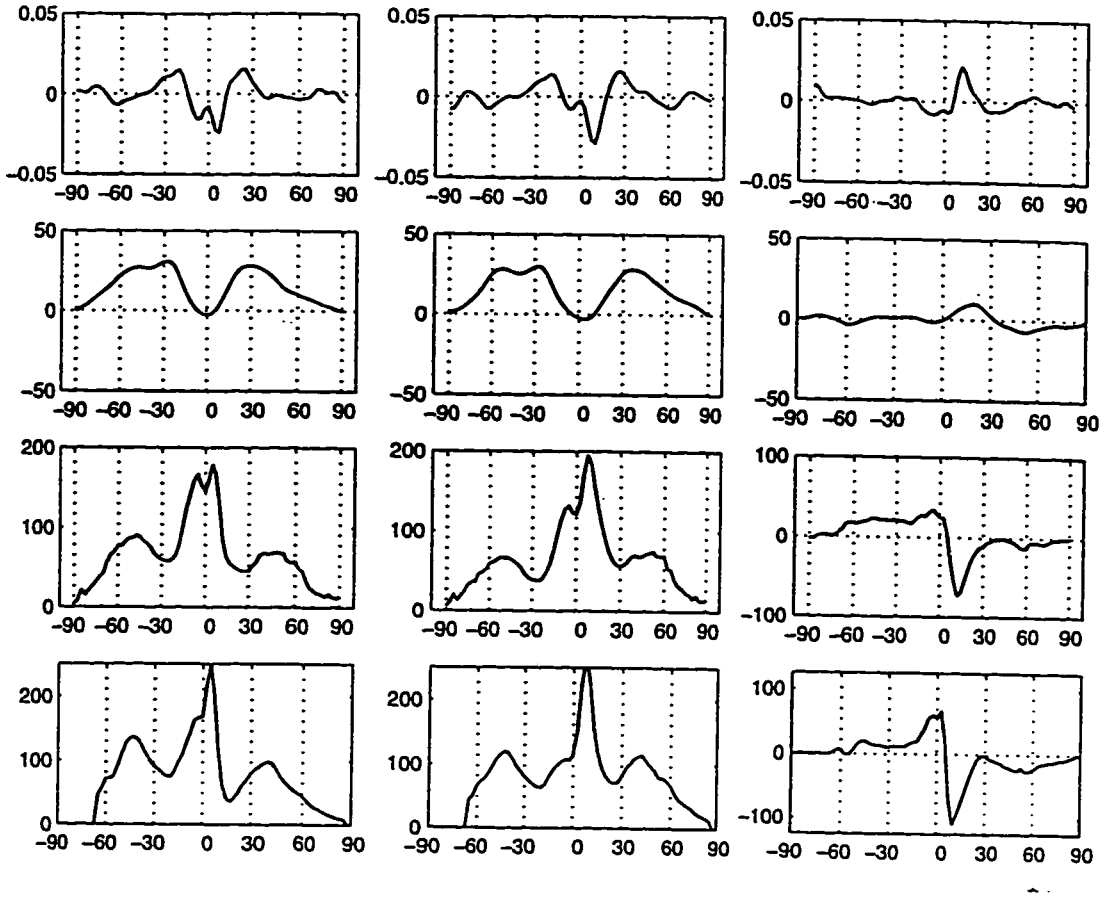

Figure 3.14:
Upper row: the pressure vertical velocity at 300 mb height in spring (left panel), fall (middle panel), difference between spring and fall (right panel);
Second row: analogous diagram for the zonal velocity field at 200 mb height;
Third row: same as in the previous row but for the latitude sections of reanalyzed precipitation;
Lower row: same as in the third row but for the merged precipitation field.

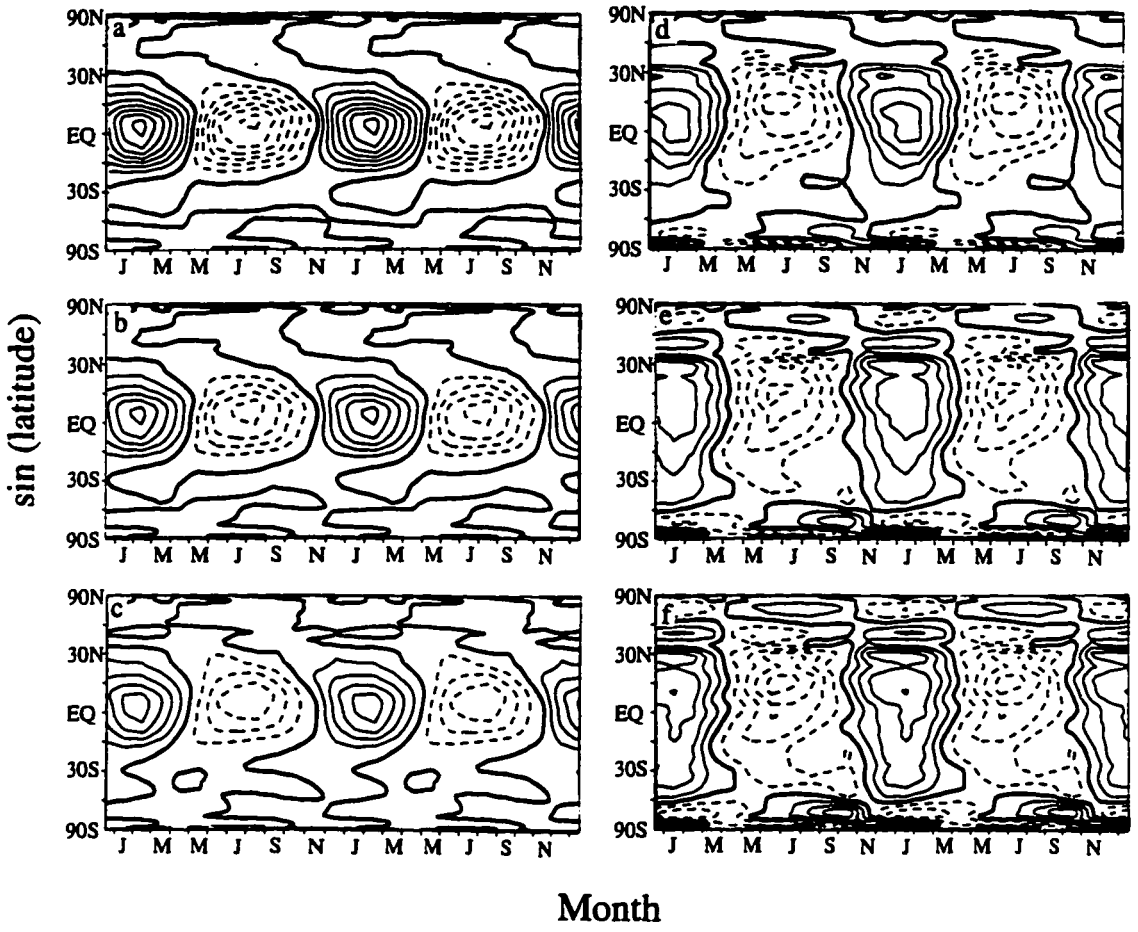

Figure 3.15: Time-latitude sections for deviations from the annual mean values of the monthly mean climatological mass stream function (NCEP/NCAR data). Negative values are shown with dashed lines

(a) Mass stream function at 250 mb. Contour interval 500 kg/s/m
(b) Mass stream function at 200 mb. Contour interval 500 kg/s/m
(c) Mass stream function at 150 mb. Contour interval 250 kg/s/m
(d) Mass stream function at 100 mb. Contour interval 50 kg/s/m
(e) Mass stream function at 70 mb. Contour interval 25 kg/s/m
(f) Mass stream function at 50 mb. Contour interval 15 kg/s/m

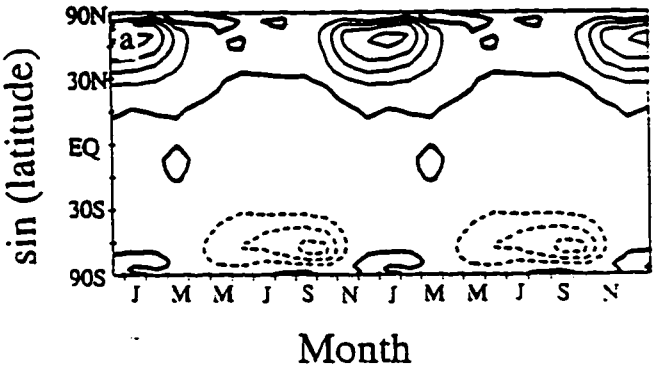

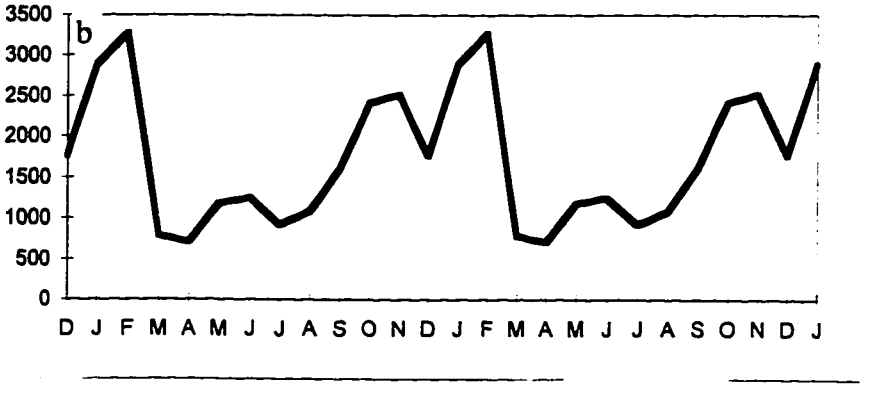

Figure 3.16: (a)Time-latitude section of the meridional eddy zonal momentum flux integrated upward from 100 mb to 1 mb height, contour interval 10 m^2/s^2.
(b) Annual march of the measure of the eddy-induced forcing constructed as the difference between the eddy zonal momentum flux at 65°N and 65°S.

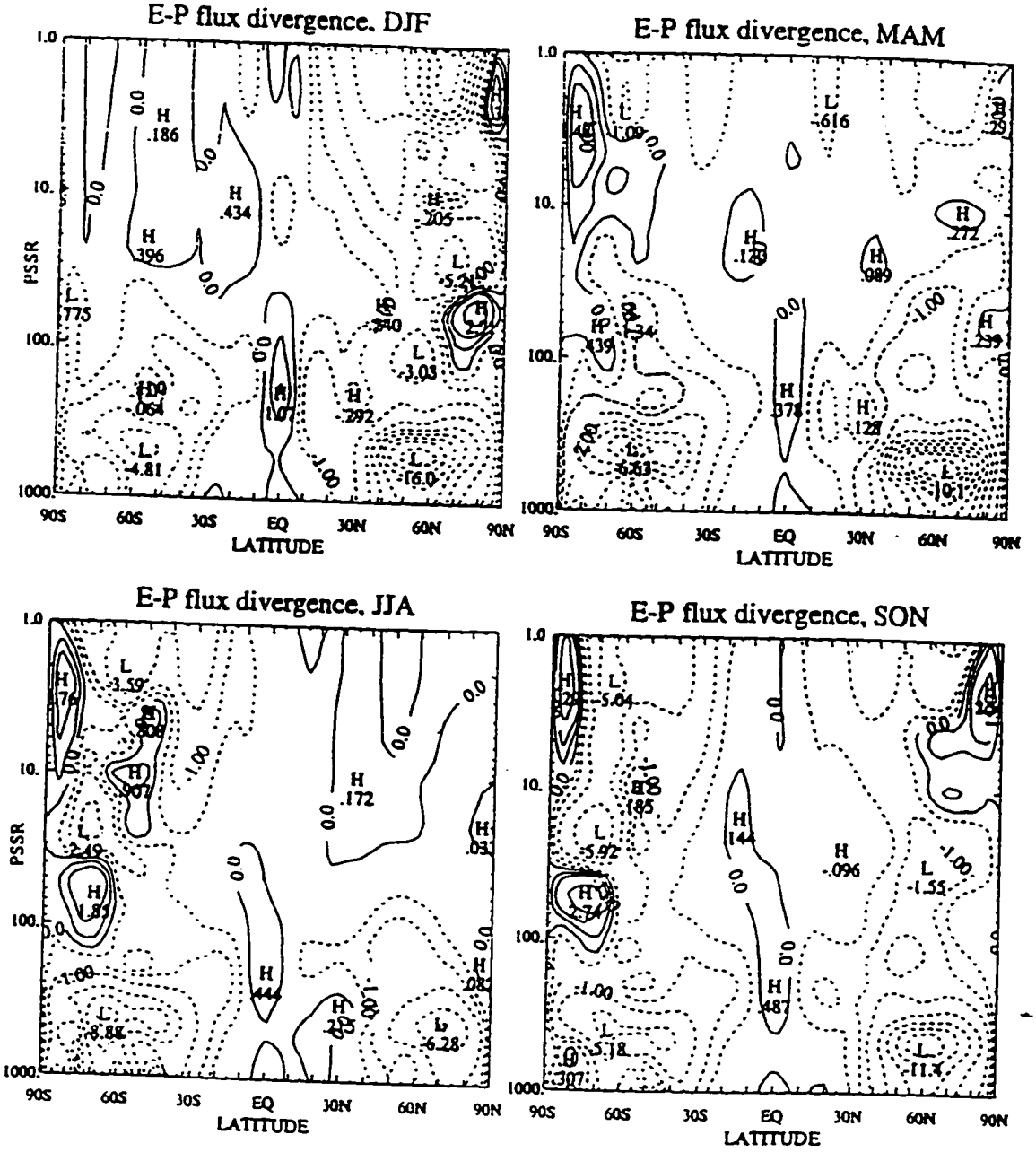

Figure 3.17: E-P flux divergence estimates in units of m/s/day, based on linear wind, temperature and momentum fluxes computed for 1979-89 UKMO geopotential height data. The contour interval is 2 m/s/day with additional contours for ± 1 and ± 0.5 m/s/day (from *Rosenlof, 1994*).

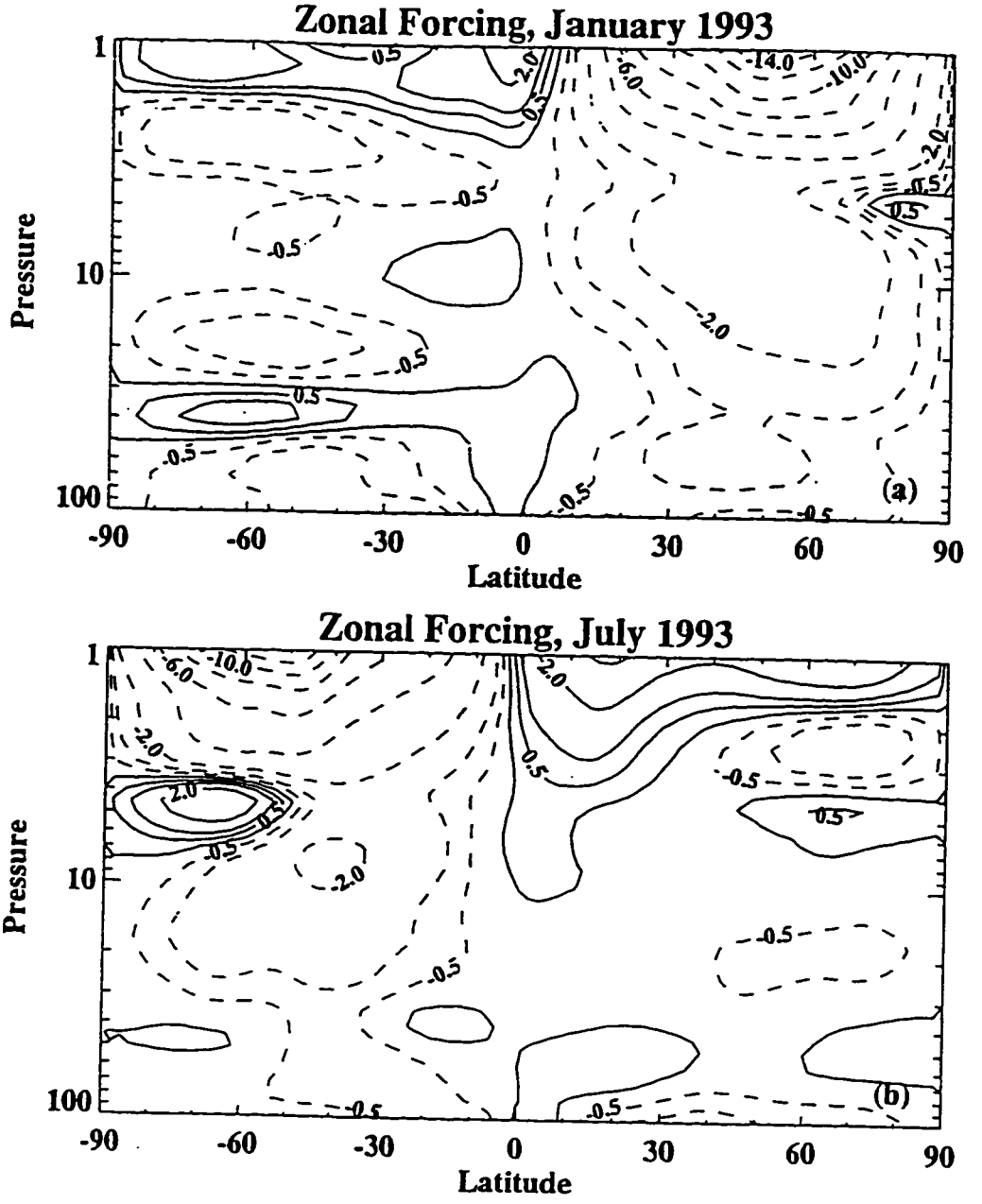

Figure 3.18: Net forcing for the zonal momentum equation computed from radiatively derived residual velocities using UKMO assimilated temperatures for (a) January 1993 and (b) July 1993. Units are m/s/day. The contour interval is 2 m/s/day, with additional contours for ± 1 and ± 0.5 m/s/day (from *Rosenlof, 1994*).

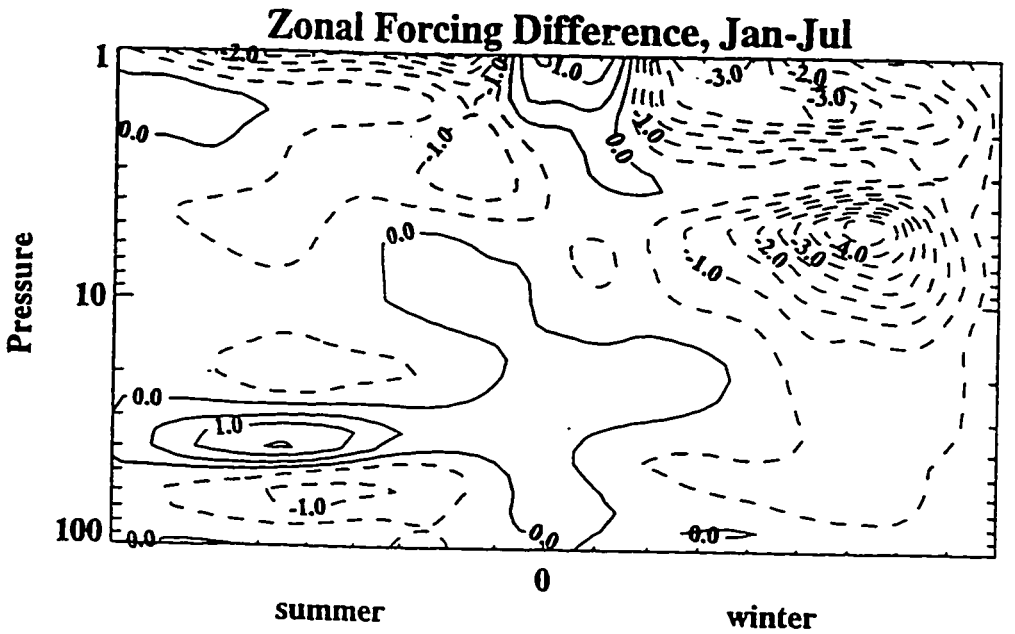

Figure 3.19: Same as in Figure 3.21 but for the January-July difference in the forcing for the zonal momentum equation computed from radiatevely derived residual velocities using UKMO assimilated temperatures (from *Rosenlof, 1994*).

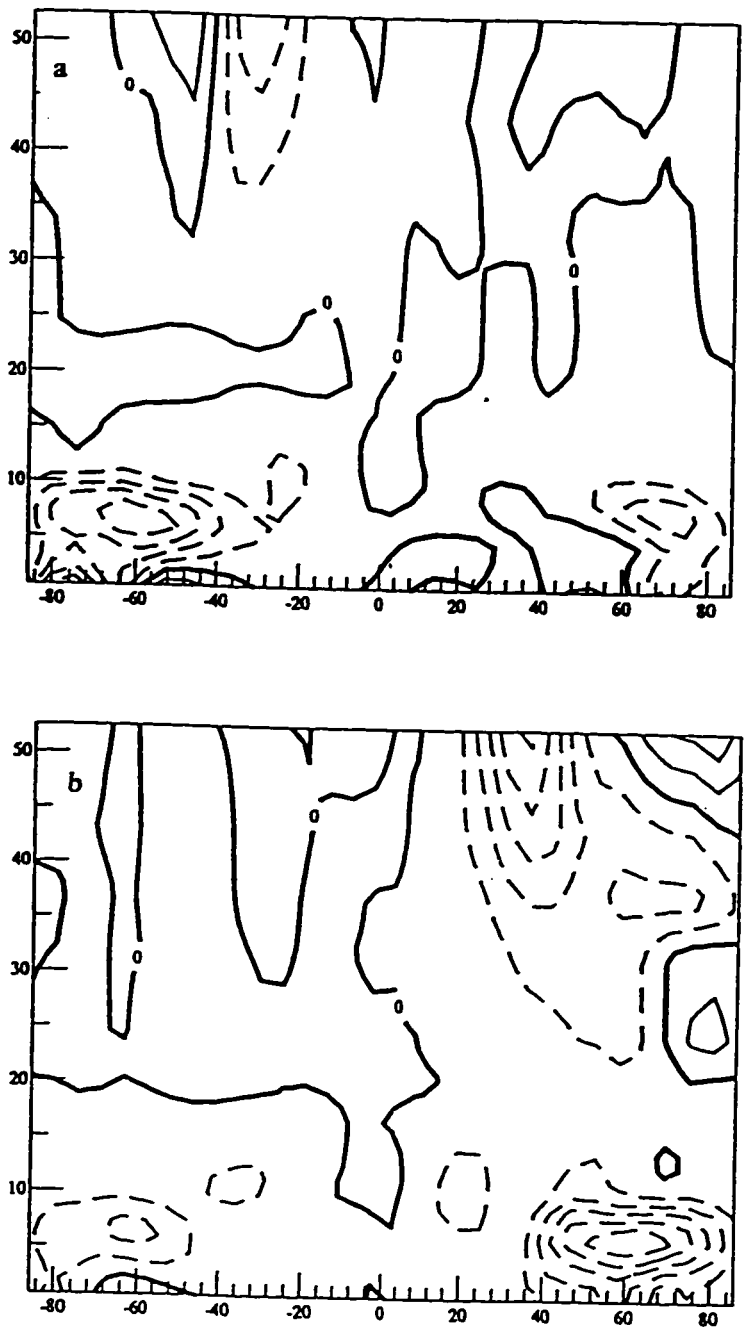

Figure 3.20 Climatological mean E-P flux divergence for (a) July and (b) January in the units m/s/day from the Atlas of the Global circulation statistics derived from the 12 years of NMC operational geopotential height analysis *(Randel, 1992)*. Contour interval 2 m/s/day.

Chapter 4 Description of the Used 2D Zonally Averaged Model

In our previous discussion we reviewed the observations of the large-scale dynamical processes in the tropics on seasonal time scales, and hypothesized that the mean meridional circulation can be explained within the framework of the "non-local" response to zonal forcing. To assess the validity of this approach we will use the 2D zonally averaged model described in this chapter to numerically simulate the dynamics in the region of the tropical tropopause (Chapters 5, 6, and 9). The simulation experiments will focus on the patterns of model response in this region to a range of different external forcing and internal parameters.

In the 2D zonally averaged semi-spectral model developed in the course of this research, the latitudinal dependence is represented by an expansion in Legendre polynomials, and the height dependence is represented by a finite difference grid. The model is based on the TEM equations in the log pressure coordinate system. In order to simulate both tropospheric and stratospheric meteorological processes, the lower boundary was placed at the 1000 mb level, and the upper boundary at the 0.5 mb level. The Chapter starts with an outline of the basic differential equations and boundary conditions. Next, the governing equations for spectral coefficients in the finite difference representation will be written down. Finally, we will discuss the grid-space representation of the various physical processes.

4.1 The Governing Equations

In an ideal situation, in order to study all the physical mechanisms involved in STE, we would like to have a 3D model in an isentropic coordinates formulation, with

fine vertical resolution both in the troposphere and stratosphere. However, it's not computationally feasible to use complex 3D models with fine vertical resolution for experiments that require long runs. In addition, as was discussed in *Yang et al [1990],* the isentropic coordinate system has a disadvantage in the specification of the lower boundary condition for the troposphere, because some isentropes intersect the ground at an angle steeper than isobaric surfaces.

Alternatively, as was discussed in Chapter 2, a 2D TEM model, which is capable of simulating the mass transport in the atmosphere can serve as a useful measure of STE. The 2D models usually use observational data for specifying the external (for the model) parameters. This allows for realistic reproduction of the global dynamical patterns on a seasonal time scale. In addition, observational data are more readily expressed in pressure coordinates, thus allowing for a simpler model, especially in the TEM framework.

Following this reasoning, we constructed a 2D zonally averaged model of the mass transport in the atmosphere. The model is spectral in horizontal direction and has a finite difference representation in vertical. Height is measured in log pressure coordinates. We use the TEM equations in the following form

$$\frac{\partial \bar{U}}{\partial t} - f\bar{v}^* + N.L. = \frac{1}{\rho \cos\varphi}\nabla F + X \tag{4.1}$$

$$\frac{\partial \bar{v}^*}{\partial t} + f\bar{U} + N.L. = -\frac{1}{a}\frac{\partial \bar{\Phi}}{\partial \varphi} \tag{4.2}$$

$$\frac{\partial \bar{\Phi}}{\partial z} = \frac{R\bar{T}}{H} \tag{4.3}$$

$$\frac{1}{a\cos\varphi}\frac{\partial}{\partial\varphi}\left(\bar{v}^{*}\cos\varphi\right)+\frac{1}{\rho}\frac{\partial}{\partial z}\left(\rho\bar{w}^{*}\right)=0 \tag{4.4}$$

$$\frac{\partial\bar{T}}{\partial t}+N.L.+N^{2}\bar{w}^{*}\frac{H}{R}=Q-\frac{R}{HN^{2}}\frac{\bar{T}_{\varphi}}{\rho}\frac{\partial}{\partial z}\rho\overline{v'T'}+\frac{1}{\rho}\frac{\partial}{\partial z}\rho\overline{w'T'} \tag{4.5}$$

Where: φ - latitude,

$z=-H\log(P/P_0)$- log-pressure height,

Ω- the angular velocity of the earth,

R - the gas constant for dry air, a - the radius of the Earth,

$\rho=\rho_0\exp(-z/H)$- basic state density,

$N^2=R/H\left(\frac{dT_0}{dz}+\frac{\kappa T_0}{H}\right)$ - static stability,

$\bar{U}$ -zonal mean velocity,

$\bar{v}^{*}$ - meridional residual velocity,

$\bar{w}^{*}$ - vertical residual velocity,

$\bar{T}$ - zonally averaged temperature,

$\bar{\Phi}$ - geopotential,

$H=\frac{RT_0}{g}$ - equivalent atmospheric depth,

∇F - the E-P flux divergence,

$Q=Q_s+Q_l$ - the total diabatic heating which is the sum of short and long wave components. Long-wave diabatic heating in most experiments is considered to be the Newtonian relaxation to the equilibrium temperature in the form $-\alpha\bar{T}$. The dissipation in the equation for the zonal and meridional velocities is treated as a Rayleigh friction with the coefficient κ_r, which represents the parameterization of

unresolved eddies. *NL* stands for nonlinear terms due to advection by the wind. The following boundary conditions are used:

at the bottom:

$$z = 0:$$

$$\nu \frac{\partial \overline{U}}{\partial z} = C_D \overline{U}$$

$$\nu \frac{\partial \overline{v}^*}{\partial z} = C_D \overline{v}^* \qquad (4.6a)$$

$$\overline{w}^* = \frac{1}{a\cos\varphi} \frac{R}{H} \frac{\partial\left(\overline{v'T'}\cos\varphi / N^2\right)}{\partial\varphi}$$

$$\frac{\partial \overline{T}}{\partial z} = F_r$$

where the drag coefficient C_D is assumed to be equal to 0.005 m s^{-1}.

F_T is a sensible heat flux calculated according to bulk aerodynamic formulae (see *Emanuel, 1991*).

at the top:

$$z = Z_T:$$

$$\frac{\partial \overline{U}}{\partial z} = 0$$

$$\frac{\partial \overline{v}^*}{\partial z} = 0 \qquad (4.6b)$$

$$\overline{w}^* = 0$$

$$\frac{\partial \overline{T}}{\partial z} = 0$$

At the side boundaries:

$$\varphi = \pm \pi/2$$

$$\overline{\psi}^* = 0 \qquad (4.6c)$$

Here $\overline{\psi}^*$ is the TEM stream function that can be defined by

$$\overline{v}^* = -\frac{1}{\rho\cos\varphi}\frac{\partial\overline{\psi}^*\rho}{\partial z}$$
$$\overline{w}^* = \frac{1}{a\cos\varphi}\frac{\partial\overline{\psi}^*}{\partial\varphi} \qquad (4.7)$$

Equation (4.1) is the prognostic equation for zonally averaged zonal velocity, (4.2) - prognostic equation for zonally averaged meridional velocity, (4.5) -prognostic zonal mean thermodynamics equation. The diagnostic equations include the hydrostatic equation (4.3) and the zonal mean continuity equation (4.4).

Let us introduce new variables describing the zonally averaged wind components, temperature and geopotential weighted by $\rho^{1/2}$:

$$\overline{U} = \overline{U}_{initial}\exp(-z/2H)\cos\varphi$$
$$\overline{v}^* = \overline{v}^*_{initial}\exp(-z/2H)\cos\varphi$$
$$\overline{w}^* = \overline{w}^*_{initial}\exp(-z/2H)\cos\varphi \qquad (4.8)$$
$$\overline{T} = \overline{T}_{initial}\exp(-z/2H)\cos\varphi$$
$$\overline{\Phi} = \overline{\Phi}_{initial}\exp(-z/2H)\cos\varphi$$

We used the factor $\exp(-z/H)$ that is proportional to $\rho^{1/2}$, in order to simplify the equations in vertical.

As was already noted, we are going to use a spectral representation in horizontal direction. The application of an efficient spectral transform method (*Bourke, 1972*), that allows quick transformation from grid space into spectral space, requires that we replace the wind components with the corresponding vorticity and divergence as follows

$$\zeta = -\frac{1}{a}\frac{\partial \overline{U}}{\partial \mu} \tag{4.9}$$

$$D = \frac{1}{a}\frac{\partial \overline{v}^*}{\partial \mu} \tag{4.10}$$

For the same reason we'll use $\sin\varphi = \mu$ as a horizontal coordinate. Thus the horizontal derivative transforms into:

$$\frac{1}{a}\frac{\partial}{\partial \varphi} = \frac{\sqrt{1-\mu^2}}{a}\frac{\partial}{\partial \mu} \tag{4.11}$$

Substituting (4.8) - (4.11) into (4.1) - (4.5), we obtain a new set of equations in the following form:

$$\begin{aligned}
&\frac{\partial \zeta}{\partial t} = -\frac{1}{a}2\Omega\frac{\partial}{\partial \mu}\left(\overline{v}^*\mu\right) - \frac{1}{a}\frac{\partial}{\partial \mu}\frac{1}{\rho a\cos\varphi}\nabla F - \kappa_r\zeta + NL1\\
&\frac{\partial D}{\partial t} = -\frac{1}{a}2\Omega\frac{\partial}{\partial \mu}\left(\overline{U}\mu\right) - \frac{1}{a^2}\frac{\partial}{\partial \mu}\left(1-\mu^2\right)\frac{\partial \Phi}{\partial \mu} - \kappa_r D + NL2\\
&\left(\frac{\partial}{\partial z} - \frac{1}{2H}\right)\overline{w}^* + D = 0\\
&\frac{\partial}{\partial t}\left(\frac{\partial}{\partial z} + \frac{1}{2H}\right)\overline{\Phi} + N^2\overline{w}^* = Q_{new} - \alpha\left(\frac{\partial}{\partial z} + \frac{1}{2H}\right)\overline{\Phi} + NL3
\end{aligned} \tag{4.12}$$

where the nonlinear terms are:

$$NL1 = e^{z/2H}\frac{1}{a}\frac{\partial}{\partial\mu}\left[\frac{\overline{v}^{\bullet}}{a}\frac{\partial\overline{U}}{\partial\mu}+\overline{w}^{\bullet}\left(\frac{\partial}{\partial z}+\frac{1}{2H}\right)\overline{U}\right]$$

$$NL2 = -e^{z/2H}\frac{1}{a}\frac{\partial}{\partial\mu}\left[\frac{\overline{U}^{2}}{a}\frac{\mu}{\sqrt{1-\mu^{2}}}\right] \qquad (4.13)$$

$$NL3 = -e^{z/2H}\left[\frac{\overline{v}^{\bullet}}{a}\frac{\partial\left(\frac{\partial}{\partial z}+\frac{1}{2H}\right)\overline{\Phi}}{\partial\mu}+\overline{w}^{\bullet}\left(\frac{\partial}{\partial z}+\frac{1}{2H}\right)\left(\frac{\partial}{\partial z}+\frac{1}{2H}\right)\overline{\Phi}\right]$$

Equations (4.12) together with the boundary conditions (4.6a,b), represent the core of our 2D model.

4.2 The Vertical Representation

The primary goal of the model is to study the circulation in both stratosphere and troposphere simultaneously. Thus, we have chosen to use log pressure coordinate in vertical direction.

To minimize truncation errors the grid points in vertical dimension are staggered as shown in Fig 4.1. Notation Z_k will indicate that an arbitrary variable Z is evaluated at the full pressure level P_k, k=1,...kx. Similarly, $Z_{k+1/2}$ is evaluated at the half level $P_{k+1/2}$. Variables $\overline{U},\overline{v}^{\bullet},\overline{\Phi}$ as well as ζ and D are evaluated at full levels, while $\overline{T},\overline{w}^{\bullet}$ are evaluated at half levels. The lowest level of the domain $P_{1/2}$ is placed at 1000 mb, the position of the top boundary depends upon the goal of the individual experiment and lies either near the tropical tropopause (for the tropospheric experiments) or in the mesosphere. In the current version of the model we have 41 equidistant levels. However, the model can be easily extended to allow for layers of varying width.

4.3 The Spectral Representation

The scalar variables $\zeta, D, \overline{T}, \overline{\Phi}$ as well as $\overline{U}, \overline{v}^*, \overline{w}^*$ are expanded in series of Legendre polynomials. The choice of Legendre polynomials was determined by the following factors.

1. Legendre Polynomials are orthogonal and they are the eigensolution of the Helmholtz equation

$$\frac{\partial}{\partial \mu}\left(1-\mu^2\right)\frac{\partial P_n(\mu)}{\partial \mu} + n(n-1)P_n(\mu) = 0 \tag{4.14}$$

As will be shown later, this kind of differential operator is involved on the left-hand side of the partial differential equation for $\overline{w}^*$.

2. They satisfy proper boundary conditions and have continuous derivatives up to the second order at the poles. In our case, the assumption of smoothness of the true solution at any point, and, particularly, at the poles, is automatically satisfied.

In the subspace of these polynomials, an arbitrary variable $Z(\mu, z, t)$ can be expanded as:

$$Z = \sum_{n=1}^{NX} Z_n(z,t)P_n(\mu) \tag{4.15}$$

where $P_n(\mu)$ is the Legendre polynomial of degree n. $P_n(\mu)$ are normalized i.e.

$$\frac{1}{2}\int_{-1}^{1} P_n^2 d\mu = 1 \tag{4.16}$$

In addition to (4.14) Legendre Polynomials have the following properties :

$$-(1-\mu^2)\frac{\partial P_n}{\partial \mu} = (n-1)\varepsilon_{n+1}P_{n+1} - n\varepsilon_n P_{n-1} \tag{4.17}$$

where $\varepsilon_n = \dfrac{n-1}{\sqrt{4(n-1)^2-1}}$

$$\mu P_n = \varepsilon_{n+1} P_{n+1} + \varepsilon_n P_{n-1} \tag{4.18}$$

These properties allow us to efficiently compute the spectral coefficients of $\overline{U}$ and $\overline{v}^{\bullet}$ from the spectral coefficient of ζ and D and vice versa.

$$\begin{aligned} \zeta_n &= \frac{1}{a}\left[n\varepsilon_n \overline{U}_{n-1} - (n-1)\varepsilon_{n+1}\overline{U}_{n+1}\right] \\ D_n &= \frac{1}{a}\left[-n\varepsilon_n \overline{v}^{*}_{n-1} - (n-1)\varepsilon_{n+1}\overline{v}^{*}_{n+1}\right] \end{aligned} \tag{4.19}$$

The procedure for transforming of the partial differential equations into the spectral domain is as follows. Let's consider a partial differential equation

$$\partial Z / \partial t = L + N \tag{4.20}$$

Here, Z is a prognostic variable whose spectral coefficients Z_n are known at time t. The linear terms are each evaluated in the spectral domain, and L denotes their sum. Linear differential operators do not present any difficulty due to the properties of Legendre Polynomials mentioned above. The nonlinear terms whose sum is denoted by N, are evaluated by the transform method (*Bourke, 1972*):

- The spectral coefficients of all the variables are transformed onto a Gaussian latitude grid.
- Nonlinear dynamical and physical process terms in each prognostic equation can now be calculated at every latitude grid point

- The appropriate nonlinear terms are transformed back to the spectral domain by inverse Legendre transformations.

After that, by substituting the spectral expansions of Z, L and N into the original partial differential equation we obtain the residual, or the error of approximation that depends upon the chosen truncation:

$$R = \partial / \partial t \sum_{1}^{NX} Z_n - \sum_{1}^{NX} L_n - \sum_{1}^{NX} N_n \qquad (4.21)$$

where NX is the number of the harmonics.

The requirement to minimize the mean square integral of the residual (4.21) at the solution gives the resulting space truncated equations in the form:

$$\partial Z_n / \partial t = L_n + N_n \qquad (4.22)$$

Practical realization of this method implies the substitution of the spectral expansions of Z, L and N into the partial differential equation (4.20), multiplication by P_n and integration over the globe applying the orthogonality property.

The above procedure was performed on the set of equations (4.12), thus transforming them to a set of equations for spectral coefficients. The only derivative left in an analytical form was the time derivative. For time differencing we chose the semi-implicit method described below.

4.4 Time Differencing Scheme

A leapfrog semi-implicit time differencing scheme is used to approximate the time

derivatives on the left-hand side of the spectral equations. The scheme can be written as

$$Z(t+\Delta t) = Z(t-\Delta t) + 2\Delta t F(Z(t)) \tag{4.23}$$

Let's examine the amplitude and phase-speed errors caused by the scheme. If a leap-frog scheme is applied to the oscillation equation in the form

$$\frac{\partial Z}{\partial t} = i\kappa Z \tag{4.24}.$$

the solution is:

$$Z(t_0+\Delta t) = e^{ik\Delta t} Z(t_0) \equiv AZ(t_0) \tag{4.25}.$$

The amplification factor A is constant from one time step to the next, and satisfies the quadratic equation:

$$A^2 - 2ik\Delta t A - 1 = 0 \tag{4.26}$$

The two roots are:

$$A_{\pm} = ik\Delta t \pm (1 - k^2\Delta t^2)^{1/2} \tag{4.27}$$

Thus, in the limit of a good numerical resolution, $A_+ \to 1$, and $A_- \to 1$.

Evidently, the numerical solution has two different modes: the physical mode corresponding to A_+ and the computational mode associated with A_-. The computational mode is an artifact of the numerical representation. Both modes are stable and neutral for the case $|k\Delta t| < 1$. When modeling more general nonlinear systems, however, the leapfrog computational mode can grow slowly and at some point it can dominate the solution. This problem can be avoided by filtering the high-frequency components of the numerical solution. To all the prognostic variables we applied the Robert time filter in the form :

$$Z_f(t) = (1-2\alpha)Z(t) + \alpha\left[Z(t+\Delta t) + Z_f(t-\Delta t)\right] \tag{4.28}$$

We chose, $\alpha = 0.03$ so that low frequency modes are only slightly damped. All the reasoning above allows us to write down the final version of the model equations which we are going to solve numerically.

4.5 Numerical Equations for the Spectral Coefficients

The prognostic vorticity equation:

$$\frac{\zeta_{k,n}^{\tau+1} - \zeta_{k,n}^{\tau-1}}{\Delta t} = -2\Omega\left[\varepsilon_n \frac{n}{n-1} D_{k,n-1}^{\tau} + \varepsilon_{n+1} \frac{n-1}{n} D_{k,n+1}^{\tau}\right] - \kappa_r \zeta_{kn}^{\tau-1} + (NL)_{kn}^{\tau} \tag{4.29}$$

The prognostic divergence equation after some manipulation was rewritten as an elliptic equation for $\overline{w}^*$ (compare with (2.9))

$$\begin{aligned} &-\left[\frac{\overline{w}^{*\tau+1}_{k+1,n} - 2\overline{w}^{*\tau+1}_{k,n} + \overline{w}^{*\tau+1}_{k-1,n}}{\Delta z^2} - \frac{\overline{w}^{*\tau+1}_{k+1,n} + 2\overline{w}^{*\tau+1}_{k,n} - \overline{w}^{*\tau+1}_{k-1,n}}{16H^2}\right] + \\ &\frac{N^2\Delta t^2}{4a^2} n(n-1)\overline{w}^{*\tau+1}_{k,n} = \delta_z D_{k,n}^{\tau-1} + \frac{n(n-1)}{a^2}\Delta t \delta_z \Phi_{k,n}^{\tau-1} - \\ &\frac{N^2\Delta t^2}{4a^2} n(n-1)\overline{w}^{*\tau-1}_{k,n} + \frac{n(n-1)}{2a^2}\Delta t^2\left[Q_{k,n}^{\tau} - \alpha\delta_z \Phi_{k,n}^{\tau-1}\right] + \\ &2\Omega\Delta t\left[\varepsilon_n \frac{n}{n-1}\delta_z \zeta_{k,n-1}^{\tau} + \varepsilon_{n+1}\frac{n-1}{n}\delta_z \zeta_{k,n+1}^{\tau}\right] - \\ &\kappa_r \Delta t \delta_z D_{k,n}^{\tau-1} + (NL)_{k,n}^{\tau} \end{aligned} \tag{4.30}$$

The continuity equation:

$$\delta_z D^{\tau+1}_{k,n} = -\left[\frac{\overline{w}^{*\tau+1}_{k+1,n} - 2\overline{w}^{*\tau+1}_{k,n} + \overline{w}^{*\tau+1}_{k-1,n}}{\Delta z^2} - \frac{\overline{w}^{*\tau+1}_{k+1,n} + 2\overline{w}^{*\tau+1}_{k,n} + \overline{w}^{*\tau+1}_{k-1,n}}{16H^2} \right] \tag{4.31}$$

and the thermodynamic energy equation:

$$\frac{\delta_z \Phi^{\tau+1}_{k,n} - \delta_z \Phi^{\tau-1}_{k,n}}{\Delta t} = -N^2 \frac{\overline{w}^{*\tau+1}_{k,n} + \overline{w}^{*\tau-1}_{k,n}}{2} + Q^{\tau}_{k,n} - \alpha \delta_z \Phi^{\tau-1}_{k,n} + (NL)^{\tau}_{k,n} \tag{4.32}$$

where:

- Δt stands for two time steps if we use the leap-frog time differencing scheme, and for a single time step if we initialize our computations with the explicit scheme;
- $\delta_z Z$ represents the finite difference analogue of $(\partial/\partial z + 1/H)Z$;
- NL represents the sum of the non-linear terms. As was discussed in 4.3, these terms are evaluated in the physical space, and then transformed into the spectral domain.

It should be noted that all the prognostic equations except for the equation for $\overline{w}^*$ (equation (4.30)) are explicit. Thus, at every time step we have to invert only one operator, which results in considerable computational savings.

4.6 Grid Point Physical Processes

We included the following grid-point physical processes into our model:

- Horizontal diffusion, some form of vertical diffusion, long and short wave

radiation, and a parameterization of the eddy-induced zonal forcing.

- In addition to Rayleigh friction which represents the effect of nonresolved eddies, we included a fourth order horizontal diffusion primarily for computational stability and because of its scale selectivity (*Gordon and Stern, 1982*). Inclusion of the tendency term into the equation for the residual meridional velocity introduces the possibility of symmetric equatorial inertial instability (*Dunkerton 1988*). To deal with this problem, we included a 4^{th} order vertical dissipation term into the equations for the zonal and meridional winds.
- We considered the surface boundary layer beneath the first level of the model to be governed by bulk aerodynamic drag laws.
- Long wave radiative cooling is considered to mimic the process of relaxation to the equilibrium temperature determined by a short-wave radiative heating and cumulus convection. The relaxation time scale depends upon the height and is treated as constant in the troposphere.
- The version of the model we are describing now does not include the a hydrologic cycle. As will be shown in Chapter 7, the inclusion of moist convection explicitly may be crucial for understanding the dynamics of the tropical troposphere.

The next three chapters present a series of experiments that were made with this model in order to describe and understand the dynamical processes in the region of the tropical tropopause. The results are compared with those from the previous models, and suggestions are made for improving existing models.

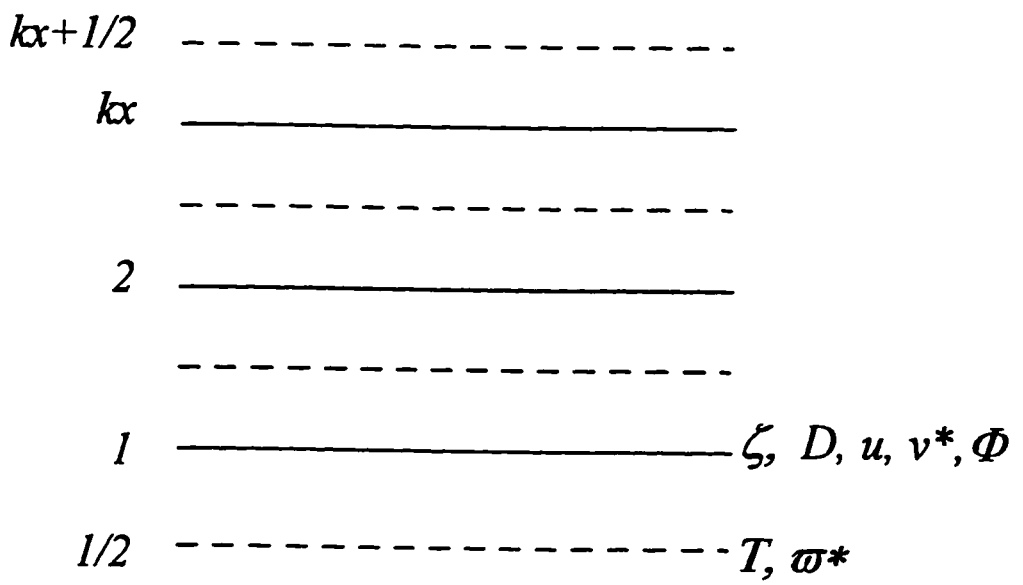

Figure 4.1 A vertical section of the model grid in log-pressure coordinates.

Chapter 5 Mean Meridional Circulations in the Stratosphere.

As was concluded in Chapter 3, atmospheric dynamics in the region of the tropical tropopause requires an understanding of both stratospheric and tropospheric circulations.

This chapter examines the stratospheric components of the dynamics of the region of the tropical tropopause, while the next one focuses on the tropical tropospheric circulation.

In this chapter we attempt to explain the circulation in the tropical lower stratosphere based on experiments with our 2D zonally averaged model. The previous prognostic 2D models used for simulation of the observed patterns will be discussed. Then we'll proceed with the application of our model to the problem described above.

5.1 The Meridional Circulation in the Stratosphere Derived from 2D Prognostic Models

There are several kinds of 2D models designed to simulate the observed features of the meridional circulation. All of them are based on the simple, well known property of rotating, stratified fluid that in a balanced, axisymmetric flow an external forcing excites a mean meridional circulation. This circulation is required to maintain the balance, and, generally, it opposes the forcing. The induced circulation then has a twofold effect, locally reducing the impact of the forcing, and causing a non-local response outside the source region in such a way as to maintain thermal wind balance everywhere. The classic illustration was provided by *Eliassen [1951]* who derived an elliptic equation for the meridional streamfunction in the form:

$$\nabla^2\psi = \frac{\partial F}{\partial z} + \frac{\partial Q}{\partial y} \tag{5.1}$$

where F and Q are appropriately normalized measures of the "body force" and diabatic heating (compare to equation 2.9). Eliassen discussed the qualitative aspects of the structure of the mean meridional circulation including the differences between mechanically forced and thermally forced circulation. However, several important questions remained to be clarified. One of the most important: what determines the scale and type of response to any given forcing? Recently, a number of 2D models have produced interesting results regarding this question. These models, with their main results and drawbacks, are briefly described below.

A model proposed by *Plumb [1982]* focused on the structure of the mean meridional circulation driven by realistic steady, zonally symmetric thermal or mechanical forcing. Plumb used the techniques of a tidal theory. Within this theory, the solution of a steady version of elliptic equation for $\overline{w}^*$ (eq.2.9) is obtained as an expansion of Hough functions. These functions are the eigenvectors of Laplace's tidal equation for a given frequency and zonal wave number (both assumed to be zero, i.e. Plumb considered the zonally symmetric stationary case). The form of these elliptic functions and their eigenvalues or "equivalent depths", which determine the corresponding vertical structure, allowed him to investigate the structure of the forced meridional circulation. Plumb showed how the position of the heating in the meridional plane affects the extent of the meridional circulation. The response to heating in the vicinity of the equator is largely confined to the tropics, but heating at middle and high latitudes drives a global circulation, often extending into the opposite hemisphere. He noted that on the seasonal time scales the primary forcing of the residual meridional circulation is mechanical via the Eliassen-Palm flux convergence.

This mechanical forcing appears in the right hand side of the elliptic equation (5.1) in the form of a vertical derivative. Thus, a localized zonal force is equivalent to a dipole in vertical thermal forcing, resulting in a circulation that has a dipole structure in vertical. At the same time, the latitudinal structure consists of a single cell elongated into the other hemisphere. Plumb concentrated mainly on the response to a localized thermal forcing and noted that the downward penetration of this response is inefficient.

Following Plumb's work, *Dunkerton [1989]* analyzed the response to a mechanical forcing localized in high and mid-latitudes.

He argued that the streamfunction amplitudes are larger below a shallow source than above, exactly what we would expect from the downward control principle.

The studies of Eliassen, Plumb and Dunkerton provided many useful insights into the processes controlling the mean meridional circulation. However, an important question not addressed in their works is the description of the adjustment of the atmosphere to externally imposed forcing. When a stratified, rotating atmosphere in quasi-geostrophic equilibrium is subject to external forcing, it can adjust to such forcing by a change in its zonally averaged temperature and wind structure, or through the mean meridional circulation.

The following types of adjustment are possible in the above described atmosphere:

- Thermodynamic heating can be balanced by infrared relaxation or by adiabatic cooling (heating) by upward (downward) motion.
- The momentum budget can adjust by means of frictional dissipation of zonal momentum or through the acceleration produced by the Coriolis torque.

The nature of these adjustment processes is crucial for understanding the response of the stratosphere to perturbations in external forcing. Addressing these issues, *Garcia [1987]* generalized Plumb's model by including, in addition to body forces, mechanical and thermal dissipation with different characteristic time scales. With this extension, he, like Plumb, used a zonally-averaged, quasi-geostrophic model to illustrate how the adjustment of the middle atmosphere to externally imposed forcing depends on the internal dissipative properties of the atmosphere and the period of the forcing.

For a slowly varying forcing the strength of the mean meridional circulation was shown to depend on the ratio κ_r/α. For small values of this ratio, it is mainly the mechanical forcing , i.e. the E-P flux divergence, that drives the circulation. In this case, most of the response to shortwave heating occurs through long-wave cooling so that the temperature structure of the atmosphere remains close to radiative equilibrium. If $\kappa_r/\alpha >> 1$ the heating is very efficient, and the adjustment takes place through the mean meridional circulation. These results are consistent with the analytical results discussed in 2.2

Throughout most of the stratosphere the ratio κ_r/α is quite small. So, Garcia argued that on the seasonal time scale a net E-P flux divergence of up to 3m/s/day, produces meridional circulation comparable to that produced by ozone heating. This mechanical forcing, centered in the midlatitudes of the winter hemisphere, drives a circulation that extends into the summer hemisphere. The meridional circulation warms high latitudes and cools the tropics in the lower stratosphere.

However, at the same time, Garcia showed that near the tropopause the meridional circulation induced by the tropospheric, seasonally varying diabatic heating

is comparable in magnitude to the circulation induced by the E-P flux divergence in the stratosphere. This similarity makes it important to consider the tropospheric circulation when describing the dynamics in the region of the tropical tropopause.

Putting all these results together, *Dunkerton [1989]* noted that the generalized body force circulation problem (*Eliassen, 1951*) should include the following effects:

- spherical geometry
- atmospheric compressibility
- mechanical friction
- Newtonian cooling
- additional feedback effects, like, radiative-dynamical coupling, and interaction between the cumulus convection and the dynamics.

These models of meridional circulation in the stratosphere are linear. Thus, they are not suitable for studying the circulation in the tropics where there exists a positive feedback between the nonlinear advection of the angular momentum and the forcing (see 2.3). Therefore, 2D nonlinear models have to be used to study the dynamics in this region.

Dunkerton [1989] was the first to apply a nonlinear 2D model to the problem of simulation of the meridional circulation of the middle atmosphere. He extended the nearly inviscid nonlinear theory of the Hadley circulation driven by a symmetric heating (*Held and Hou, 1980)* to the region of the tropical stratosphere characterized by the asymmetric radiative heating. The Hadley circulation induced under these conditions conserves angular momentum *(Schneider 1977)*. Thus, Dunkerton argued that the inclusion of the nonlinear advection in the angular momentum equation is critical for obtaining a strong meridional circulation in the tropical stratosphere during

the solstice periods. The main results derived from his model are as follows:

- The semi-realistic height dependent thermal relaxation rate causes the splitting of the Hadley circulation driven by the asymmetric heating into two components: tropospheric and stratospheric

- The meridional circulation in the stratosphere consists of one cell, with rising in the summer hemisphere and descending into the winter hemisphere.

- The lines of the mass streamfunction in the steady state in the stratosphere are parallel to the constant angular momentum surfaces (in the inviscid steady state) and are symmetric about the equator.

- The simulated circulation was still weaker than the observed one (*Solomon et al, 1986*). However, the horizontal advection of the angular momentum was sensitive to the wave-induced forcing. The addition of a wintertime extratropical eddy forcing enhances the circulation and extends it into the winter hemisphere. Thus, the mean meridional circulation in the stratosphere in his model may be thought of as a hybrid Hadley/wave-induced circulation driven by radiative heating and E-P flux convergence in extratropics.

Dunkerton's work, however, did not clarify the comparative role of the thermal and mechanical forcing in inducing the residual mean meridional circulation in the tropical lower troposphere. Specifically, the remaining question could be posed as

follows: "under what conditions does the meridional circulation in the tropical stratosphere behave like Hadley circulation induced by asymmetric thermal forcing and when is it mostly non-locally controlled by the extratropical wave-induced forcing?" This question will be discussed below based on the results of a set of experiments with our 2D model.

5.2 Some Features of the Meridional Circulation in the Stratosphere Derived from our 2D Model

The results discussed above and the yet unresolved problems of 2D prognostic modeling of the stratospheric meridional circulation inspired us to apply our model (see Chapter 4) to studying the dynamics in the tropical stratosphere. The model can be considered an extension of the *Dunkerton's [1989]* model because of the following features:

- The meridional velocity equation now contains nonlinear terms as well as the tendency term (the role of the tendency term near the equator has not been studied yet and should be explored further, especially in the tropical region).
- The model is spectral (in comparison with the finite difference model used by Dunkerton) and so we do not bring in additional horizontal dissipation due to the first and second order spatial differentiations.
- N^2 varies both with latitude and height.

All these improvements allowed us to simulate a dynamical response in the tropical region to a realistically specified forcing. We focused on three major issues dealing with the circulation in response to forcing.

1. The first question we addressed was: What determines the type of adjustment

of the stratospheric dynamics to the external forces?

To answer this question we examined the response in the stratosphere first, to externally specified heating and, second, to wave-induced zonal forcing. In the first case, as was discussed in 2.2, the long-wave part of heating (in Newtonian cooling representation $-\alpha\overline{T}$) depends upon the temperature and, hence, upon the dynamics itself. It follows, that this part of the diabatic heating can not be specified externally. The externally specified short-wave radiative heating in K/day is shown in Fig. 5.1 (a). It is asymmetric about the equator and approximately corresponds to that at the time of the Southern hemisphere summer solstice.

Fig 5.1 (b) shows the lines of the streamfunction of the response to this heating. The following parameters are used:

- the radiative relaxation time is 10 days
- the dynamical dissipation time is 5 days
- thus, the ratio $\kappa_r/\alpha = 2$

The contour interval for the streamlines is 200 m^2/s , the maximum corresponds to 1.8e3 m^2/s. The circulation is deep and broad. The response to the same forcing but in an atmosphere with a smaller dynamical dissipation ($\kappa_r/\alpha = 0.2$) is shown on Fig. 5.1 (c). In comparison with the previous result, the circulation is less than half as strong. It is also shallower and not so broad in the latitudinal direction.

The corresponding zonal velocity fields are shown on Fig 5.1 (d) and (e). The wind for the case $\kappa_r/\alpha = 0.2$ (e) is very strong in comparison with $\kappa_r/\alpha = 2$ (d). In addition, for the case when $\kappa_r/\alpha = 2$, the wind decays more rapidly with height, which leads to greater departures from radiative equilibrium in the temperature field.

We consider next the steady-state response to the dynamical forcing, exemplified

by the divergence of the E-P flux of the planetary waves.

The simple pattern of the E-P flux divergence is specified as shown on Fig. 5.2 (a). This corresponds to mean flow acceleration of about 3m/s/day centered at 35 km and 60°N. As in the previous experiment, the streamfunction is shown for two different cases: first, $\kappa_r/\alpha = 2$ (Fig. 5.2b) and second, $\kappa_r/\alpha = 0.2$ (Fig. 5.2c). The response in the second case is stronger and much deeper than for the atmosphere with strong dissipation. The corresponding zonal velocity fields are shown on Fig. 5.2 (d) and (e).

The mass streamfunction distribution produced by the combined effect of thermal and mechanical forcing specified above is shown in Fig. 5.3:

- Fig. 5.3 (a) corresponds to the case with large mechanical dissipation ($\kappa_r/\alpha = 2$). The response in this case extends well into the summer hemisphere due to the important role of the heating.
- As shown in Fig. 5.3 (b), the response in the atmosphere with $\kappa_r/\alpha = 0.2$ differs significantly from that described above. The induced flow is nearly totally downward with the streamlines parallel to the latitude lines. It is also nearly twice as strong. In accordance with the previously discussed downward control principle, in this case there is no appreciable model response in the meridional circulation in tropics.

2. The second question that we investigated with the model was : "How does the response to the remote zonal forcing in the tropics depend upon the location, strength and period of oscillation of the forcing?"

To answer this question, we examined the response dependence on the latitude of

the location of the forcing, and its time period. The amplitude of the forcing was normalized by the cosine of latitude so, when integrated over the domain, total forcing value would be the same for all regions.

Fig. 5.4 shows a response to a steady forcing located at 35km and at 60°N. The dashed lines show the location and pattern of the forcing. The contour interval is $5m^2/s/day$, the maximum value is 10 $m^2/s/day$. The contour interval for the mass streamfunction is 10 kg/m/s. The response, shown in Fig. 5.4, is a classic illustration of the downward control principle (see 2.2). The streamfunction lines away from the forcing are lines of constant latitude. The streamfunction at any location is controlled by the distribution of wave-induced forcing. Thus, the forcing located at high and mid - latitudes does not influence the tropical regions.

For a non-steady forcing the model response changes significantly. Fig. 5.5 shows the response to forcing with a 360 day period of oscillation located at 60°N. The dashed lines show the location and pattern of the forcing. The contour intervals are the same as in Fig. 5.4. The streamlines penetrate into the summer hemisphere and the zero line is located at around 15°S. To estimate the response in tropics we integrated the mass flux over the tropical tropopause region (at 100 Pa and from 20S° to 20N°). The resulting mass flux is 2.2×10^{15} (kg m/s).

The response to the same forcing, but located at 40°N, is shown in Fig 5.6. The dashed lines indicate the location and pattern of the forcing. The contour intervals are the same as in Fig. 5.4. The estimated mass flux integrated over the tropics in this case is 6.6×10^{15} (kg m/s). This mass flux is only three times larger than for the forcing located at 60° N. This comparison reveals a clear response in the region of the tropical tropopause to the forcing located as high as at 60°N and oscillating with a seasonal

time scale.

3. The third question we addressed was: "To what extent does the radiative stratospheric heating determine the dynamics in the tropical stratosphere?"

To investigate the role of heating in a simple manner we assumed the following:

- the radiative equilibrium temperature is proportional to the first Legendre polynomial. $T_{rad} = T_0\mu$;
- the thermal relaxation rate depends on height and is shown on Fig. 5.7
- the ratio $\kappa_r/\alpha = 0.1$

The streamfunction of the response is shown at Fig. 5.8 with the contour interval of 100 m^2/s. As shown in the picture, the circulation in the stratosphere is antisymmetric about the equator, the air rises in the summer hemisphere and descends in the winter hemisphere. Thus, this mechanism tends to oppose the upward motion in the winter tropical lower stratosphere caused by the remote eddy-induced forcing.

These results represent a preliminary outcome of the "Hadley cell" approach (i.e, an approach to the mean meridional circulation in the stratosphere as a circulation induced by some local diabatic heating) and its potential for explanation of the observed meridional circulation in the tropical lower stratosphere. At this point we can state, that the behavior of this induced meridional circulation depends, to a large extent, upon the externally specified radiative equilibrium temperature. To deal with this problem we should include a radiation module that computes realistic long and short-wave heating/cooling rates as dependent upon the distribution of radiatively active constituents and temperature, which, in their turn, are determined by the atmospheric dynamics.

Summarizing the experiments described above, our results (as was expected from the analytical discussion) showed that the meridional circulation in the tropical stratosphere is strongly influenced by the wave-induced forcing in the middle and high latitudes. The strength and scale of the response depend upon the location of the eddy-induced forcing and its variations in time. Thus, further experiments should take into account the realistic time dependence of the eddy-induced forcing.

The next chapter deals with the meridional circulation in the tropical troposphere. The same set of questions: "Under what conditions does the meridional circulation in the tropical troposphere behave like the Hadley circulation determined by the local heating, and when is it mostly non-locally controlled by the extratropical wave-induced forcing?" will form the core of our discussion.

a

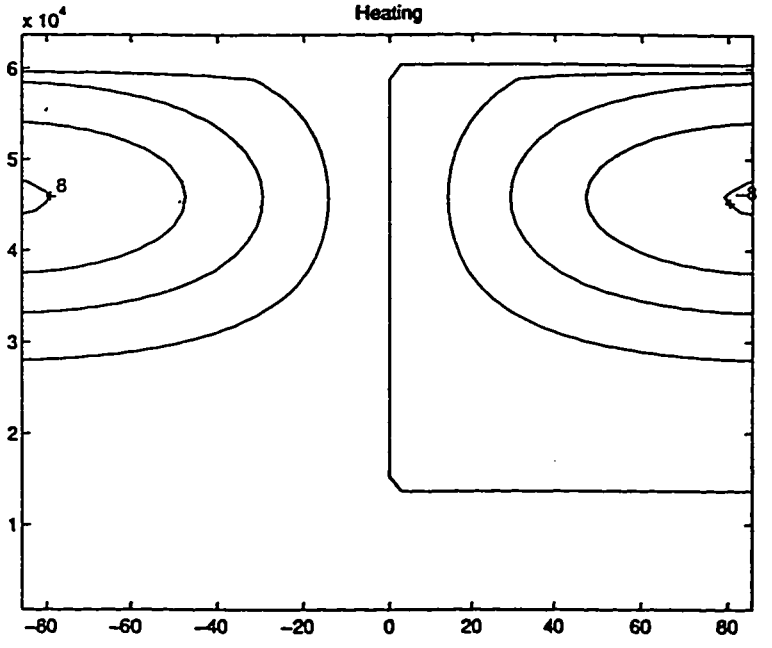

b

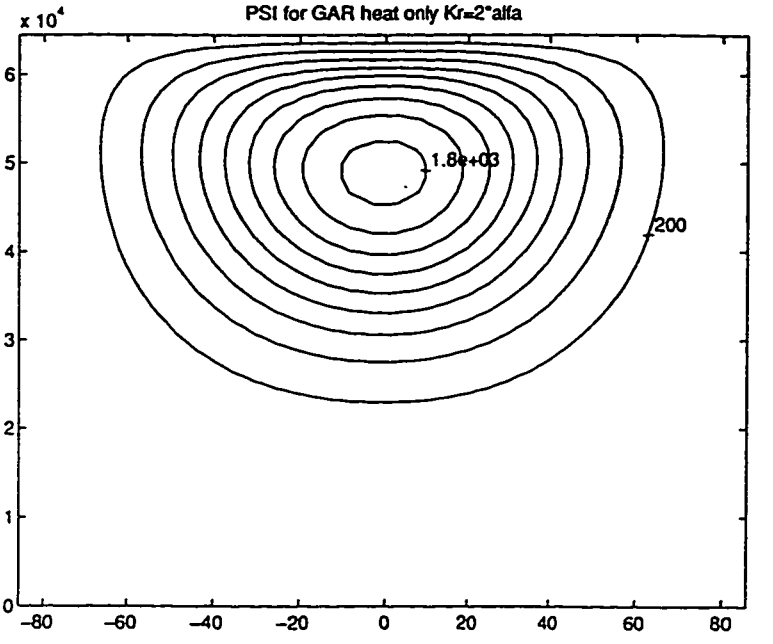

Figure 5.1: (a) Externally specified short-wave radiative heating in K/day; Contour interval is 2K/day; (b) The contours of the streamfunction of the response to the specified in (a) heating for $\kappa_r/\alpha = 2$. The contour interval for the streamlines is 200 m^2/s , the maximum corresponds to 1.8×10^3 m^2/s.

c

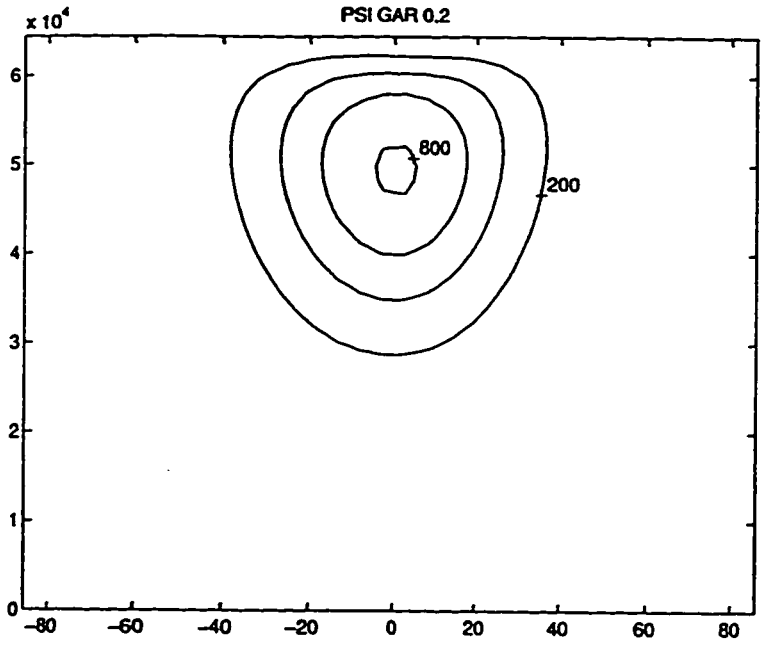

d

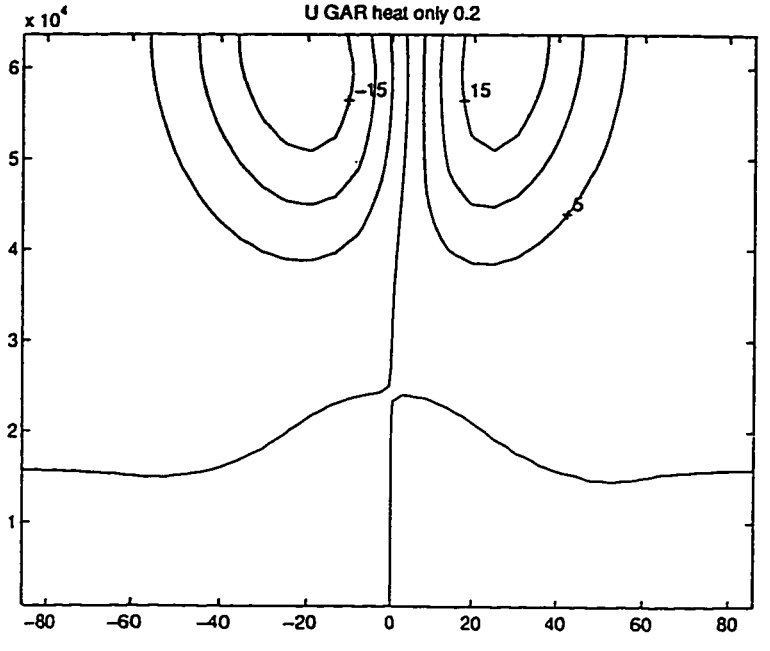

Figure 5.1 (continued):

(c) Same as in (b) but for $\kappa_r/\alpha = 0.2$,

(d) Corresponding zonal velocity field $\kappa_r/\alpha = 0.2$,

e

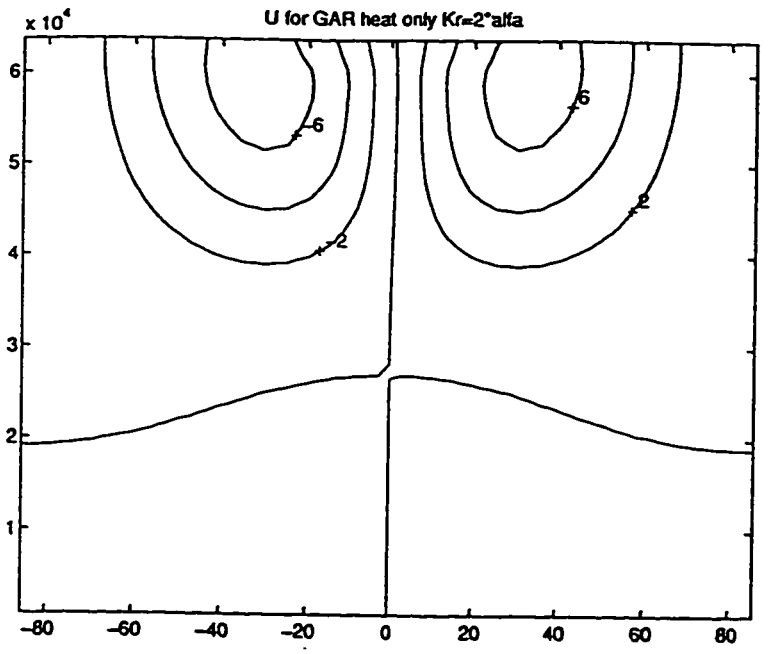

Figure 5.1 (continued): (e) Same as (d) but for $\kappa_r/\alpha = 2$

a

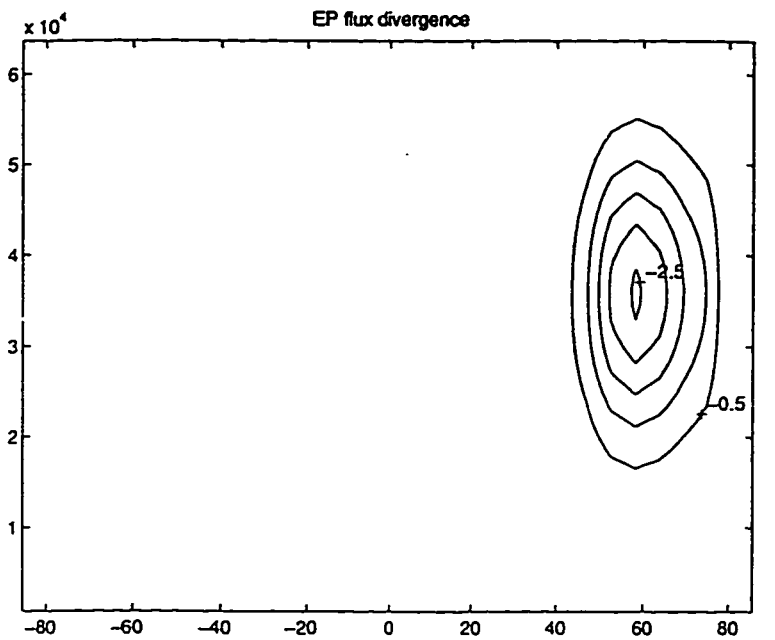

Figure 5.2: (a).Externally specified E-P flux divergence, corresponding to a mean acceleration of about -3 m/s/day.

b

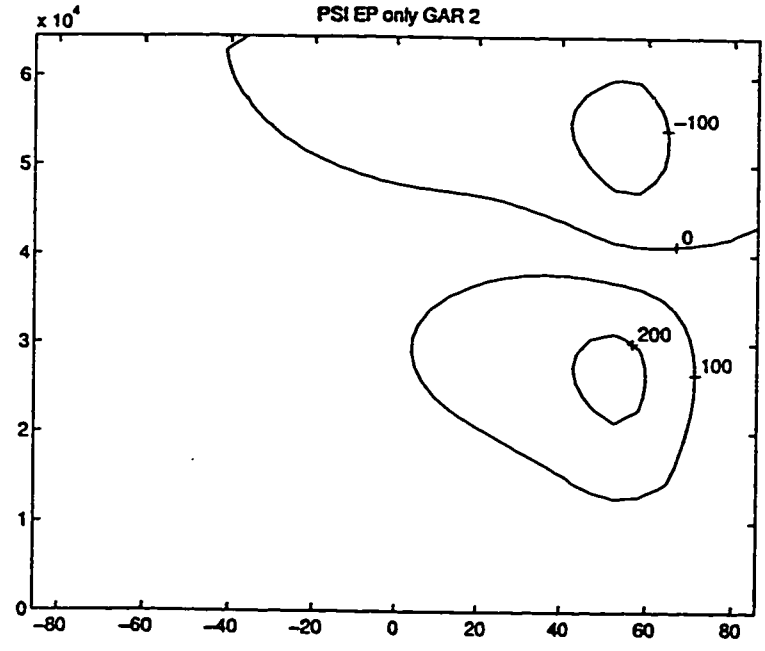

c

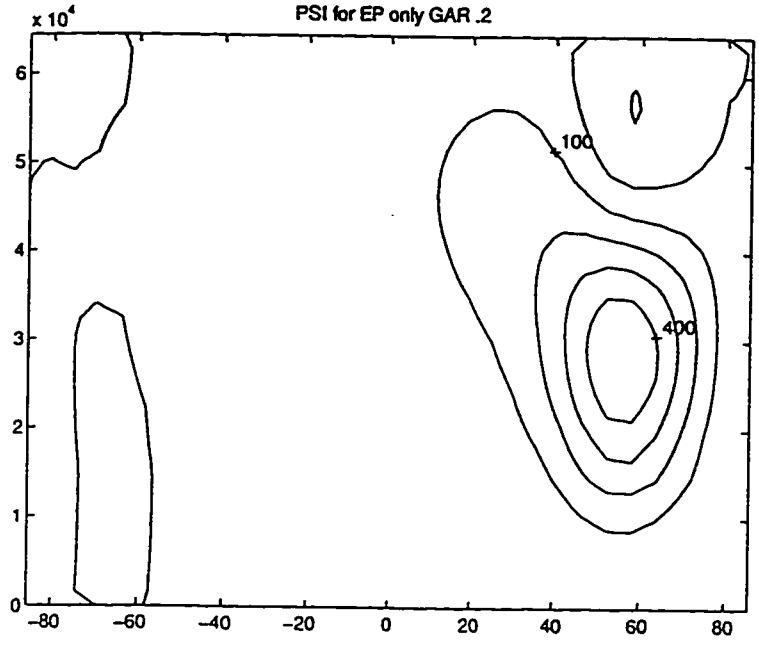

Figure 5.2 (continued): (b) The contours of the streamfunction of the response to the specified in (a) zonal forcing for $\kappa_r/\alpha = 2$. The contour interval for the streamlines is 100 m^2/s , maximum corresponds to 300 m^2/s; (c) Same as in (b) but for $\kappa_r/\alpha = 0.2$

d

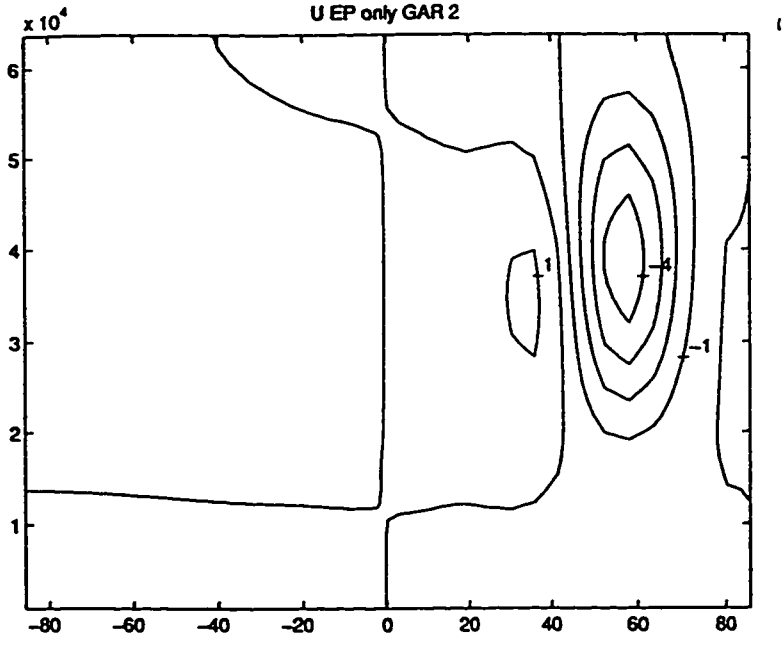

e

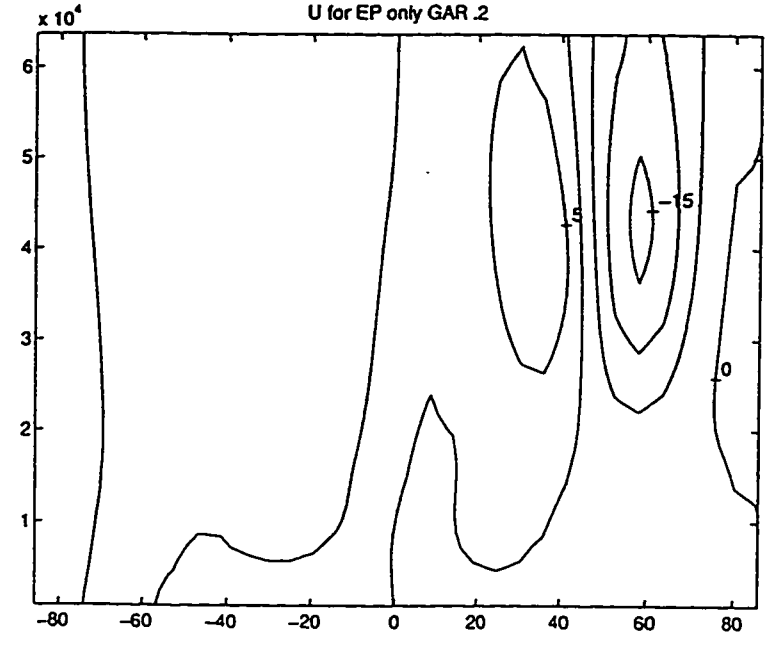

Figure 5.2 (continued): (d) Corresponding zonal velocity field $\kappa_r/\alpha = 2$; (e) Same as (d) but for $\kappa_r/\alpha = 0.2$

a

b

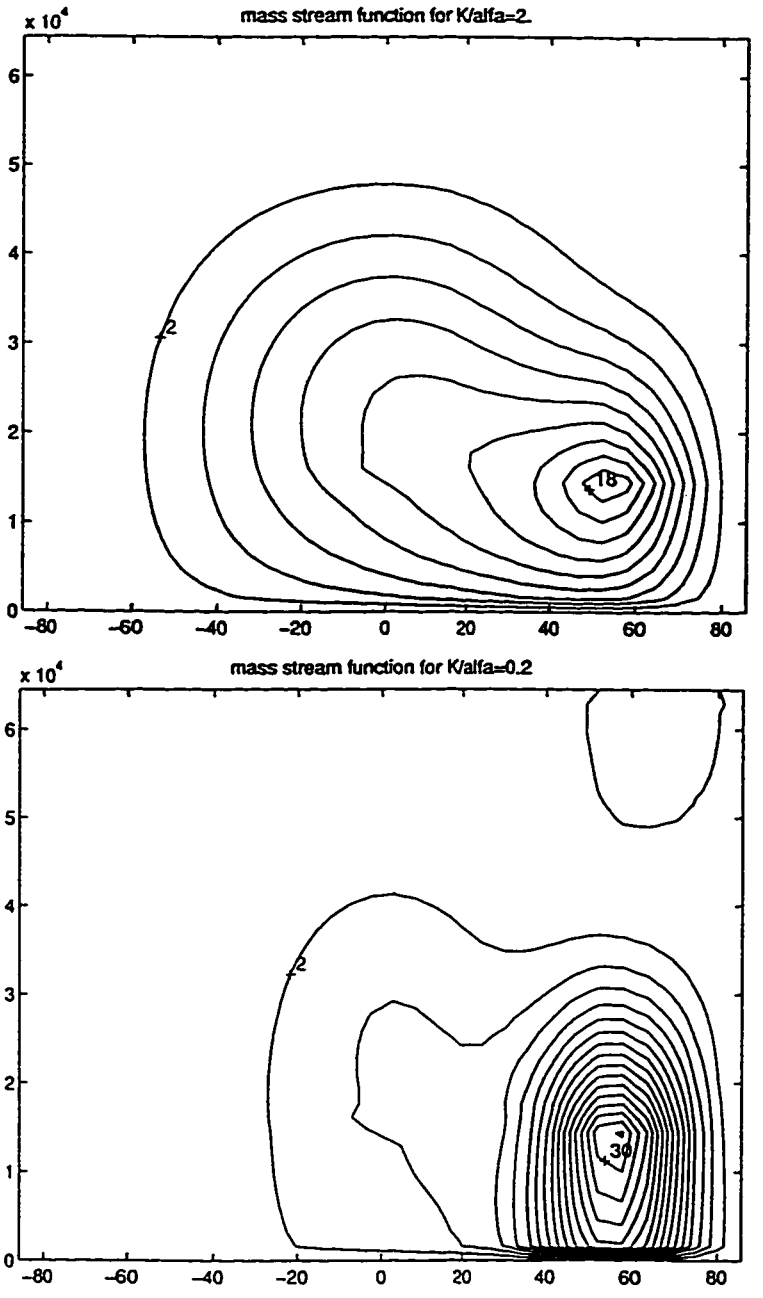

Figure 5.3: Mass streamfunction distribution of the response to the combined thermal (5.1 a) and mechanical (5.2 a) forcing. The contour interval is 2 kg/m/s. (a) Mass streamfunction for $\kappa_r/\alpha = 2$; (b) Same as (a) but for $\kappa_r/\alpha = 0.2$

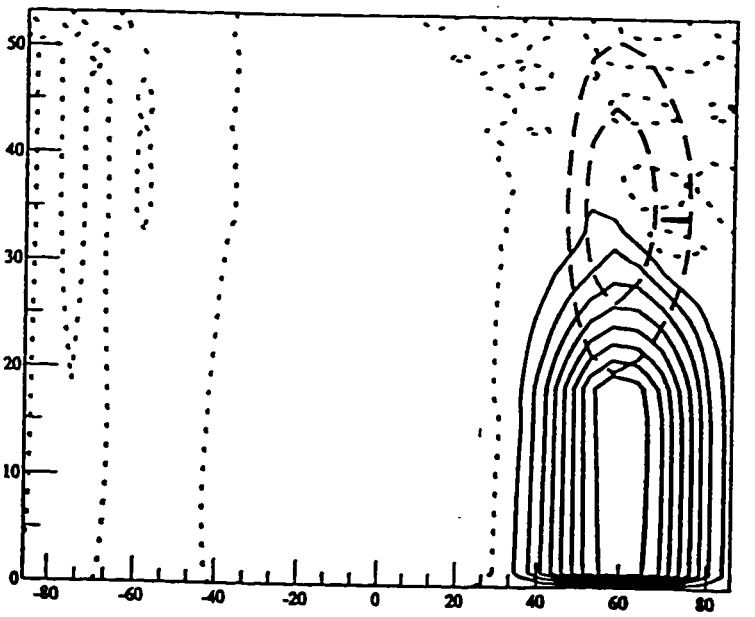

Figure 5.4: The response to the steady forcing located at 35km and at 60°N. The dashed lines show the location and pattern of the forcing. The contour interval is 5m^2/s/day, the maximum value is 10 m^2/s/day. The contour interval for the mass streamfunction is 10 kg/m/s.

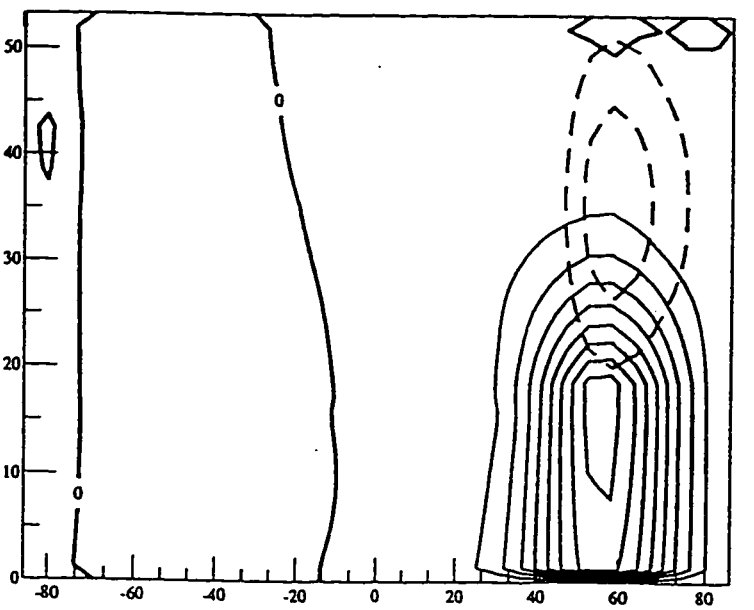

Figure 5.5: Same as in Figure 5.4 but for forcing that oscillates with a period of 360 days.

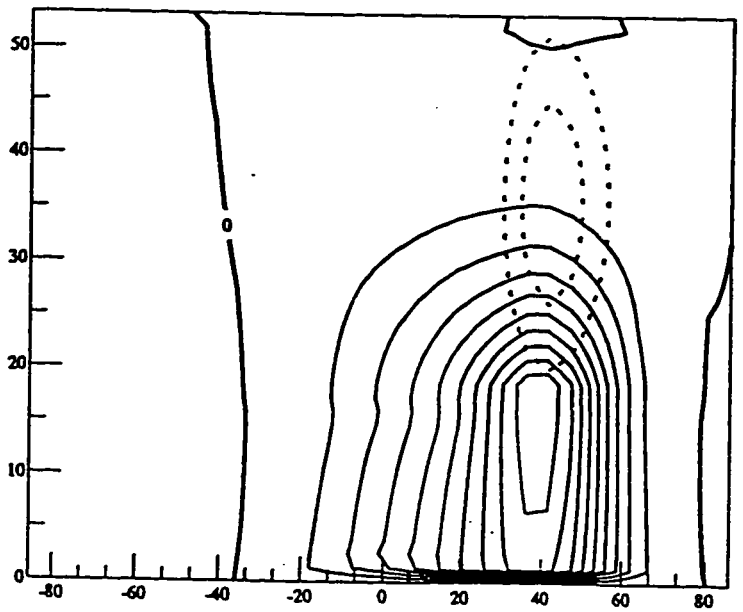

Figure 5.6: Same as Figure 5.5 but for the forcing located at 40°N

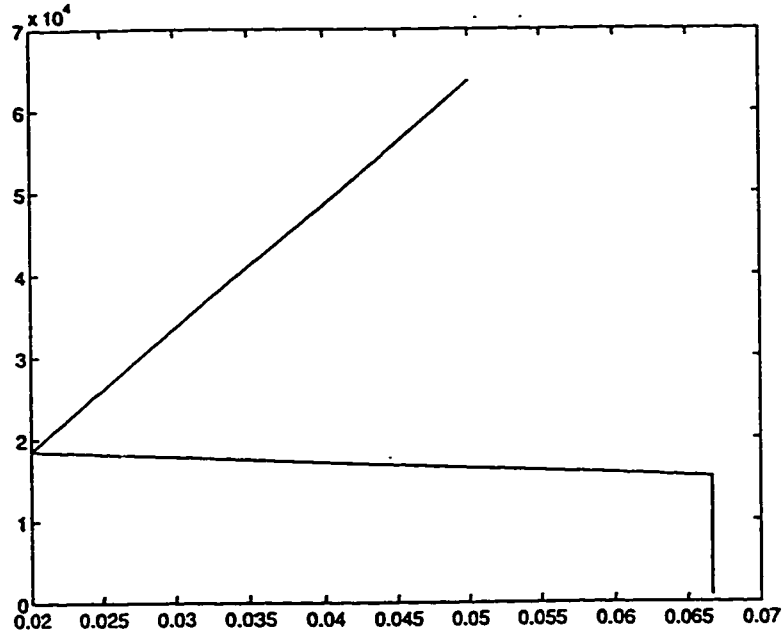

Figure 5.7: Thermal relaxation rate depending on height.

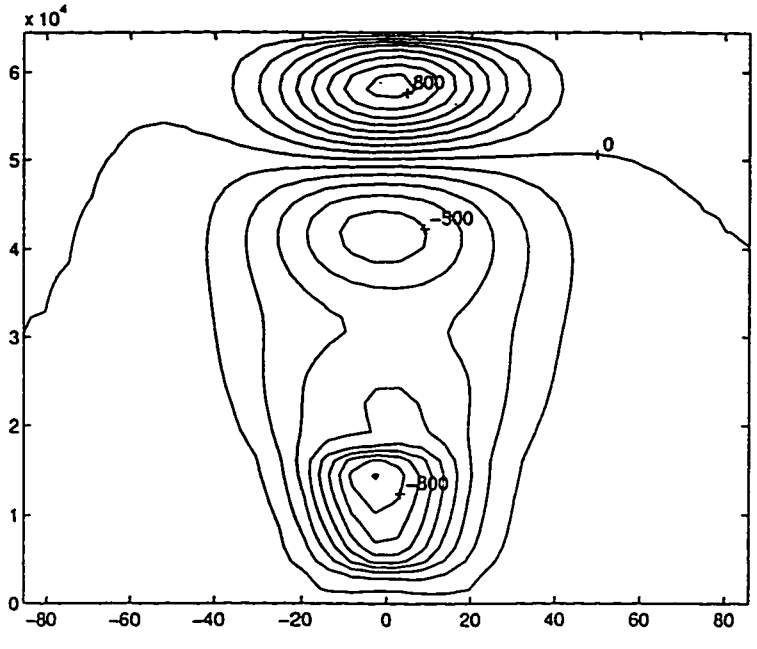

Figure 5.8: The streamfunction of the response to the thermal forcing antisymmetric about the equator. Contour interval is 100 m^2/sec.

Chapter 6 Mean Meridional Circulation in the Troposphere.

This chapter discusses the second vital counterpart of the complex dynanamical mechanism that determines large-scale circulation in the region of the tropical tropopause. For consistency, we will follow the historical development of the views on the mean meridional circulation in the troposphere. Our discussion will be also partly based on the review of the symmetric circulation models by *Lindzen [1990]*. Following *Lindzen [1990]*, we start with an examination of the likely behavior of the troposphere in the absence of eddies, and discuss the classical axisymmetric models of the troposphere. A comparison of the model responses with observations will be the basis for analysis of the mechanism responsible for inducing the observed zonally averaged state. In particular, the observed discrepancies reveal the role of eddies in maintaining the zonal average state. Finally, a conceptual model of the tropical circulation non-locally controlled by eddy-induced zonal forcing is presented and verified with the model.

6.1 Hadley Circulation in the Axially Symmetric Atmosphere

Lindzen [1990] provided a comprehensive review on the development of the theory of the zonally symmetric circulation in the troposphere. This section presents a summary of his survey of the main theoretical and numerical models describing this circulation.

The first theory of the zonally symmetric circulation in troposphere was developed by *Hadley [1735]*. In an attempt to explain the prevailing easterly

tradewinds in the tropics and westerlies in middle latitudes, he presented the following arguments:

- Warm air rises at the equator and flows poleward at upper levels approximately conserving angular momentum. Therefore, large westerly currents are produced at high latitudes.
- The observed westerly currents are smaller than the predicted ones. Therefore, friction should reduce westerly currents and the return flow at the surface will have a momentum deficit, leading to tropical easterlies.

The fact that this model predicted northwesterly surface winds in midlatitudes whereas observations showed southwesterly winds, led to further development of the theory. *Ferrel [1856]* and *Thompson [1857]* argued that at a latitude where the zonal flow is zero, there must be a pressure maximum. Therefore, within the friction layer next to the surface, a shallow flow will be established down pressure gradient, leading to a reversed cell (nowadays referred to as the Ferrel cell).

A large number of numerical models have been used for simulation of the observed zonally averaged structure of the troposphere. However, there remained many discrepancies between the empirical data and model responses.

A comprehensive description of the Hadley circulation in the troposphere was given by *Schneider [1977].* He proposed a nonlinear axially symmetric steady state model of the troposphere which could be used as a good tool for understanding the behavior of the symmetric circulation. *Held and Hou [1980]* (HH) expanded on *Schneider's* work, exploring his approximation in more details as follows.

The governing equations in HH were the steady zonally symmetric nonlinear equations for a Boussinesq fluid of depth H in the form:

$$\nabla(\vec{V}U) - fv - \frac{Uv\tan\varphi}{a} = \frac{\partial}{\partial z}\left(\nu\frac{\partial U}{\partial z}\right)$$

$$\nabla(\vec{V}v) + fU + \frac{UU\tan\varphi}{a} = -\frac{1}{a}\frac{\partial\Phi}{\partial\varphi} + \frac{\partial}{\partial z}\left(\nu\frac{\partial v}{\partial z}\right)$$

$$\nabla(\vec{V}\Theta) = \frac{\partial}{\partial z}\left(\nu\frac{\partial\Theta}{\partial z}\right) - \frac{\Theta-\Theta_e}{\tau} \qquad (6.1)$$

$$\frac{\partial\Phi}{\partial z} = g\frac{\Theta}{\Theta_0}$$

$$\nabla\vec{V} = 0$$

where U is the zonal velocity,

$\vec{V} = (v, w)$ are meridional and vertical velocities,

f is the Coriolis parameter,

a is the radius of the Earth,

Θ is the potential temperature,

Θ_e is the radiative equilibrium potential temperature,

τ - radiative relaxation time.

The following assumptions were made:

- The dissipation in the dynamical and thermodynamical equations is in the form of vertical diffusion $\frac{\partial}{\partial z}\nu\frac{\partial}{\partial z}$;
- The radiative heating is supposed to be in the form of Newtonian relaxation towards an externally specified radiative equilibrium potential temperature;
- This radiative equilibrium potential temperature is in the form :

$$\Theta_e(\varphi, z) = \Theta_0\left(1 - \Delta_H\left(\frac{1}{3} + \frac{2}{3}P_2(\sin\varphi)\right) + \Delta_v\left(\frac{z}{H} - \frac{1}{2}\right)\right) \qquad (6.2)$$

where $P_2(x) = 0.5\cdot\left(3x^2 - 1\right)$, Δ_H - the fractional potential temperature drop from equator to the pole, Δ_v - the fractional potential temperature drop from H to the

ground, τ -the radiative relaxation time.

- The boundary conditions are:

at z=H:

no stress: $\frac{\partial U}{\partial z} = \frac{\partial v}{\partial z} = 0,$ (6.3a)

no heat conduction: $\frac{\partial \Theta}{\partial z} = 0,$ (6.3b)

rigid top: $w = 0,$ (6.3c)

at z=0:

no heat conduction: $\frac{\partial \Theta}{\partial z} = 0,$ (6.4a)

rigid bottom: $w = 0,$ (6.4b)

linearized surface stress conditions:

$$\nu \frac{\partial U}{\partial z} = CU$$
$$\nu \frac{\partial v}{\partial z} = Cv \qquad (6.4c)$$

- Symmetry about the equator was also assumed:

$v = 0$ at $\varphi = 0$ (6.5)

(later we are going to trace the changes in circulation should this condition be violated).

For the inviscid case ($\nu = 0$), the set of equations (6.1) has an exact solution, that can be described as follows. The atmosphere is in radiative equilibrium, specified in the absence of: meridional circulation, and has a zonal velocity, U_e , satisfying the thermal wind balance in the form:

$$\frac{\partial}{\partial z}\left(fU_e+\frac{U_e^2\tan\varphi}{a}\right)=-\frac{g}{a\Theta_0}\frac{\partial\Theta_e}{\partial\varphi} \tag{6.6}$$

Setting U_e to be 0 at the bottom we can integrate (6.6) and obtain

$$\frac{U_e}{\Omega a}=R\cos\varphi\frac{z}{H} \tag{6.7}$$

where $R=\frac{gH\Delta_H}{(\Omega a)^2}$ (assuming $R<<1$)

Schneider [1977] argued that this thermal equilibrium (TE) solution can not be a steady solution of the symmetric equation in the presence of any, even small, viscosity (and if the diffusive friction is in the form of downgradient turbulent momentum fluxes). This statement is an extension of *Hide's [1969]* result regarding the location of the extrema in the total angular momentum distribution.

Hide's theorem can be formulated as follows: In the presence of downgradient viscous fluxes, the total angular momentum per unit mass,

$$M\equiv\Omega a^2\cos^2\varphi+Ua\cos\varphi \tag{6.8},$$

cannot have a local extremum in the interior of the atmosphere. Instead (because of the boundary condition we assumed above), M may have a maximum at the surface in the region of surface easterlies. (The proof of the theorem is simple, and can be found in *Schneider, 1977* or *Lindzen, 1990*). The upper bound for M is given by its value at the equator when $U=0$. Therefore, $M_{max}<\Omega a^2$.

This contrast contradicts the TE assumptions about U_e (see equation (6.7)). Thus, the TE solution cannot be realized, and a mean meridional circulation strong enough to produce a temperature field consistent with the angular momentum distribution, must be present. This temperature field must have very small horizontal gradients in the tropics.

The strength, height and width of this meridional circulation are obtained theoretically from the following three constraints:

- continuity and conservation of the potential temperature
- conservation of the angular momentum

Solving for the Hadley circulation analytically is not simple even within the highly simplified model of HH. Thus, one has to turn to numerical computations. *Lindzen [1990]* summarized the Hadley circulation simulated with the HH zonally symmetric model and the discrepancies between the observed and modeled circulations as follows:

- The symmetric simulations yield an upper level jet in about the right place but it is stronger than the observed.
- The symmetric simulations yield surface winds of the right sign in about the right place. In the absence of vertical diffusion, the wind magnitudes are too small. Vertical diffusion (that might be provided by cumulus clouds in the form of cumulus friction as was suggested by *Schneider and Lindzen, 1976*) increases the magnitudes.
- The calculated Hadley cell has a finite extent. It cannot carry heat between the tropics and the poles, and therefore affect observed equator-pole temperature gradient.
- The calculated temperature distribution does not have a pronounced equatorial minimum at the level of the tropopause
- The intensity of the simulated Hadley circulation is weaker than is observed.

In summary, these simulations clarified the origins and causes of the meridional

circulation. They also explained the observed surface easterlies. However, the remaining discrepancies between the model and the observations still need to be understood.

Lindzen [1990] argued that HH's model provides an inadequate description of the real atmosphere due to the three deficiencies:

- the overly simplified assumption of symmetry about the equator,
- the neglect of eddy effects,
- the partly external prescription of heating which does not take into account either the coupling between the cumulus convection and the dynamics or dynamical-radiative coupling.

Consequently, model improvement should follow these 3 directions. Below, we consider each of the shortcomings from the perspective of its influence on the model response.

6.2 Role of Asymmetry about the Equator

As was discussed in 3.2, the Hadley circulation is strongly asymmetric about the equator. Fig 6.1 (*Oort, 1983*) shows the meridional circulation for solstitial conditions. The circulation actually consists of one cell that extends from summer hemisphere far into winter hemisphere. The circulation in the tropics of the summer hemisphere is very weak.

Lindzen and Hou [1988], and later *Plumb and Hou [1992],* improved the HH model by allowing the center of the heating to be located off the equator. Specifically, they replaced equation (6.2) by

$$\Theta_e(\varphi, z) = \Theta_0\left(1 - \Delta_H\left(\sin\varphi - \sin\varphi_0\right)^2 + \Delta_v\left(\frac{z}{H} - \frac{1}{2}\right)\right) \qquad (6.9)$$

In this equation, φ_0 is not zero and the heating is asymmetric about the equator.

In the HH model, the requirement of continuity of the potential temperature in the vicinity of the edge of the cell (φ_h):

$$\overline{\Theta}(\varphi_h) = \overline{\Theta_E}(\varphi_h) \tag{6.10 a}$$

and the requirement of no net heating (i.e. 'equal area' argument):

$$\int_0^{\varphi_h} \overline{\Theta} \cos\varphi d\varphi = \int_0^{\varphi_h} \overline{\Theta}_e \cos\varphi d\varphi \tag{6.10 b}$$

helped to determine analytically the horizontal extent of the cell and the potential temperature at the equator, which, in the symmetric case, is supposed to be the latitude of separation between 'summer' and 'winter' cells. However, in the case of asymmetric heating, the latitude of separation is shifted off the equator and does not coincide with the center of the heating, φ_0. *Lindzen and Hou [1988]* calculated this bounding latitude, φ, as well as the latitudes of the edges of 'summer', φ_{H+}, and 'winter', φ_{H-}, cells as functions of φ_0 (Fig 6.2). They showed that latitude of separation of the cells shifts away from the equator even for small φ_0. At the same time, φ_{H-} grows significantly when φ_{H+} and φ_0 approach each other. This result is consistent with the observed weak summer cell and strong and pronounced winter cell. *Lindzen and Hou* also showed that a small shift of the center of heating off the equator is accompanied by a great enlargement and intensification of the 'winter' cell along with a corresponding reduction of the 'summer' cell. In addition, at the tropical tropopause level the potential temperature is symmetric about the equator and has a local minimum on the equator.

The introduction of asymmetry about the equator diminishes the discrepancy between the model and the observations. However, several problems remain unresolved:

- The winter high tropospheric jet is still much stronger than observed
- The low level easterly jet on the winter side of the equator is consistent with observations but the surface wind magnitudes are now excessive.
- The Hadley cell model still does not simulate the observed equator-pole temperature gradient.

Lindzen [1990] concluded that such extension of the axisymmetric model leads only to modest improvement in the discrepancies between the model and the observation mentioned in *section 6.1*. Therefore, he argued that it is necessary to consider eddy-induced forcing and its non-local influence on the meridional circulation in the tropics.

6.3 Non-locally Controlled Hadley Circulation

The inconsistency in the Hadley circulation obtained as a result of the axially symmetric model, on the one side, and obtained as zonal and time average of the observations, on the other side, suggests that baroclinic waves should play a significant role in determining and maintaining the observed Hadley circulation.

Schneider [1984] investigated the influence of the eddy momentum flux forcing on the Hadley cell in his zonally averaged model. He concluded that " As long as there is sufficient friction for a steady state to exist, the Hadley circulation mass flux does not respond strongly to changes in the strength of the horizontal eddy momentum forcing, but does respond strongly to changes in the distribution of the tropical thermal forcing"(p. 1093). This result is consistent with ours. As was shown in Chapter 5, in the presence of a strong dynamical dissipation the response in meridional circulation is determined by heating. On the contrary, the response in the

inviscid limit is non-locally determined by the eddy-induced zonal forcing.

Dunkerton [1989] reopened the question of non-local control of Hadley circulation by the extratropical eddy forcing in the context of the stratosphere. He argued that the modeled tropical Hadley circulation is weaker than the observed unless the "sideways influence" due to eddy forcing is included. Therefore, even from this perspective, the remote influence of the extratropical forces should be included in comprehensive analysis of the meridional circulation.

There are two aspects of this non-local control in the troposphere. First, eddy induced extratropical zonal forcing causes a meridional circulation that can be described in the framework of the "suction pump" mechanism discussed in Chapter 2. Second, this induced meridional circulation is coupled with cumulus convection, which maintains this meridional circulation by changing the effective static stability *(Emanuel, 1991)*. This coupling between the non-locally induced large-scale dynamics and cumulus convection in the tropical region will be considered in Chapter 7. Below we discuss the first aspect of the non-local control of the Hadley circulation.

We examined the response in the Hadley circulation to the extratropical Rossby wave-induced forcing. For this purpose a set of experiments with the 2D TEM model (described in Chapter 4) was performed. In order to separate the effects of the radiative heating and the non-local zonal eddy forcing, we specified the radiative equilibrium temperature to be symmetric about the equator. The results for the solstice conditions in radiative cooling/heating will be discussed in Chapter 9. All the experiments used the following set of parameters :

- $\kappa_r = (100 \text{ day})^{-1}$,
- $\alpha = (10 \text{ day})^{-1}$,

- N^2=1.5e-4 s^{-2}
- The atmosphere was assumed to be dry.
- The coefficient of mechanical friction near the surface was assumed to be on the order of 1 day^{-1}
- All other constants are as discussed in Chapter 4.

In the **first experiment**, the radiative equilibrium temperature (Fig. 6.3) was specified to be symmetric about the equator. Due to the assumption of no planetary-scale eddies, the boundary conditions (4.6a) transforms into $\overline{w}^*$ at the bottom. The model was allowed to relax to the radiative equilibrium temperature.

As we would have expected from the simulations with the previous nonlinear axially symmetric models, the resulting basic state has a weak meridional circulation symmetric about the equator (Fig. 6.4b). The latitude of separation of the "winter" and "summer" cells coincides with the center of heating, and is located at the equator. The zonal wind field is also symmetric about the equator (Fig. 6.4a). Maximum westerlies are observed near the tropopause. Weak easterlies exist at the surface near the equator. In the following discussion we will refer to this state as the reference state.

The **second set of experiments** introduced an additional zonal forcing into the zonal momentum equation corresponding to the E-P flux divergence in July (Fig 6.5a). This forcing has strong negative values of an order of -10 m/s/day at 7 km and at 60°S. It should be noted that in the tropics the forcing is very weak and is overall negative. Near the surface there exist positive patches of E-P flux divergence.

Fig. 6.5 (b) shows the corresponding horizontal eddy temperature fluxes ($\overline{v'T'}$

fluxes). The $\overline{v'T'}$ fluxes have large negative values in the mid and high-latitudes of the Southern hemisphere of an order of 16 K m/s. The boundary conditions at the bottom are now in the form (4.6 a)

Fig. 6.5 (c-h) shows the model response to this additional zonal forcing. We obtain it as a residual of the model response to both zonal forcing and diabatic heating, and the model response to the diabatic heating alone (Fig. 6.4).

Fig. 6.5 (c) shows the TEM streamfunction of the response. The maximum absolute value is 2500 m^2/s and is located at 5 km and 50°S. The response is mainly in the 'winter hemisphere'. The conventional EM diagnostic, shown on Fig. 6.5 (e), demonstrates the existence of a thermally direct, single Hadley cell with rising motion in the summer hemisphere, and extending into the winter hemisphere. A Ferrel cell exists in the middle latitudes of the winter hemisphere. Fig. 6.5 (g) shows the corresponding response in the zonal wind field. It should be noted that the addition of zonal forcing improves the zonal wind field in comparison with the previous models by decreasing the upper level westerlies and increasing the lower level easterlies.

In the **third set of experiments**, an additional tropical heating corresponding to the idealized effects of cumulus convection heating in July was externally specified. The cumulus heating in this case is parameterized in the same fashion as the radiative heating in the first experiment. We prescribed radiative equilibrium temperature with the same spatial distribution as the cumulus heating observed in July. Fig. 6.6 (a) shows this part of the prescribed radiative equilibrium temperature. It is centered at 5°N off the equator with a maximum value of 40°K. As in the first experiment, the model temperature is allowed to relax to this externally specified radiative equilibrium temperature.

Fig. 6.6 (b) shows the TEM streamfunction of the response to this heating. In comparison with the previous case, the circulation is more symmetric about the equator. It is also stronger. The maximum of the mass streamfunction (Fig. 6.6c) is shifted upward. The residual circulation is seen to be thermally direct over the entire Southern Hemisphere with the maximum intensity in low latitudes.

The corresponding conventional EM streamfunction (Fig. 6.6d) reveals a Hadley circulation nearly symmetric about the equator. The winter cell is a little bit stronger than the summer cell. Ferrel cells exist in both hemispheres, though the one in the winter hemisphere is more pronounced.

The **fourth set of experiments** combines the above described mechanical and thermal forcing. The resulting meridional circulation is shown in Fig. 6.7. In this figure the pronounced 'winter' cell is stronger than in the previous cases. However, it is not a simple algebraic sum of the two previous responses, due to the nonlinearity.

The residual circulation is seen to be thermally direct over the entire winter hemisphere with a secondary maximum intensity in the middle latitudes. It is considerably more intense than the conventional Eulerian mean meridional circulation (panel c).

The circulation is still weak in comparison with observations. Nevertheless, we have achieved a qualitative correspondence since the distribution of the surface easterlies and the tropopause westerlies is closer to the observed zonal wind distribution.

The main conclusion following from these simulations is that the Hadley circulation in tropics obviously "feels" the influence of the remote zonal forcing induced by the eddies in middle latitudes. Our experiments suggest that the

pronounced asymmetry about the equator (under non-solstice conditions in the radiative heating/cooling distribution) is at least to some extent determined by eddies. It should be noted that, although the Hadley circulation induced by the extratropical eddy forcing alone is not as strong as the observed meridional circulation, its seasonal variability may be affected by the annual cycle in the zonal forcing.

At this point, the main direction of the model improvement is in obtaining a stronger meridional circulation which would better correspond with the empirical data. For this purpose, the following mechanisms should be added:

- The basic state, as we determined it, was symmetric about the equator. We didn't take into consideration the asymmetry of the short-wave radiation and thus the asymmetry of the basic state. The nonlinearity of the problem could lead to stronger response under this conditions
- More interesting and important, the cumulus heating was externally prescribed and the coupling between the dynamics and moist convection was omitted.

Incorporating these mechanisms may result in a stronger, more realistic pattern of mean meridional circulation.

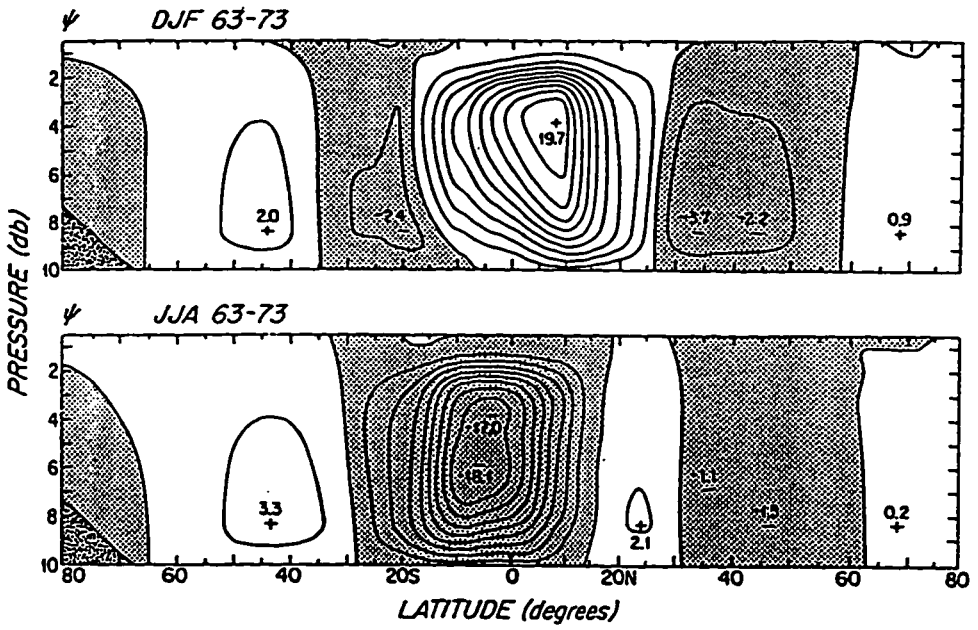

Figure 6.1: Time average meridional-height cross section for the streamfunction of the mean meridional circulation. Units, 10^{10} kg/s, contour intervals 0.2×10^{10} kg/s. (from *Oort, 1983*)

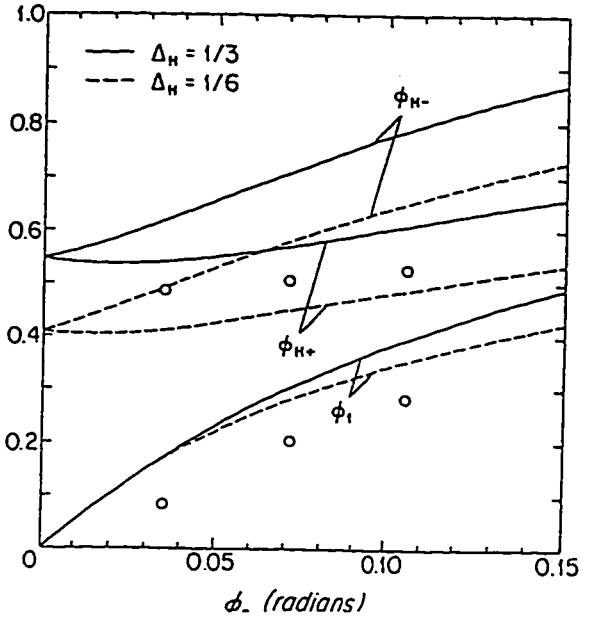

Figure 6.2: The latitude of separation φ, as well as the latitudes of the edges of 'summer' φ_{H+} and 'winter' φ_{H-} cells as functions of φ_0. (from *Lindzen and Hou [1988]*)

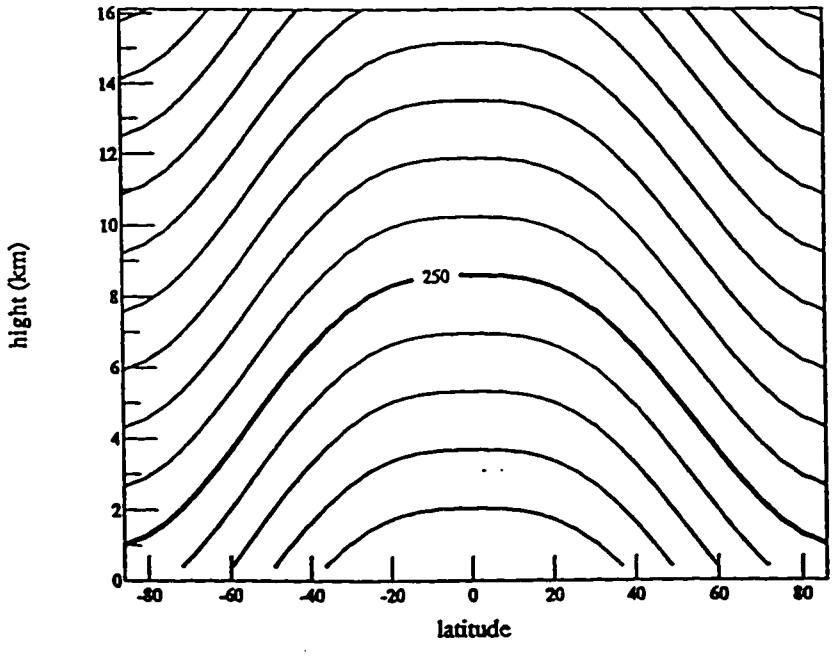

Figure 6.3: Radiative equilibrium temperature specified to be symmetric about the equator; contour interval 10 K

a

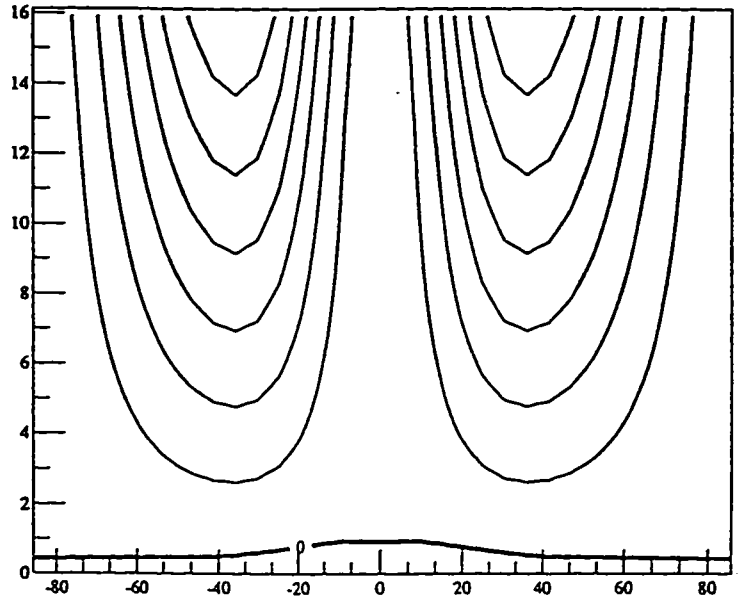

Figure 6.4: Response to the heating specified in Figure 6.3.
(a) zonal wind field; contour interval 5m/s

b

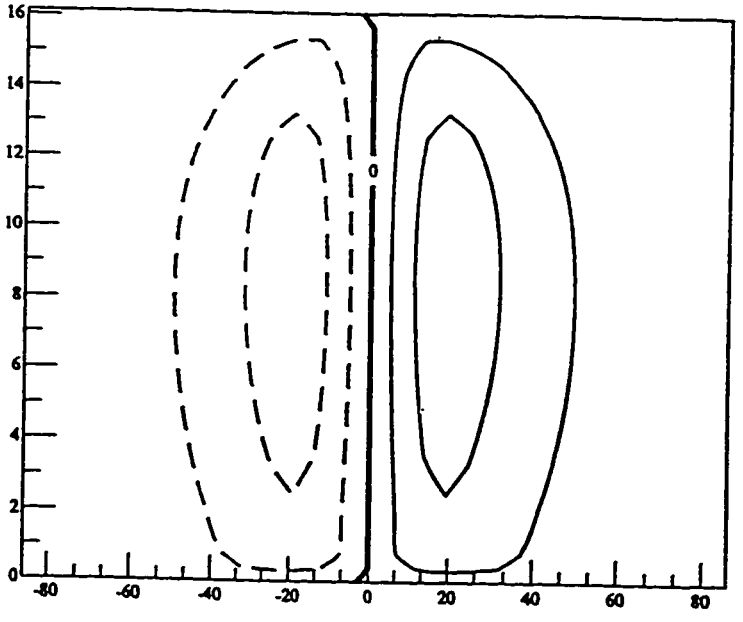

c

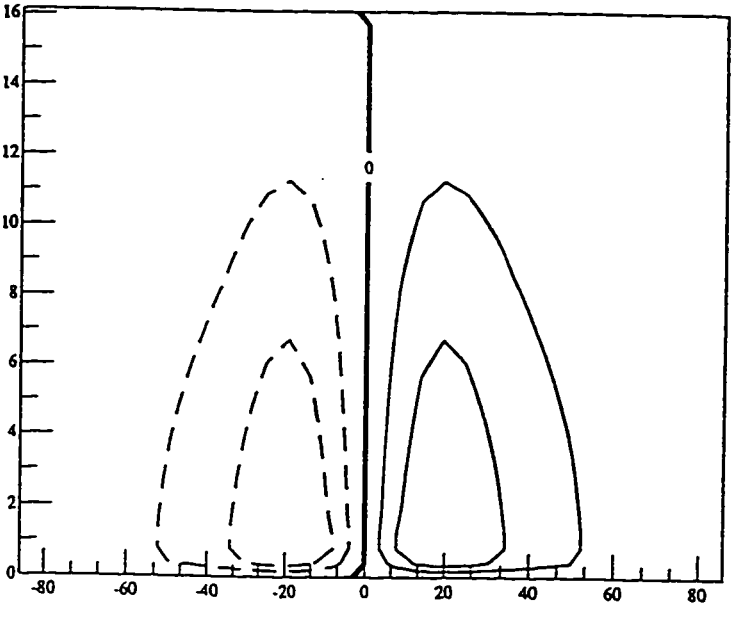

Figure 6.4 (continued): (b) streamfunction; contour interval 100 m^2/s;
(c) mass streamfunction; contour interval 50 kg/m/s

a

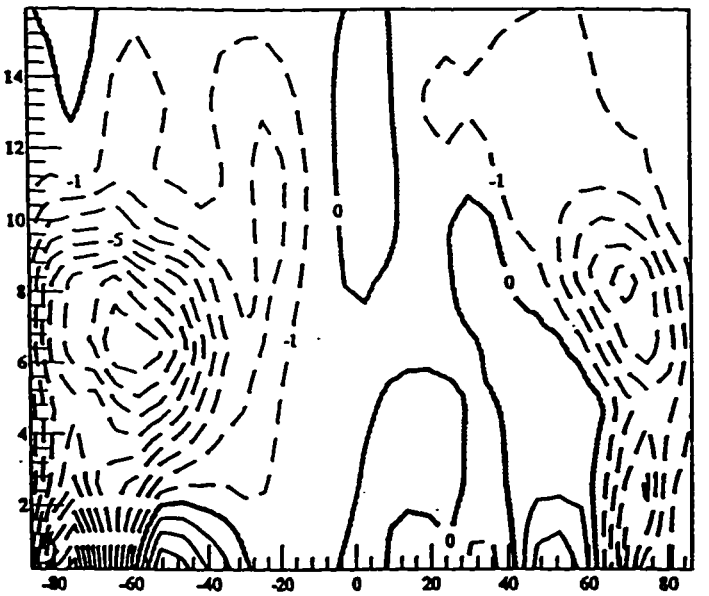

b

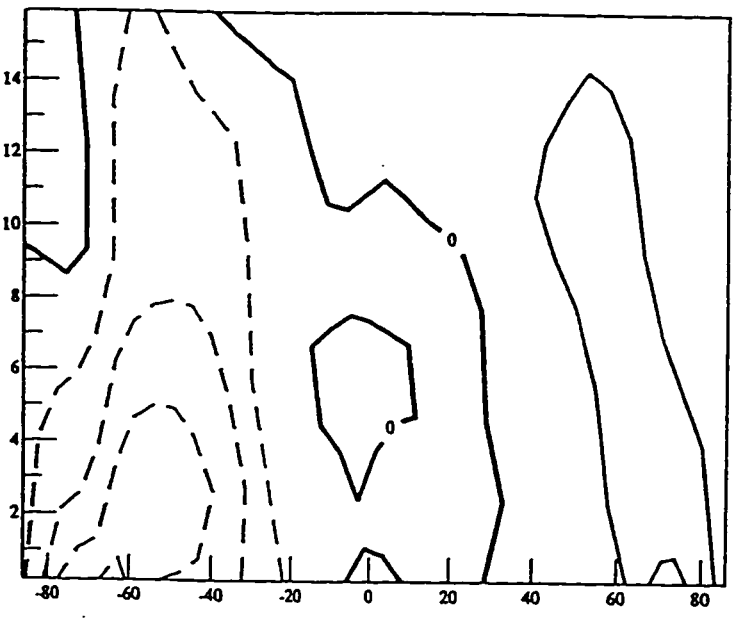

Figure 6.5: (a) zonal forcing in the zonal momentum equation corresponding to the E-P flux divergence in July *(Randel, 1992)*; contour interval 1 m/s/day
(b) corresponding $\overline{v'T'}$ fluxes; contour interval is 4 K×m/s.

c

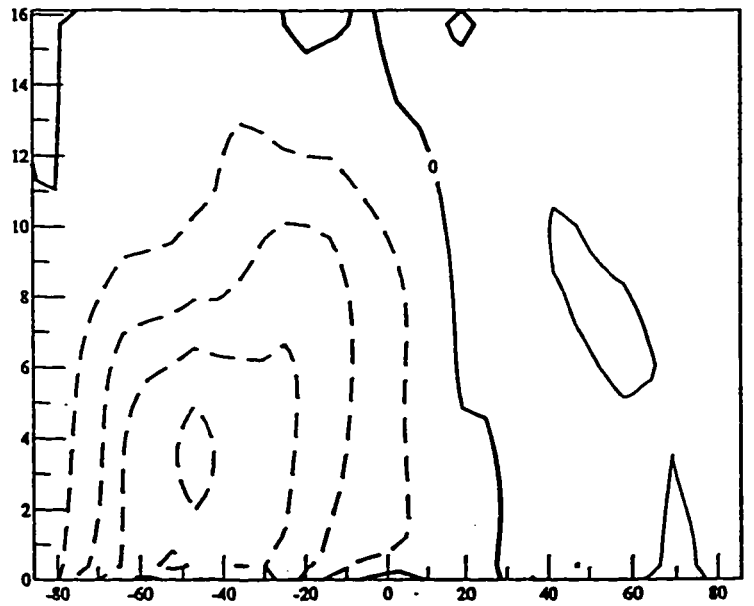

d

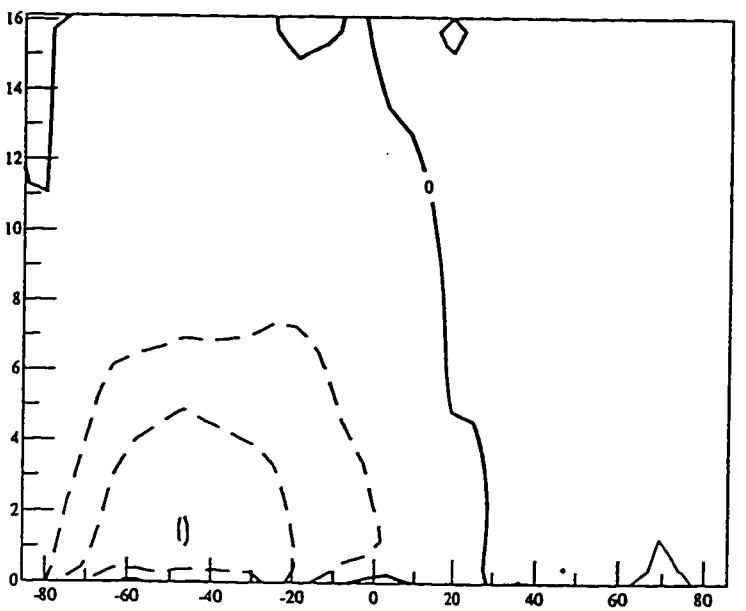

Figure 6.5 (continued) the response to the zonal forcing shown in panel (a). (c) the TEM streamfunction of the response, contour interval is 500 m^2/s, maximum absolute value is 2500 m^2/s; (d) corresponding residual mass stream function, contour interval is 500 kg/m/s

e

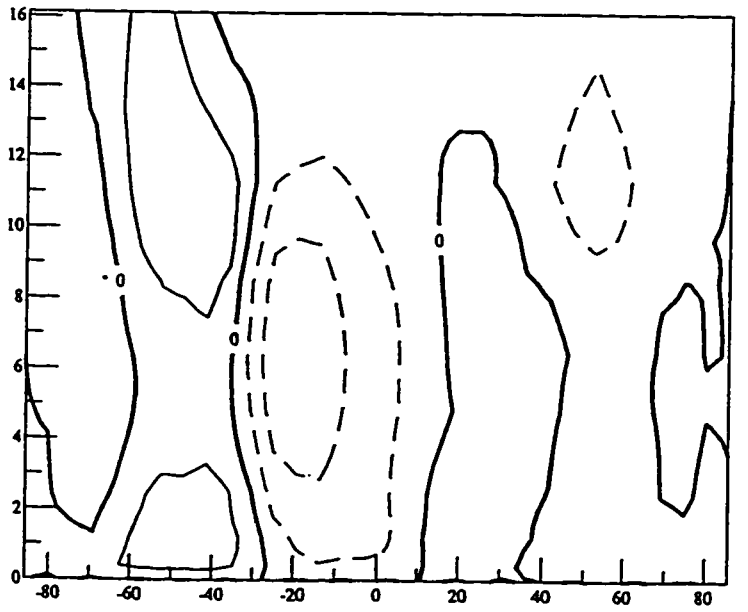

f

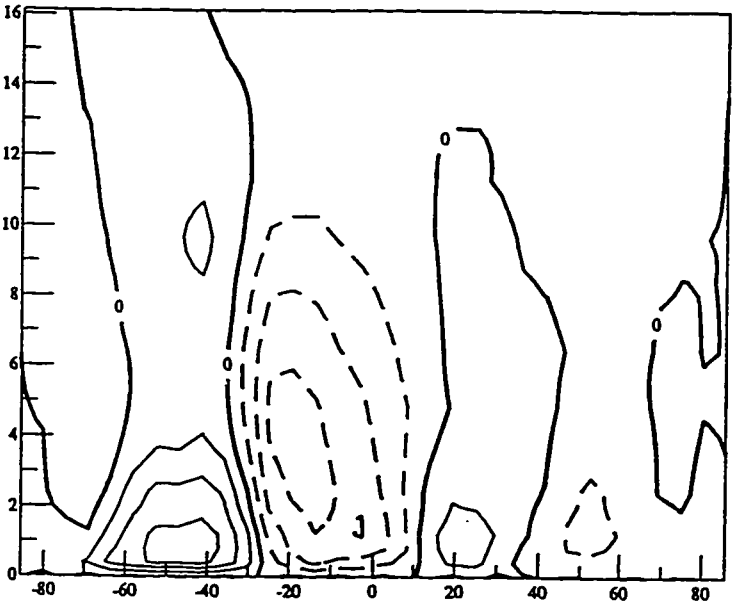

Figure 6.5 (continued): (e) conventional EM diagnostic; streamfunction lines, contour interval is 500 m^2/s; (f) corresponding mass streamfunction lines, contour interval is 200 kg/m/s

g

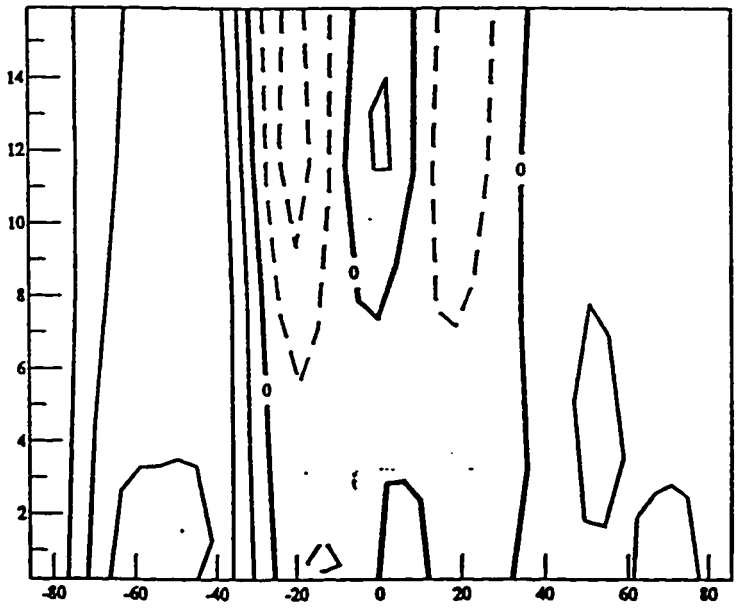

h

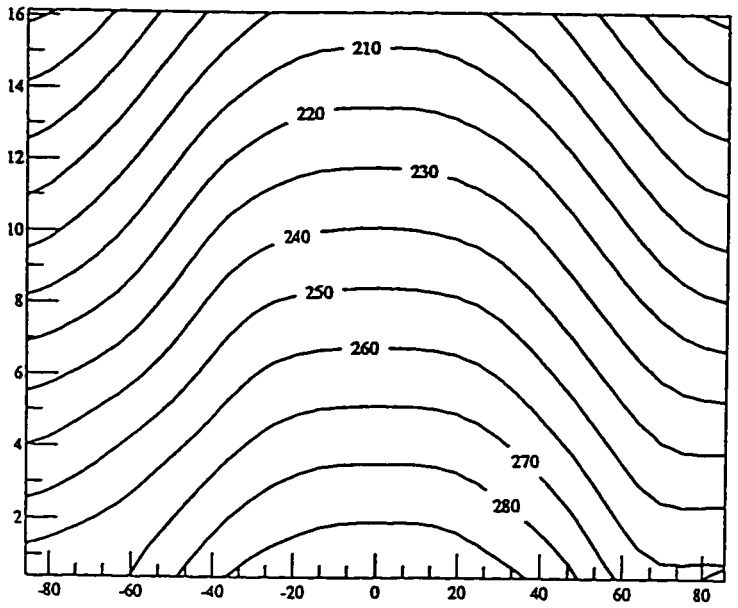

Figure 6.5 (continued): (g) the corresponding response in the zonal wind field (the deviation from the reference state shown in Fig 6.4a); contour interval is 2.5 m/s. (h) the corresponding temperature distribution

a

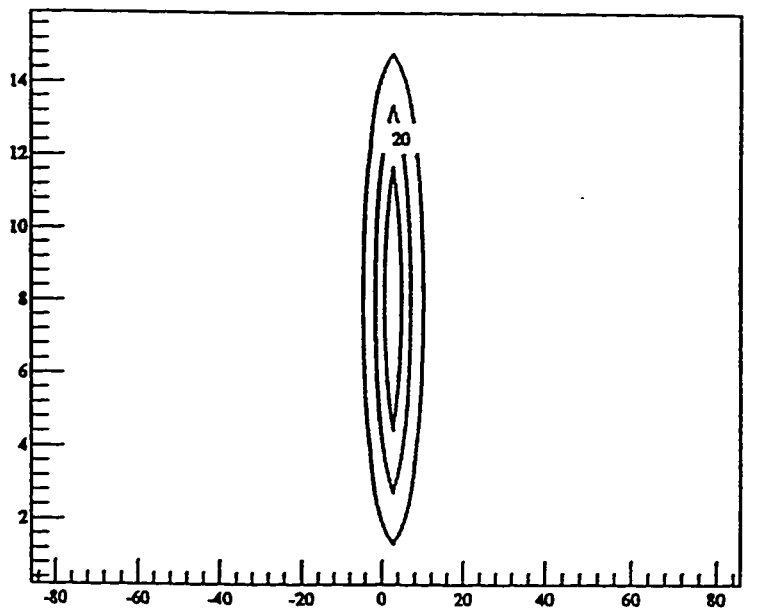

Figure 6.6: Response to an externally specified additional tropical heating corresponding to the idealized effect of cumulus convection heating in July. (a) The prescribed deviation from the symmetric radiative equilibrium temperature in July. The contour interval is 10°K, maximum value is 40°K.

b

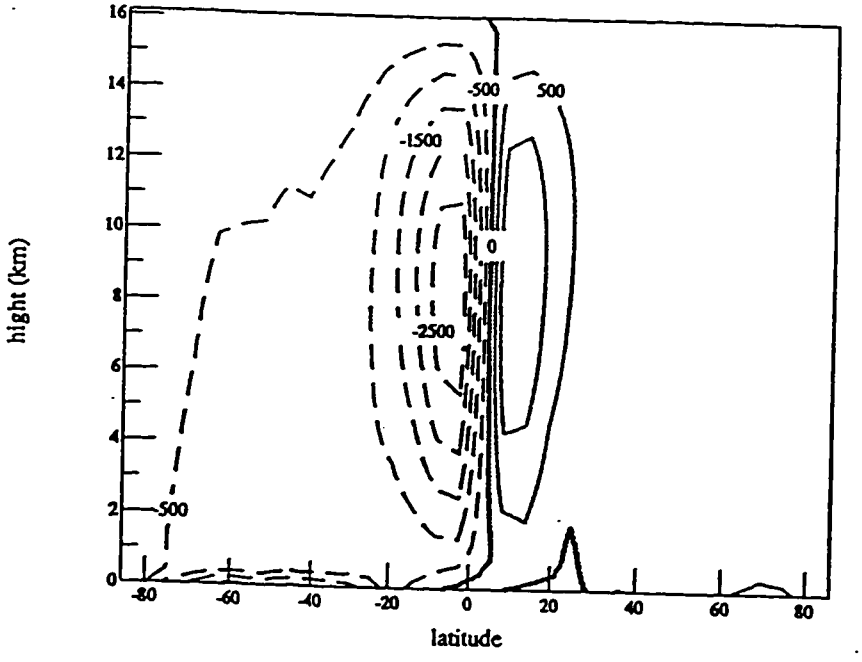

c

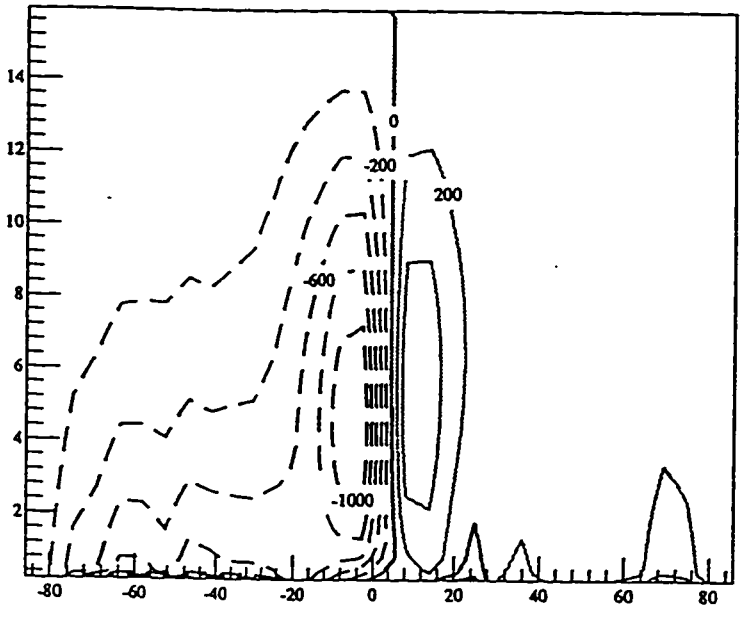

Figure 6.6 (continued): (b)The TEM streamfunction of the response to the heating specified in (a). Contour interval is the same as in Figure 6.5 (c); (c) corresponding residual mass stream function, contour interval is 200 kg/m/s

d

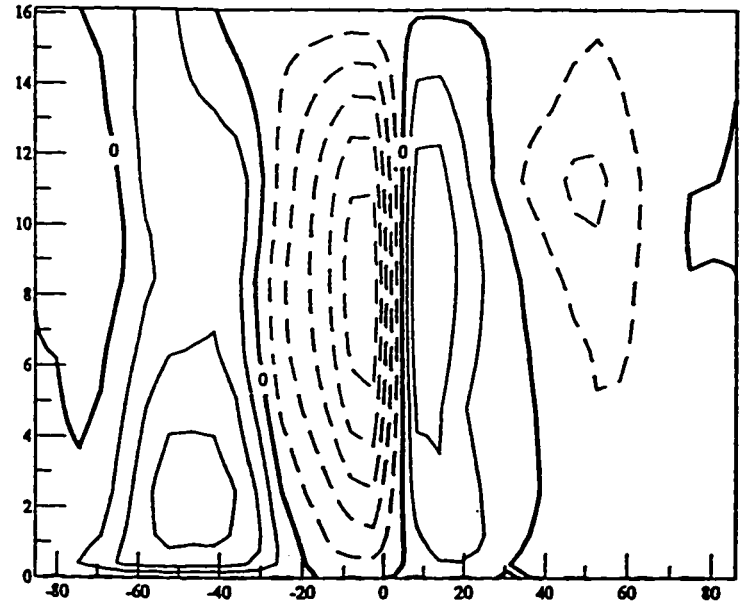

e

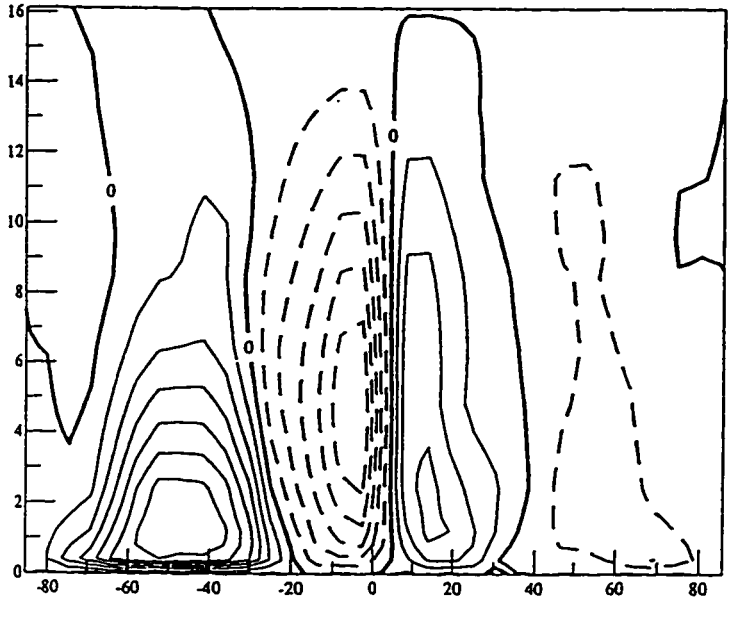

Figure 6.6 (continued): (d) EM stream function of the response to the cumulus heating; contour interval is 500 m^2/s; (e) corresponding mass streamfunction lines, contour interval is 200 kg/m/s

f

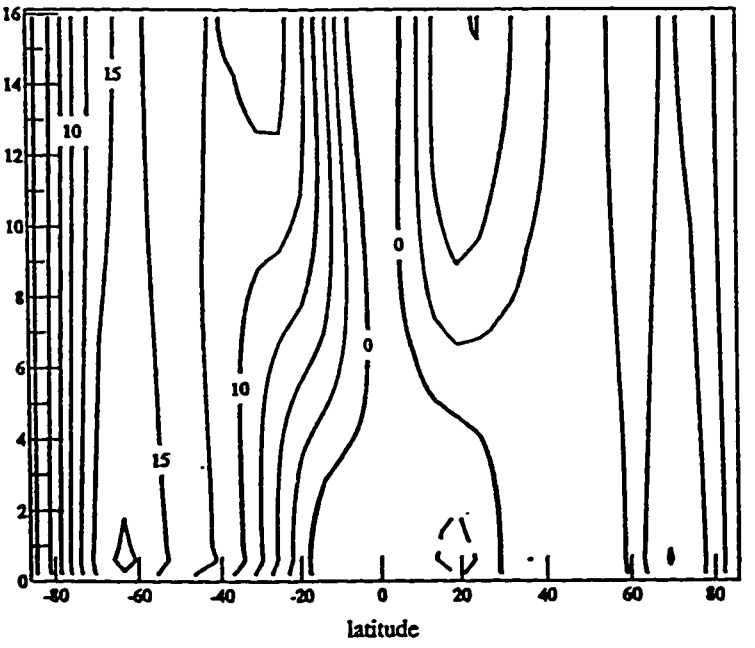

g

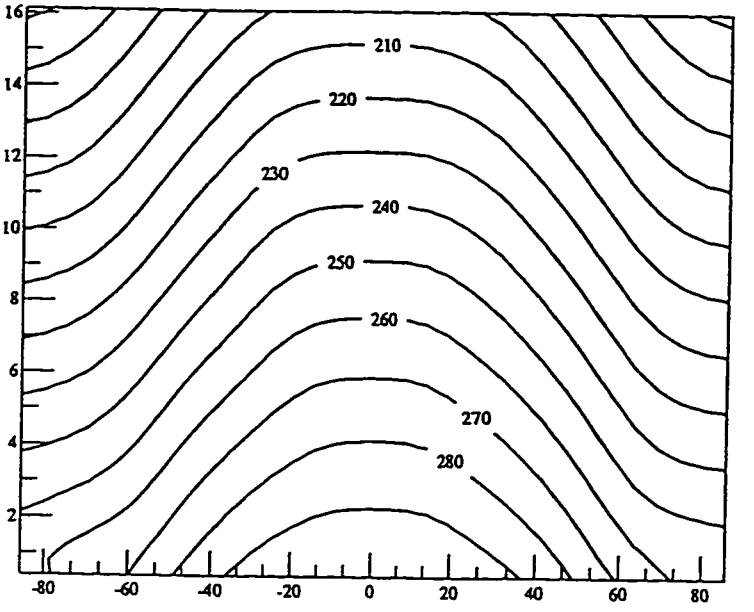

Figure 6.6 (continued): (f) the corresponding response in the zonal wind field (the deviation from the reference state shown in Fig 6.4a); contour interval is 2.5 m/s; (g) the corresponding temperature distribution.

a

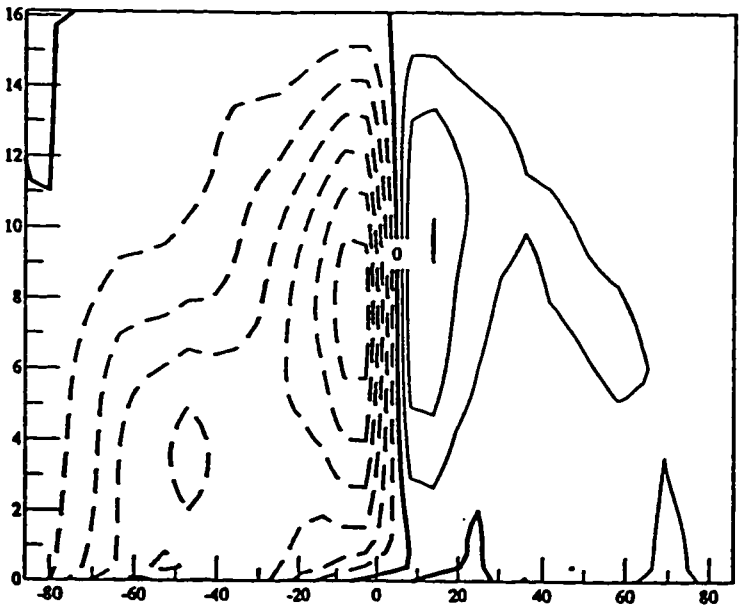

b

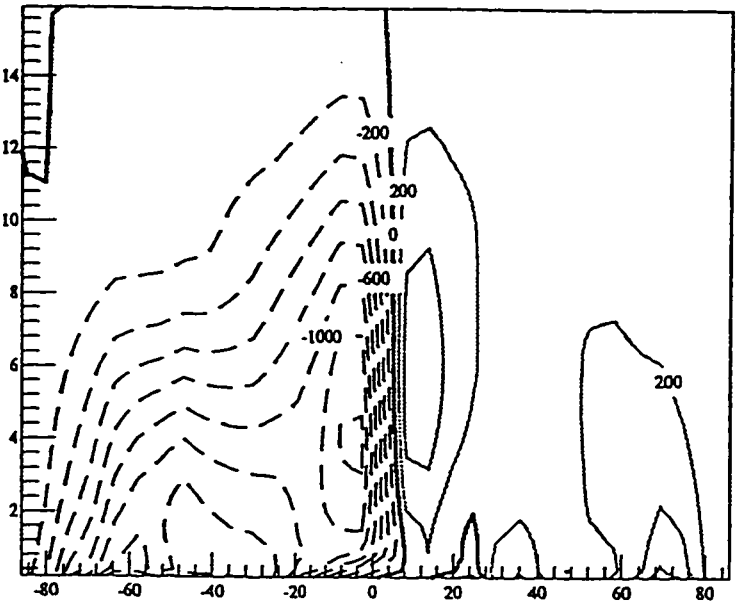

Figure 6.7: Response to the combined effect of the above described mechanical and thermal forcing: (a) the TEM streamfunction of the response, contour interval is 500 m^2/s, maximum absolute value is 2500 m^2/s; (b) corresponding residual mass stream function, contour interval is 500 kg/m/s

c

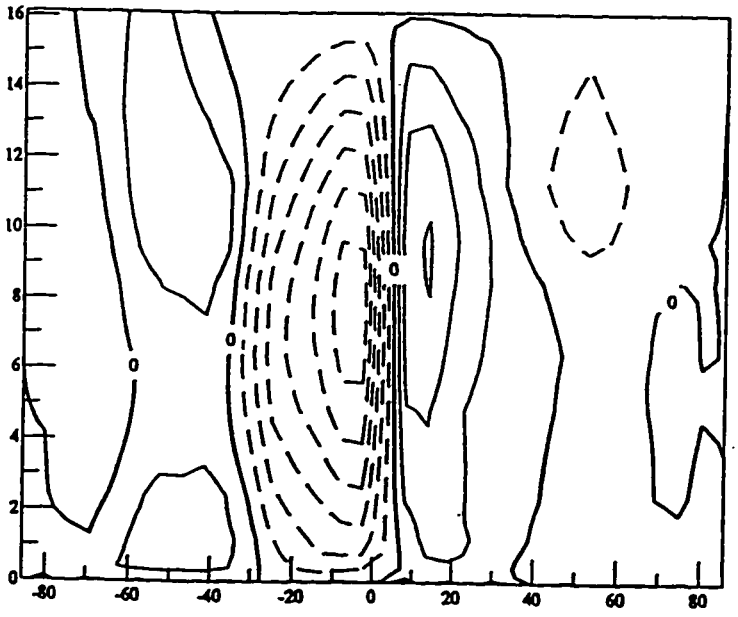

d

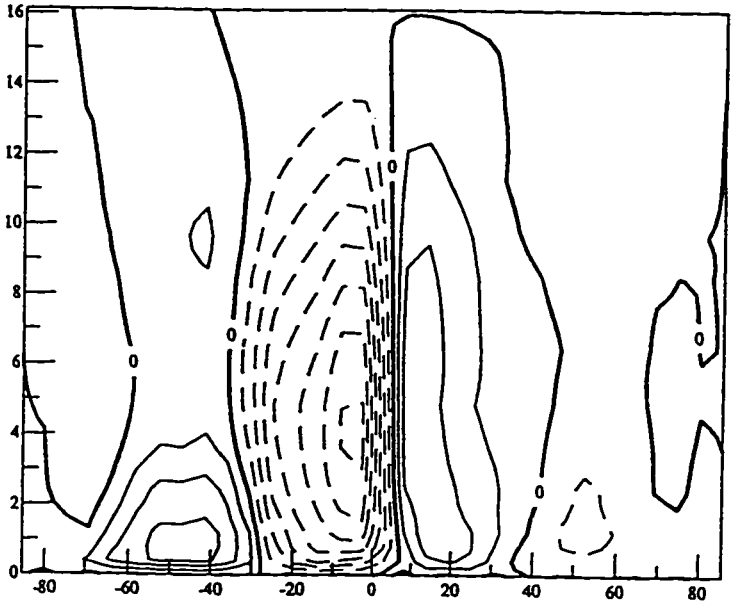

Figure 6.7 (continued): (c) conventional EM diagnostic; streamfunction lines, contour interval is 500 m^2/s; (d) corresponding mass streamfunction lines, contour interval is 200 kg/m/s

e

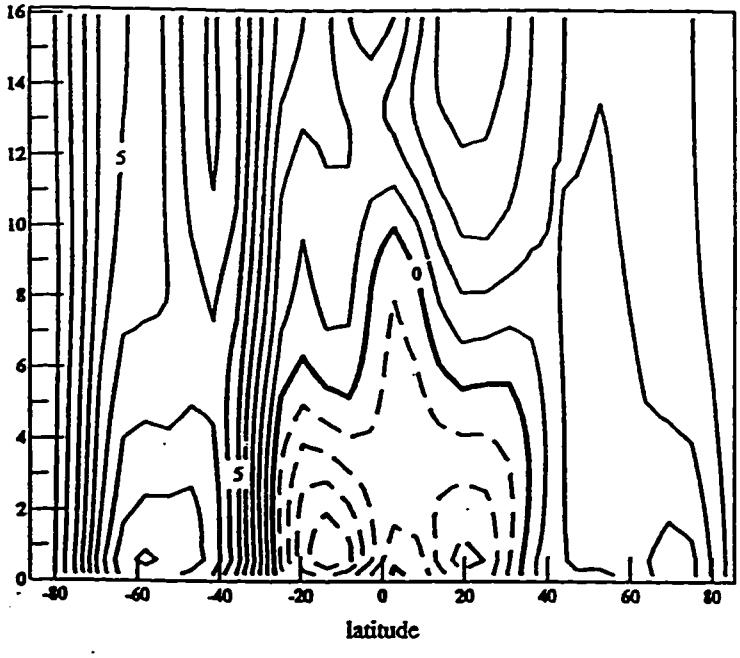

f

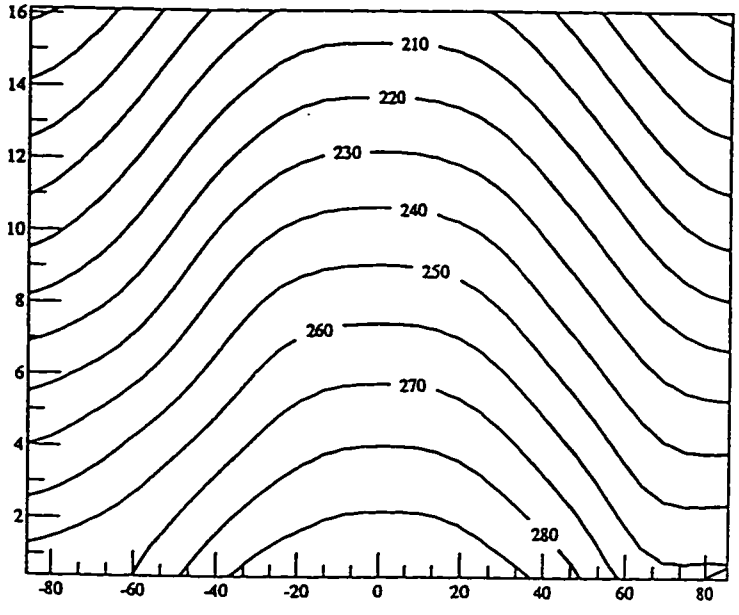

Figure 6.7 (continued): (e) the corresponding response in the zonal wind field (the deviation from the reference state shown in Fig 6.4a); contour interval is 2.5 m/s ; (f) the corresponding temperature distribution.

Chapter 7 Convective Processes and Tropical Atmospheric Circulation.

As was discussed in the previous chapter, diabatic heating plays an important role in the tropical dynamical circulation. Many of the simplified models of tropical dynamics often ignore the interaction between the dynamics and cumulus convection, which limits their applicability. In this chapter we will discuss the possible mechanisms of this interaction within the framework of the quasi-equilibrium theory for moist convection (*Arakawa and Schubert [1974]*).

The Betts-Miller computational convection scheme, which maintains the atmosphere in a state of near neutrality to reversible saturated ascent, will be presented and implemented in our model.

7.1 Conditional Instability vs Statistical Equilibrium

The following discussion is based on the *Emanuel et al. [1994]* review of the cumulus convection mechanism.

For a long time the dominant concept for describing the interaction between large-scale atmospheric circulation and moist convection implied that the convection acts as a heat source for the large-scale circulation, while the circulation supplies water vapor to the convection. *Charney and Eliassen [1964]* introduced the Conditional Instability of the Second Kind (CISK) theory to describe this kind of interaction. The main purpose of their theory was to explain the finite scale of the ascent region in developing tropical cyclones. Thus, *Charney and Eliassen* looked at convection as a heat source in an otherwise unsaturated atmosphere. Central to their concept was the idea that surface friction could promote the development of disturbances by inducing

convergent inflow and thus increasing the supply of moisture to the disturbances. In response, the heating due to precipitation strengthens the disturbance, which in turn, strengthens the convection. The central assumption in this theory was that the atmosphere is conditionally unstable to moist convection. This means that convection increases the potential energy of the column of air and thus serves as a source of energy that can be converted into the kinetic energy of the large-scale circulation. This implicitly assumes that the available potential energy (APE) contained in the conditionally unstable atmosphere can be converted to kinetic energy of the large-scale disturbance, i.e. heating itself leads to production of kinetic energy.

However, there exist serious discrepancies between the CISK theory and the observations. The CISK mechanism implies that the correlation between the heating and temperature fluctuations is positive. This positive correlation requirement for the disturbance energy to be produced is an inherent result of the external specification of heating in this case. However, observations show that, most probably, there is negative correlation between these variables (*Emanuel et al., 1994*)

Recently, the concept of conditional instability of the mean tropical atmosphere has been further undermined by observational data. Conditionally unstable soundings were only found in a few continental areas where severe convective storms originate.

In the tropics, large-scale upward motion is, certainly, associated with latent heat release, but the latent heating is nearly balanced by the combination of radiative and adiabatic cooling.

Betts [1982] was the first to note the correspondence between observed atmospheric profiles and a virtual moist-adiabatic lapse-rate(*) . *Xu and Emanuel*

(*)Virtual potential temperature is defined as the potential temperature that dry air would have if its

[1989] found that tropical profiles can be approximated by the virtual moist adiabatic profiles. All these observations reveal that convecting plumes probably carry the condensed water to at least some height. Thus, the process goes along a reversible virtual adiabat, rather than along irreversible moist adiabat, where the condensed water precipitates immediately. The observed near neutrality of the atmosphere to moist convection is then the result of rapid convective release of conditional instability whenever it appears.

Back in 1974 *Arakawa and Schubert [1974]* applied the theory of quasi, or statistical equilibrium to the problem of interaction between the convection and large - scale dynamics. This theory was later developed and summarized in *Emanuel et al [1994].*

In the framework of this approach, the large-scale circulation in convecting atmosphere is considered a result of the following:

- The real atmosphere is not conditionally unstable but rather nearly neutral to moist convection. Most of the convective systems are nearly in statistical equilibrium with their environment;
- The amount of convective available potential temperature (CAPE) in a moist convecting atmosphere, while not zero, is in most cases approximately invariant;
- The virtual temperature of a convecting atmosphere has approximately a one-to-one relationship with subcloud-layer entropy. Thus, predicting the response of subcloud layer entropy to large-scale disturbances would account for the major effects of convection.
- There is a small but nonzero response time of convection to large-scale forcing.

---

pressure and density were equal to those of a given sample of moist air.

The small departures from statistical equilibrium lead a negative correlation between convective heating and disturbance temperature and, thus, to damping of disturbances. The direct interaction of large-scale disturbances with convection is thus better described as moist convective damping (MCD) than as CISK.

The subcloud entropy can be changed in a few different ways. *Emanuel et al [1994]* argued that the most dramatic changes in the subcloud entropy are produced by convective downdrafts that, in turn, are caused by large-scale updraft motions. On the global scale of the zonally symmetric circulation, these updraft motions can be induced either locally by short wave radiative heating or non-locally by eddy-induced zonal forcing . The increasing large-scale updraft motion increases convection and therefore convective downdraft. Thus, these motions reduce the boundary layer entropy and, correspondingly, the free atmosphere temperature. In other words, the large-scale ascent "feels" an effective, positive static stability that, under typical conditions, is about an order less than the dry static stability *(Neelin et al, 1987).*

Recently several convection schemes based on statistical equilibrium thinking have been developed *(Betts and Miller, 1986; Emanuel, 1991).*

In the next section of this chapter, we will present the Betts-Miller scheme, and implement it in our model for studying of the meridional circulation in the tropical troposphere.

7.2 The Betts-Miller Scheme

The Betts-Miller scheme was designed to directly represent the quasi-equilibrium state established by convection. Quasi-equilibrium implies that the convective cloud field constrains the temperature and moisture structure of the atmosphere. The

scheme is based on observations that show the existence of quasi-equilibrium between the tendency of convection to stabilize the atmosphere, and the tendency of large scale forcing to destabilize it. If the model vertical column becomes unstable, then the model temperature and humidity profiles relax back to empirically derived quasi-equilibrium profiles over a small, but finite, timescale. As was discussed in *7.1*, the stability is assumed to be relative to a moist virtual adiabat which retains its condensed water. Different reference thermodynamic structures are used for shallow and deep convection. For deep convection, the reference profile is unstable with respect to a moist virtual adiabat extending from cloud base to the freezing level. Above the freezing level, the reference profile is approximated as an ice adiabat. For shallow convection, the reference profiles for temperature and moisture are assumed to lie along a constant mixing line between cloud base and the level of the inversion.

The convective scheme involves five computational steps:

1. Specification of the adjustment time scale.
2. Finding cloud base and cloud top using empirical formulas derived by *Bolton [1980].*
3. Determining first-guess reference profiles for shallow and deep convection
4. Correction of the first-guess reference profiles to satisfy the following set of constraints for shallow and deep convections.

Shallow convection does not precipitate but simply redistributes heat and moisture in the vertical. Thus, at each level we separately correct T and q to satisfy two separate energy constraints:

$$\int_{p_t}^{p_b} c_p\left(T_{ref} - \bar{T}\right)dp = \int_{p_t}^{p_b}\left(q_{ref} - \bar{q}\right)dp \qquad (7.1)$$

In deep convection, the total enthalpy remains constant and we modify the first-guess profiles until they satisfy the total enthalpy constraint

$$\int_{p_t}^{p_b} \left(k_{ref} - \bar{k}\right) dp \tag{7.2}$$

where $k = c_p T + Lq$ and the integral is through the depth of the convection layer.

5. Convective adjustment is then applied to the separate temperature and moisture fields as two tendencies

$$\left(\frac{\partial \bar{T}}{\partial t}\right)_{conv} = \frac{T_{ref} - \bar{T}}{\tau} \tag{7.3}$$

$$\left(\frac{\partial \bar{q}}{\partial t}\right)_{conv} = \frac{q_{ref} - \bar{q}}{\tau} \tag{7.4}$$

In order to satisfy these equations, the quantity:

$$\Delta k = \frac{1}{\Delta P_c} \int_{p_t}^{p_b} \left(k_{ref} - \bar{k}\right) dp \tag{7.5}$$

is calculated. T_{ref} is then adjusted at each level by an amount that changes k by Δk while maintaining the subsaturation at the same prescribed amount.

(The subsaturation parameter P is defined as $P = p^* - p$, where p^* is pressure at the saturation level). The first-guess reference profile is constructed through the low level equivalent temperature(*), thus the lowest level temperature remains unchanged.

(*) Equivalent potential temperature is defined as the potential temperature a parcel of air would have if all its water vapor were condensed and the latent heat converted into sensible heat.

This meets the requirement for the conservation of moist static enthalpy that adjusts the reference profiles and forces drying and cooling of the boundary layer. The precipitation rate in this case is given by :

$$PR = \int_{p_0}^{p_T} \frac{q_{ref} - \bar{q}}{\tau} \frac{\partial p}{g} = -\frac{c_p}{L} \int_{p_0}^{p_T} \frac{T_{ref} - \bar{T}}{\tau} \frac{\partial p}{g} \qquad (7.6)$$

If precipitation is less than zero, the shallow cloud scheme is called.

The application of the Betts-Miller scheme is attractive to us because of its conceptual simplicity, and the fact that within it the convection occurs solely in response to buoyancy and not from external factors like moisture convergence . This scheme was used in several atmospheric models and was reported to produce reasonable results *(Slingo et al, 1993, Seager and Zebiak, 1993)*

Before presenting the results of the implementation of the Betts-Miller convection scheme in our model, we will test it in a straightforward one dimensional case, and compare it with the results of Emanuel's convective scheme.

7.3 A Simple Radiative-Convective Equilibrium Calculation in the Presence of Large-Scale Ascent.

As a simple test of the new scheme a radiative-convective equilibrium calculation was performed. Assuming the atmosphere to be under some characteristic conditions over the tropical ocean (see *Emanuel, 1991*), the radiative cooling was specified to be 3×10^{-5} K/s. The compensating latent and sensible heat fluxes from the ocean were calculated according to bulk aerodynamic formulas.

The model was initialized using the sounding from the tropical western Pacific provided by Emanuel *(Emanuel, 1991)*, Fig 7.1, panels b,c,d. We ran the model for 40 days, and then averaged the fields over the last 5 days of the simulation. In this simple

case the net convective heating balances the radiative cooling everywhere, except for the boundary layer, where sensible and latent heat fluxes from the ocean are important.

Our next experiment included the effect of an imposed large-scale ascent. We introduced a large-scale upward velocity field by specifying a pressure velocity omega in the form:

$$\omega = 4\omega_m \left(\frac{(p_0 - p)(p - p_1)}{(p_0 - p_1)^2} \right)$$

where $\omega_m = -30mb/day$, p_0=1000 mb, p_1=150 mb. The profile of the vertical pressure velocity profile is plotted in panel (a) of Fig. 7.1 together with the initial temperature distribution (panel c), humidity distribution (panel d) and radiative cooling (panel b). The results are shown in Fig. 7.1 panels (e) - (l) together with the results obtained using Emanuel's scheme *(Emanuel, 1991)*.

The panels (e) and (g) show the total temperature tendencies for Emanuel's scheme and the Betts-Miller scheme, respectively. Except for the boundary layer, the convective heating compensates the radiative and advective cooling. The corresponding tendencies for the water vapor are shown in panels (f) and (h). Again, except for the boundary layer with latent heat fluxes from the ocean, the convection fully compensates the advective term.

The mechanism of this compensation can be easily understood by examining the profiles on Fig. 7.1. The convective heating has a maximum in the middle troposphere, thus compensating for the additional adiabatic cooling due to large-scale upwelling (see panels (i) for Emanuel's scheme and (k) for the Betts-Miller scheme). The net drying of the troposphere due to convection (panels (j) and (l) respectively) also

compensates the moistening by the large-scale flow.

The one dimensional experiment with the Betts-Miller scheme described above produces reasonable profiles of temperature and relative humidity. The results do not differ significantly from the experiments with Emanuel's scheme. Thus we can be confident that the Betts-Miller scheme works correctly. We have chosen to use Betts-Miller scheme (as opposed to the Emanuel's scheme) for parameterization of the cumulus convection in our zonally averaged model because of the following:

- its conceptual simplicity
- the absence of the closure parameters that have to be tuned for the model
- the relatively short time required for computation.

In the next section we will discuss the results of the implementation of Betts-Miller convection scheme in our model, and the influence of the cumulus heating upon the mean meridional circulation in the tropical troposphere..

7.4 The Influence of the Internally Specified Cumulus Convection on the Tropical Mean Meridional Circulation in the 2D Model

As was discussed in the previous sections, it is important to examine not only the role of the diabatic cumulus heating itself in maintaining the tropical circulation in the troposphere, but also the nonlinear interaction between the dynamics and cumulus convection. In this section we describe an experiment that was specially designed for this purpose.

The 2D model described in Chapter 4 was used with the following initial conditions and specified forcing. In the troposphere (1000 mb - 100 mb) we specified the temperature profile which corresponds to an idealized approximation of the

radiative equilibrium temperature in July. The maximum in the temperature distribution is shifted northward off the equator (Fig. 7.2a). The initial distribution of humidity is shown in panel (d) on the same figure.

The first run of the model contained neither convection nor zonal forcing terms. The temperature was just allowed to relax toward radiative equilibrium. The meridional circulation obtained is shown in Fig. 7.3b. The circulation consists of two cells, with air ascending in the tropics of the Northern Hemisphere and then descending in mid-latitudes of the Northern and Southern Hemispheres. Overall, the circulation is fairly weak. The corresponding zonal velocity is shown in Fig. 7.4b. The westerly jets are located at the tropopause level. In the winter hemisphere, the jet is more intense and is located closer to the equator. The zonal velocities at the equator are weak and easterly. This circulation pattern differs significantly from the observations, therefore, the following set of experiments was performed.

The eddy-induced zonal forcing, the distribution of which is shown in Fig. 7.2b, was included in the next run (however, this run still did not contain cumulus convection). The corresponding horizontal eddy temperature fluxes are shown in Fig. 7.2c. The resulting circulation (Fig. 7.3a) is more than twice as intense than the previous one. Ferrel cells exist in both Southern and Northern Hemispheres. The zonal velocity at the equator (Fig. 7.4a) becomes larger. Though this circulation is closer in intensity to the observed circulation, its pattern is still very different.

In the third experiment we examined the role of the cumulus convection alone. We excluded the zonal forcing, but included the Betts-Miller parameterization of the cumulus convection, The streamfunction in this case (Fig. 7.3d) is much stronger than in the two previous experiments. The maximum of the mass stream function is shifted

upward toward the 400 mb level. The corresponding zonal velocity (Fig. 7.4d) is stronger, especially in the summer hemisphere. Overall this run shows better correspondence to the observed circulation in the summer hemisphere, but the simulated pattern in the winter hemisphere still differed significantly from the observations.

The last experiment combined both diabatic heating and mechanical eddy zonal forcing. The resulting meridional circulation shown in Fig 7.3c looks more realistic than the meridional circulation in the previous runs. The maximum in the mass stream function is located in the tropics of the Southern Hemisphere at around 7°S and at 400 mb. The secondary Hadley cell in the summer hemisphere is much weaker. It is nearly as intense as the Ferell cell in the Southern Hemisphere at this time.

The zonal velocity field shown in Fig. 7.4c exhibits strong mid latitude westerly jets near the tropopause. The winter jet is much stronger than in all the previous cases. The easterlies at the equator are also stronger in this case. Thus, including both cumulus heating and eddy-induced zonal forcing dramatically improves the results of the simulation in both intensity and pattern.

We can examine the role of different mechanisms in maintaining the meridional circulation by a simple subtraction of the results from the runs where only the mechanism we are not interested in was present from the last complex run.

The effect of large-scale cumulus convection is shown in Fig. 7.3e. The streamfunction formed as a difference between the streamfunction obtained from the experiment with convection and eddy forcing, and the streamfunction obtained from the experiment with eddy forcing only, consists of two Hadley cells with the winter cell being broader and much more intense. The Hadley cell in the summer hemisphere

is comparable to the Ferell cell in the winter hemisphere. The maximum of the mass flux is lifted from the 800 mb to the 400 mb level.

By comparing Fig. 7.3d and Fig. 7.3e we note that there is a nonlinear interaction between the cumulus convection and the eddy induced circulation. This nonlinear effect is shown in panel f (the streamfunction presented in this panel was constructed by the following rule: $\psi_f = \psi_c - ((\psi_d - \psi_b) + (\psi_a - \psi_b))$, where subscripts denote the panels' names). The meridional circulation due to this nonlinear interaction is comparable in strength to the circulation induced by the asymmetry of the radiative equilibrium temperature. The circulation is strengthened in the Northern Hemisphere. This nonlinear term produces a wide cell with the upward motion in the tropics of the Northern Hemisphere and descent in the Southern Hemisphere. This Hadley cell is accompanied by a narrow Ferell cell in the Southern Hemisphere.

The experiments discussed above can be summarized as follows:

- The cumulus heating and eddy zonal forcing play significant roles in maintaining the meridional circulation in the tropical troposphere.
- If the cumulus heating is parameterized in the framework of the quasi-equilibrium theory, the nonlinear interaction between the cumulus convection and eddy zonal forcing is comparable to the effect of radiative cooling of the atmosphere due to asymmetry about the equator.
- The cumulus heating not only intensifies the Hadley circulation, but it also lifts the maximum of the mass flux from the lower into the middle-upper troposphere.
- The EP fluxes themselves are responsible for the appearance of the Ferell cells in both hemispheres. They also intensify the easterlies at the equator in the upper troposphere.

The last physical mechanism that we have not discussed yet is radiation and its coupling with the large-scale atmospheric dynamics. The next chapter focuses on incorporation of a radiative code into our model.

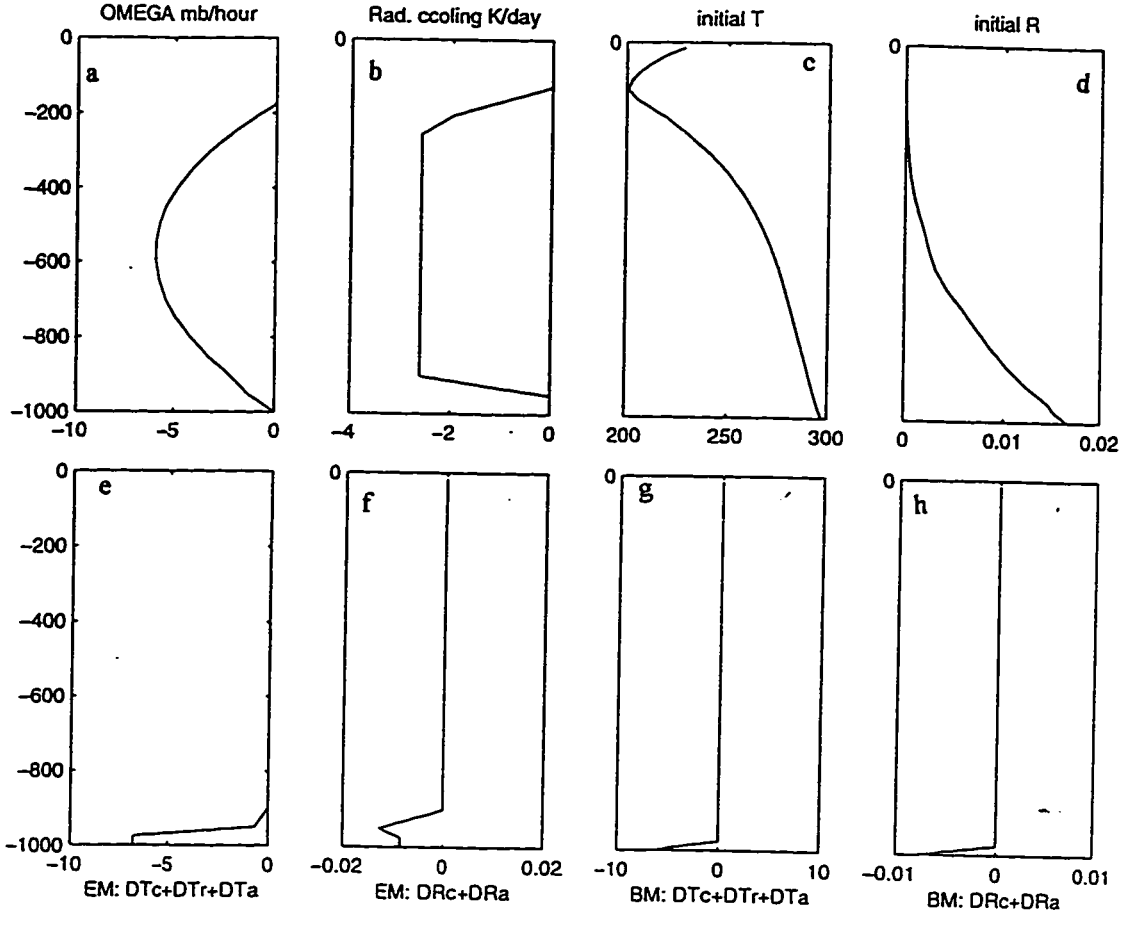

Figure 7.1: Vertical profiles of: (a) the vertical pressure velocity in mb/hour; (b) radiative cooling in K/day; (c) the initial temperature distribution; (d)initial humidity distribution; (e) total temperature tendency for Emanuel's scheme; (f) total humidity tendency for Emanuel's scheme; (g) same as (e) but for the BM scheme; (h) same as (f) but for the BM scheme.

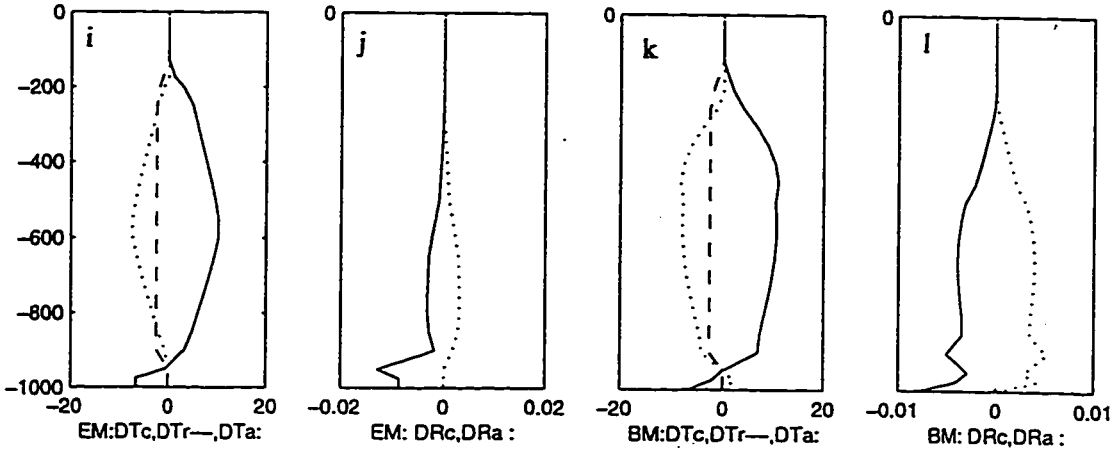

Figure 7.1 (continued): (i) the convective heating (solid line), radiative cooling (dashed line) and advective heating (dotted line) for the Emanuel's scheme; (j) same as (i) but for the humidity tendencies; (k) same as (i) but for the BM scheme; (l) same as (k) but for the humidity.

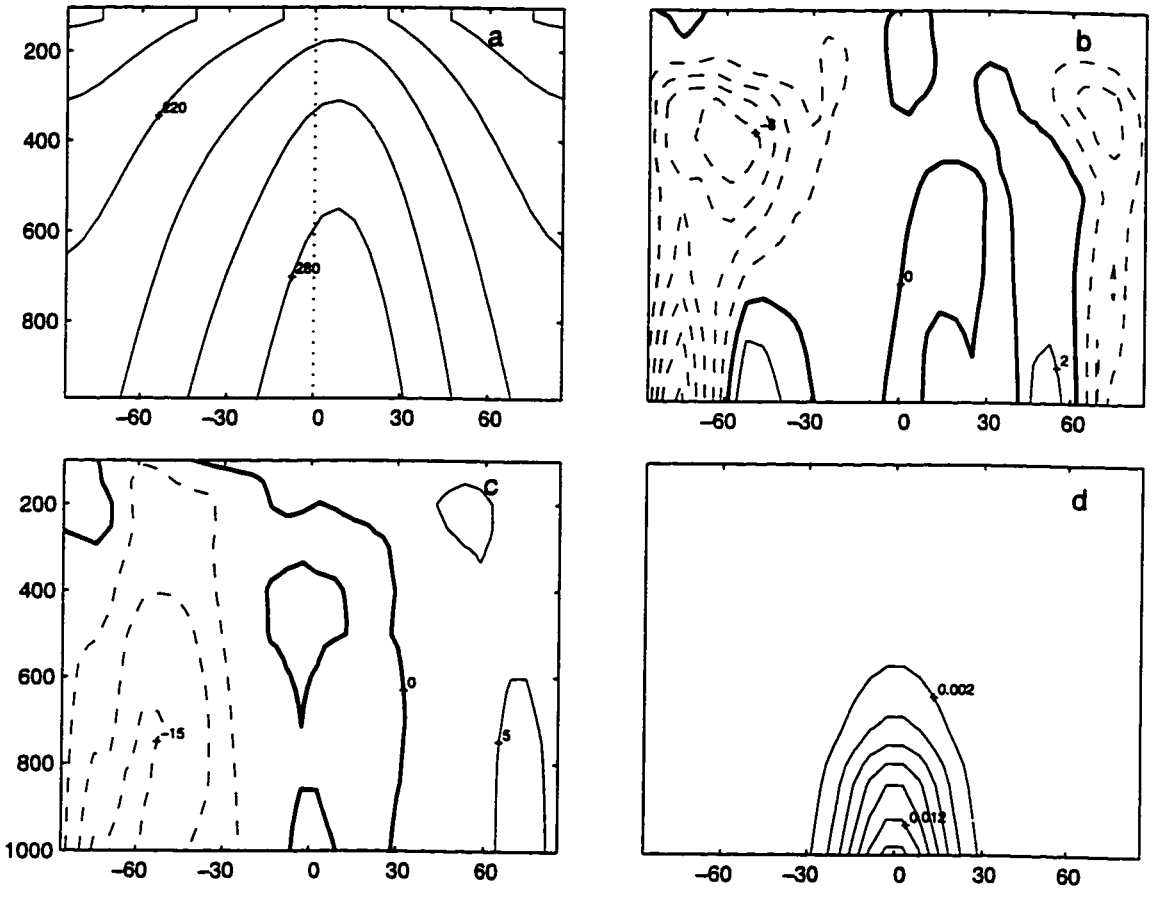

Figure 7.2: Height-latitude sections of some meteorological variables in July. (a) temperature field, contour interval 20K; (b) EP flux divergence, contour interval 2m/s/day; (c) meridional temperature eddy flux, contour interval 5 K·m/s ; (d) water vapor, contour interval 2 g/kg; The data is based on the NCAR/NCEP reanalysis data and NCAR *(Randel, 1992)* data

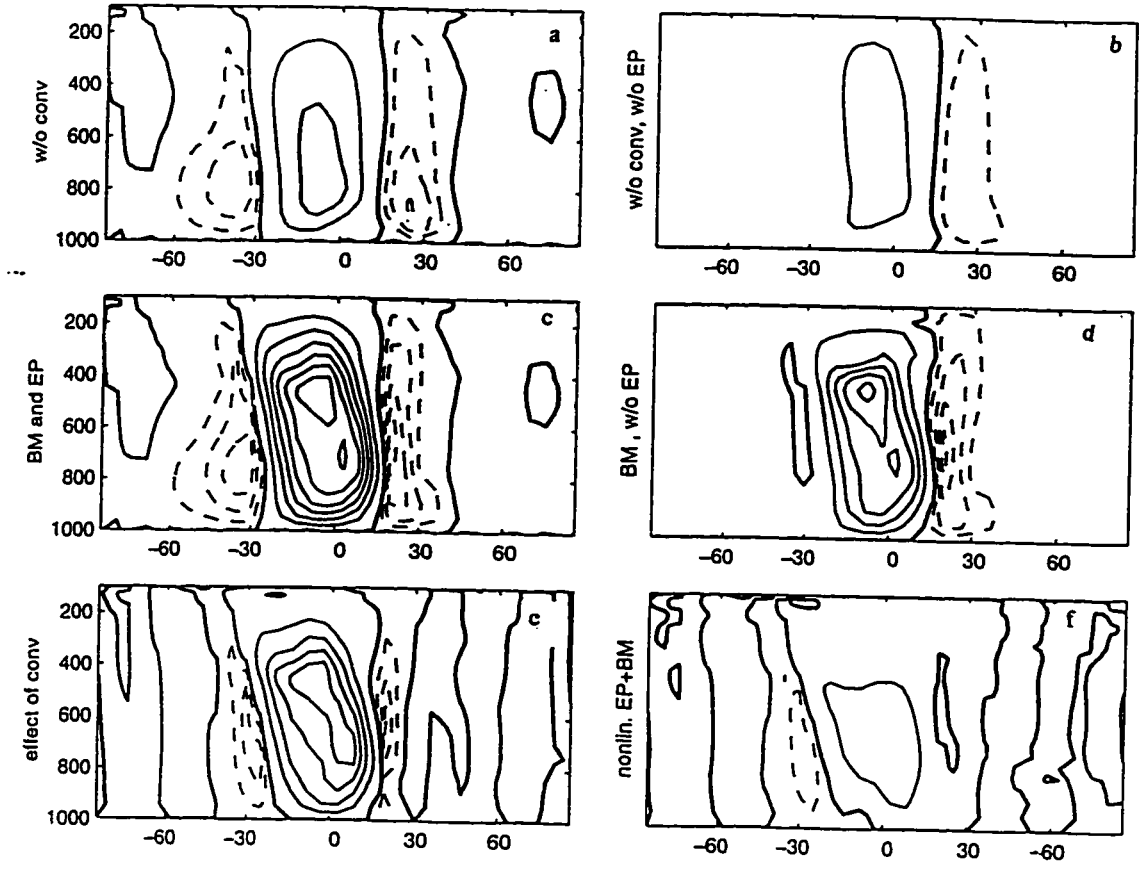

Figure 7.3: The EM mass streamfunction distribution resulting from the experiment containing (a) eddy zonal forcing without convection; (b) neither eddy forcing, nor convection; (c) convection and eddy forcing; (d) convection without eddy forcing; (e) difference between (c) and (a); (f) nonlinear coupling between the convection and zonal eddy forcing.

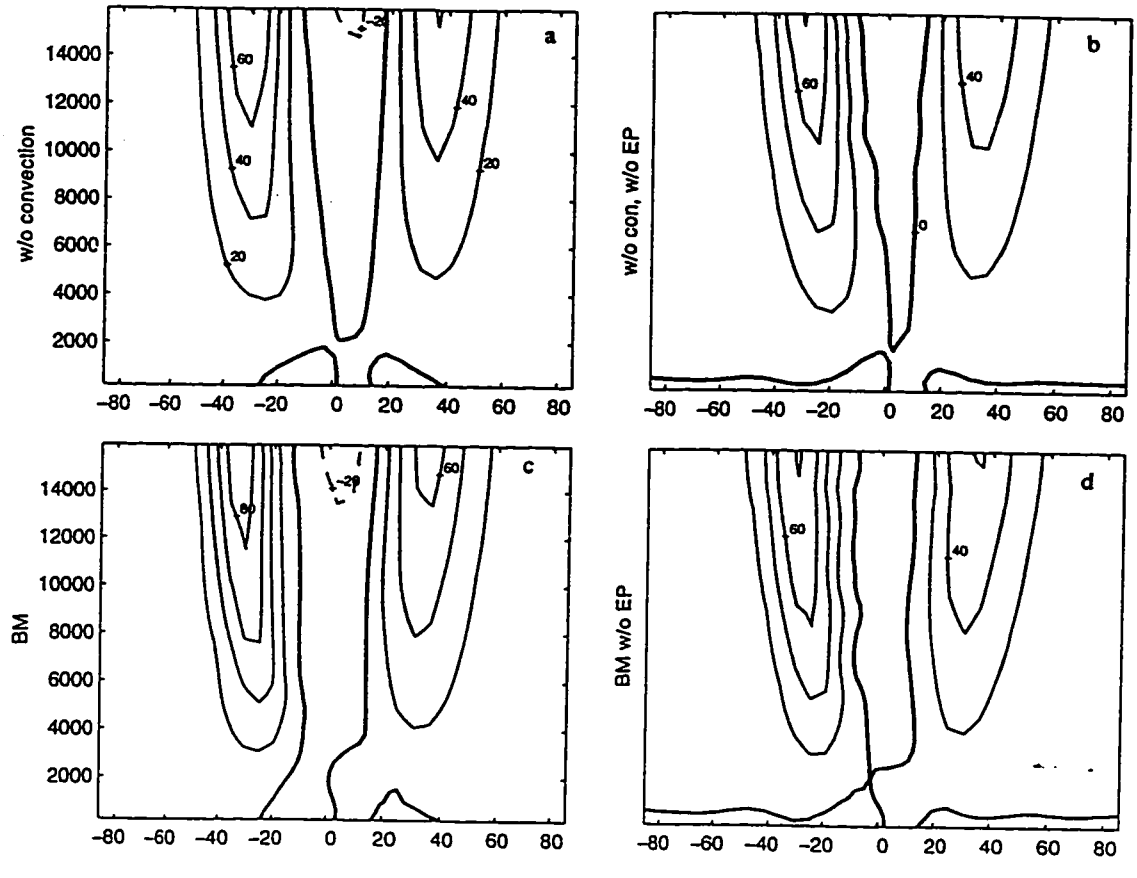

Figure 7.4: The zonal wind velocity distribution resulting from the experiment containing (a) eddy zonal forcing without convection; (b) neither eddy forcing, nor convection; (c) convection and eddy forcing; (d) convection without eddy forcing.

Chapter 8 Radiative Processes.

The next step in the model development involves a more detailed representation of radiative processes. The implementation of the radiative code, with the emphasis on the feedback mechanisms between the radiation, dynamics and cumulus convection is the focus of this chapter.

Previously, the radiative part of the diabatic heating (except for the relaxational Newtonian cooling) was specified in the model externally (see *Chapter 4*). The drawbacks of this kind of parameterization are that it can lead to significant deviations from observed heating rates and does not include the radiative - dynamical coupling. By contrast, internally computed diabatic heating in a radiative module would produce heating rates that are coupled through the temperature field with the dynamics and cumulus convection.

This chapter starts with a description of the radiative code we utilized, its main advantages and possible drawbacks. It is followed by a description of the climatological distribution of the main input chemical species in the troposphere and stratosphere. At the end we will briefly discuss the radiative heating/cooling rates calculated with this radiation code for the specific months.

8.1 Radiation and its Coupling with the Large-Scale Dynamics

In Chapter 5 we noted that accurate calculation of the mean meridional circulation induced by diabatic heating requires that the feedback between the dynamics and the radiative transfer be incorporated into the model. The importance of such computations for deriving of the meridional transport circulation in the stratosphere

have been recently emphasized in works of *Solomon et al., [1986]; Rosenfield et al., [1987]; Olaguer et al., [1992]*.

Stephens [1984] in a conceptual review of modern radiative codes, distinguished between three main components of radiative heating:

- longwave cooling,
- shortwave heating, and
- cloudiness

As to the first component, a model implementation of **infrared (IR) codes** depends upon the purpose of the model. Diagnostic models typically use more sophisticated and time consuming algorithms, such as line-by-line computational models (see *Fels and Schwarzkopf, 1981*). To the contrary, prediction models implement more numerically efficient, though less accurate algorithms.

The treatment of the second component, **solar heating,** is more straightforward, though the inclusion of multiple scattering poses some difficulties (see *King and Harshvardhan, 1986*).

The third component, dealing with the effect of **the clouds** , is also very important for correct radiative computations, though less studied and more difficult in formulation (*Haigh, 1984*).

Recent diagnostic studies of the stratospheric radiation field *(Pawson and Harwood, 1989; Rosenfield et al., 1987; Kiehl and Solomon, 1986*) have shown that the main difficulties in evaluating of the net radiative heating arise in the region of the tropical tropopause, where the equatorial lower stratosphere is very close to the radiative equilibrium. It follows, that the radiative code should be both sufficiently comprehensive and accurate (especially for the region of the tropical tropopause), and

also fast enough to be used in our prognostic model.

An appropriate kind of radiative code was developed and tested by *Olaguer et al. [1992].*They demonstrated that the exclusion of the clouds from both long and short-wave radiative algorithms does not have any significant effect on the net heating in the stratosphere. However, it significantly affects the tropospheric heating rates. Their research emphasized a proper treatment of the IR absorption of ozone, which would result in a better balance in the region of the tropical tropopause. Full descriptions of this code can be found in *Yang et al. [1991]* and *Olaguer et al. [1992]*; here we briefly summarize its main features:

- The code consists of two modules:
  a solar heating computation, with input fields: O, O_3, H_2O, N_2O, CO_2;
  an IR heating computation, with input fields: CO_2, O_3, H_2O, CH_4, N_2O
- The code includes the effect of multiple scattering
- Input of the vertical profile of temperature is required.
- The effect of the clouds is also included (the clouds are parameterized for each specific month)

The code (hereafter referred to as Olaguer-Yang-Tung (OYT) code) was originally designed and tested for calculation of the diabatic heating rates in the stratosphere. We tested this radiative code for the tropospheric climatological monthly mean heating rates computation, and found it to be suitable for our model calculation of the diabatic heating rates in both stratosphere and troposphere.

8.2 Description of the Input Data Used to Examine the Seasonal Variability

For the purposes of our studies of the seasonal behavior of the large-scale dynamics in the region of the tropical tropopause, we need to calculate the monthly mean radiative heating rates in the troposphere and stratosphere. The diabatic heating was computed using the OYT code with the combined HALOE V17 (ozone, water vapor and methane) and UARS (NO, N_2O) climatological mean data, prepared by K. Rosenlof (personal communication) for the period 1992 - 1995. The constituents data were put into the UARS standard grid vertically which extends vertically from 1000 to 1 mb, with 49 levels. The latitude grid is equidistant starting at 87.5°S with 5° interval. A constant value of CO_2 at 350 ppm was used. The distribution of ozone (panel b) and water vapor (panel c) for July and January are plotted in Fig. 8.1 and Fig. 8.2 respectively. Qualitatively these fields bear a close resemblance to the SBUV, LIMS and Nimbus 7 SAMS observations discussed in *Yang et al [1991]* . The temperature fields for January and July are shown in Fig. 8.1a and Fig. 8.2a.

The model total radiative heating rates for January and July calculated using the above inputs are shown in Fig. 8.1d and Fig. 8.2d. These results may be compared with the heating rates reported by *Olaguer et. al. [1992]*. The discrepancies of a few tenths of K/day in the lower stratosphere are due to the use of different input data. However, qualitatively, the heating rates do not differ significantly. Thus, we can proceed with implementing the radiative code in our 2D model.

Since the radiative code is very time-consuming we recalculated the heating rates every 24 hour (compared to the 5 - 10 min dynamical time-step). The input for the radiation block during the perpetual January or July runs remained the same except for the input temperature and water vapor distributions, which were taken from the

last time step of the dynamical part.

Of course, the above described radiation computation is oversimplified and does not take into consideration the transport of the chemical species in the troposphere and stratosphere. However it does account for the feedback between the dynamics, radiation and cumulus convection through the recalculation of the heating rates with the temperature and the water vapor profiles modified by the dynamical processes in the previous time step. Thus this radiation transfer parameterization is quite appropriate for study of the seasonal variability of the tropical dynamics in a 2D model.

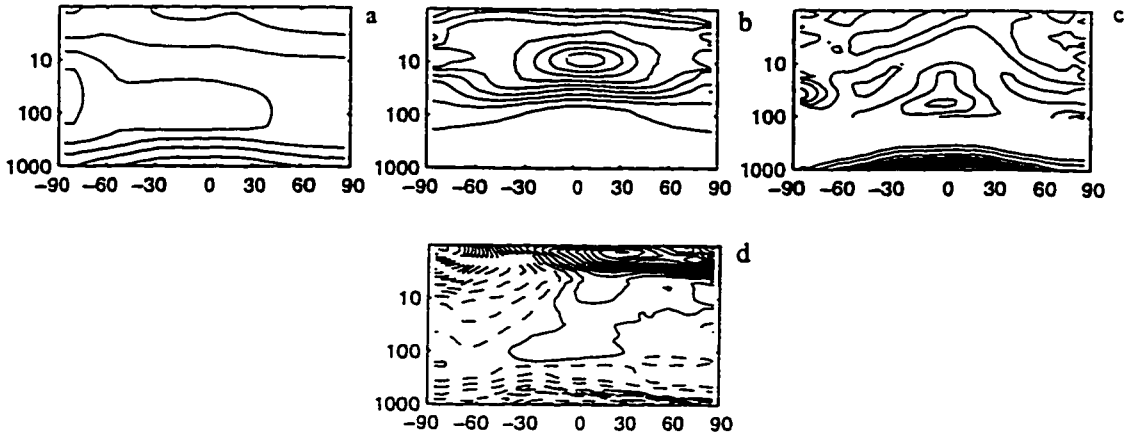

Figure 8.1: The distribution of the radiative block input fields for January: (a) temperature, contour interval 20 K, minimum value in the stratosphere 200K ; (b) ozone, contour interval 1 ppmbv, maximum in the tropical lower stratosphere is 10 ppmbv ; (c) water vapor , contour interval 1 ppmbv in the stratosphere, local maximum in the tropics there is 4 ppmbv; contour interval in the troposphere is 1000 ppmbv; (d) resulting radiative cooling/heating, contour interval is 0.5 K/day.

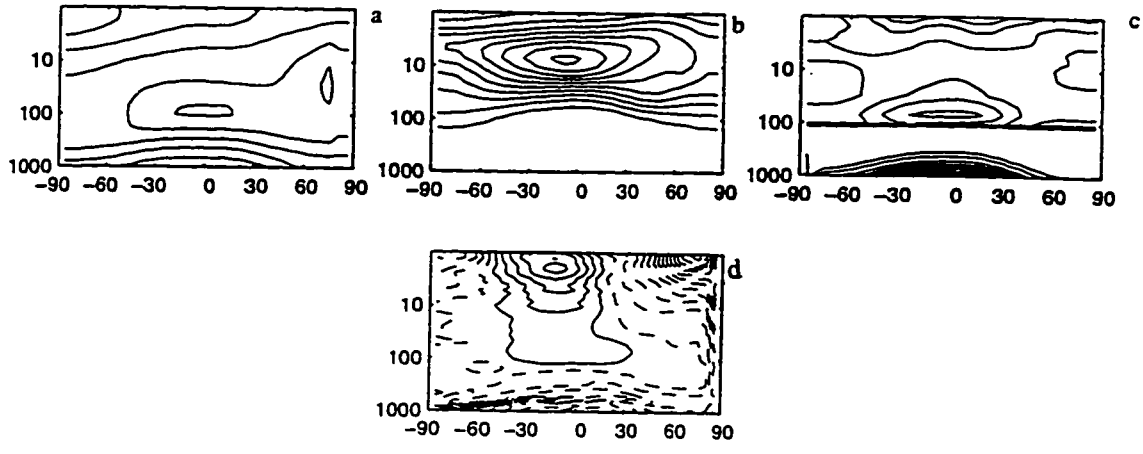

Figure 8.2: Same as in Figure 8.1 but for July.

Chapter 9 Simulation of the Seasonal Variability of the Upward Mass Flux in the Region of the Tropical Tropopause.

As discussed in Chapters 1 - 6, the observed seasonal variability of the vertical mass flux through the tropical tropopause is a manifestation of the annual variability of the meridional circulations in the stratosphere and the troposphere. These annual marches can be caused by a number of physical mechanisms including seasonal variability in radiative heating/cooling, in eddy zonal forcing and in cumulus convection coupled with the tropospheric dynamics. The dynamical processes in the tropics are inherently nonlinear, therefore an analytical description of the meridional circulation in this region is practically impossible. Thus, the only way to test the relative roles of the different physical mechanisms involved in this variability is to run numerical experiments with a model. A specially designed zonally symmetric spectral model was discussed in Chapter 4. We also described the different parameterizations of the cumulus convection and radiative heating that were incorporated into the model. With all the reasonable physical mechanisms included, we ran the experiments which helped us to clarify the role of the processes described above in maintaining the observed monthly mean climatological state. This chapter documents these experiments and discusses the main results.

9.1 January-July Difference in the Upward Mass Flux in the Region of the Tropical Tropopause.

The primary purpose of the first set of experiments was to determine the relative role of the eddy forcing in maintaining the observed upward mass flux in the region of

the tropical tropopause. All the common input parameters for the model experiments were taken to be the same as described in Chapters 5 and 6.

First, the zonally averaged circulation maintained by the radiative heating/cooling alone in the stratosphere and by the radiative heating/cooling and cumulus heating in the troposphere (hereafter referred to the basic state) was obtained. The cumulus heating was parameterized using the Betts-Miller scheme discussed in Chapter 7. The initial distribution of water vapor for the perpetual January run is shown in Fig. 8.1 (panel c) along with the initial temperature distribution (panel a). The spatial distributions of the chemical species involved in the radiative heating computations were discussed in Chapter 8 and are shown in Fig. 8.1. We ran the model for 3 months and then averaged the last month of output data.

The resulting latitude profile of the meridional mass stream function at the 100 mb level is shown in Fig. 9.1 (b). In comparison with the latitude section of the climatological mean meridional mass stream function in January deduced from the NCAR/NCEP reanalysis data (Fig. 9.1c), the upward mass flux of the simulated basic state is three times weaker. The simulated meridional cell extends from 50°N to 60°S, wider than the observed meridional circulation, which extends from 40°N to 30°S. This result suggests that radiative heating/cooling and cumulus heating alone can not maintain the observed meridional circulation, therefore an additional physical mechanism should be taken into consideration.

As was noted in our previous discussion, the eddy induced zonal forcing should be considered as a potentially important physical mechanism maintaining the observed seasonal variability of the meridional circulation in the region of the tropical tropopause. Thus, the *second set of experiments* included the eddy induced forcing,

shown in Fig.9.2. The EP flux divergence was calculated using the NCAR/NCEP data for the poleward eddy momentum and temperature fluxes (*Randel, 1992*). As in the previous case, we ran the perpetual January computation for 3 months, and averaged the results for the last 30 days. The meridional profile of the mass stream function at the 100 mb level is shown in Fig. 9.1 (a). The pattern bears remarkable similarity to the observed circulation (panel c). The northward meridional cell is confined between approximately 40°N and 30°S. The strength of the mass flux does not differ significantly from the observed one and reaches its maximum of 480 $kg \cdot m^2/s$ in the tropics of the Southern Hemisphere.

An analogous set of experiments was performed for perpetual July conditions with the initial temperature and water vapor distribution shown in Fig. 8.2 (a, c). The results are shown in Fig. 9.1, panels d-f.

The "basic state" circulation (i.e. with only radiative forcing) is in the opposite direction of the observed circulation and is extremely weak. Inclusion of the eddy induced zonal forcing shown in Fig. 9.2 (b) greatly improves the meridional circulation. Panel (d) presents latitude profile of the simulated mass stream function for this case. The shape of the pattern in the low and middle latitudes closely resembles the shape of the observed southward meridional circulation. The absolute maxima of about 100 $kg \cdot m^2/s$ are reached at around 30°S and 15°N - 20°N. The main difference is observed in the high latitudes of the Southern Hemisphere. A strong thermally direct meridional circulation is present in the high latitude region of the Southern Hemisphere in the observed NCAR/NCEP data. However, the cause of this part of the circulation is beyond the topic of our study and will not be discussed in this Chapter.

The third set of experiments was designed to separate the effects of the stratospheric and tropospheric eddies. This set of experiments differed from the previous one in only one aspect: the eddy zonal forcing in the troposphere was considered to be zero. The resulting 100 mb mass stream functions (not shown here) for January and July do not differ significantly from the mass stream function shown in panels (a) and (d).

The main results of our simulation experiments can be summarized as follows:

- The radiative heating/cooling in the stratosphere and radiative heating/cooling combined with the cumulus heating produce, at the 100 mb level, a meridional circulation which significantly differs from the observed one. It is very weak, and its direction does not always coincide with the direction of the observed meridional circulation. The tropical cell in the simulations is wider, than the observed one.
- Inclusion of the eddy zonal forcing significantly improves the simulated circulation. The tropical pattern in this case closely resembles the observed circulation, and the strength of the mass flux is comparable to the observed.
- Exclusion of the eddy induced zonal forcing in the troposphere does not alter the 100 mb mass stream function from that based on the full eddy forcing.

Therefore, the main difference between the upward mass fluxes in July and January is caused by the difference in the EP-flux divergence patterns in the stratosphere, and the seasonal variability in the region of the tropical tropopause is maintained by the seasonally varying eddy zonal forcing in the stratosphere. These modeling results confirm our previous hypothesis concerning the role of the eddy forcing in maintaining the observed annual march of the upward mass flux in the region of the tropical tropopause (*Chapter 3*).

Another interesting question raised in Chapter 3 is the role of the eddy induced zonal forcing in maintaining the seasonal variability in the middle troposphere. Can the observed difference in the circulation during the transition periods April-May (hereafter referred to as spring) and October-November (hereafter referred to as fall) be explained solely by the difference in the cumulus heating, or should the seasonal variability of the eddy induced zonal forcing also be taken into consideration? The next section discusses the modeling results on this subject.

9.2 The Differences Between the Spring and Fall Circulation.

The patterns of the zonally averaged circulation in the troposphere during two transitional seasons were compared and contrasted in Chapter 3. We described the differences between the observed spring and fall circulations, and speculated on the possible causes of these differences. The main question that remains to be answered is whether the observed differences in the meridional circulation and in the zonal wind velocity fields can be explained by the differences in the cumulus heating alone, or should the eddy induced zonal forcing also be taken into the consideration?" To address this question we performed a set of numerical experiment with our 2D zonally averaged model described in Chapter 4.

First, we ran the model for perpetual fall and spring zonally averaged conditions excluding eddy induced zonal forcing. The temperature and cumulus heating distribution were deduced from the reanalysis data shown in Fig. 3.13 and Fig. 3.14 (see Chapter 3), and repeated in Fig. 9.5. Thus, in contrast to the previous experiments discussed in section 1, the cumulus heating was externally specified, and not given by the Betts-Miller parameterization. As in previous experiments, the

model was run for three months, and the results for the last month were averaged. Fig. 9.3 (a) depicts the differences between the simulated fall and spring zonal velocity fields. The Northern Hemisphere mid-latitude westerly jet stream is closer to the equator during spring than during fall. At the same time in April-May we observe relatively weak westerlies in high latitudes of the Northern Hemisphere and in mid-latitudes of the Southern Hemisphere. Although the distribution of the simulated zonal wind bears a qualitative resemblance to the observed zonal wind shown in Fig. 9.3g, there still exist a few discrepancies that can be summarized as follows:

- The difference between the April-May and the October-November maximum wind in the simulated mid-latitude westerly jet is stronger than observed;
- In comparison to the observations, the position of the Southern Hemisphere region of relatively weak April-May westerlies is shifted toward the equator;
- In mid-latitudes of the Northern Hemisphere the simulated westerly zonal wind is stronger during the spring time than during the October-November, whereas the observed wind in this region exhibits the opposite tendency.

The simulated meridional circulation difference shown in Fig. 9.3 (d) also agrees with the observed (Fig. 9.3 h) quite well in the tropics, but the cell in the northern subtropics is too weak, and the cell centered at the equator is too wide.

These discrepancies between the model results and the observed circulation suggest that some additional forcing should be included in the experiments. Thus, the second set of experiments included as input the eddy-induced zonal forcing, which was also deduced from the NCAR data analysis. The distribution of the EP-flux divergence for the spring and fall transition periods are shown in Fig. 9.4, panels (a) and (b) respectively. The difference between these two seasons is depicted in panel

(c) of the same figure. As in the first experiment, we ran the model for perpetual spring and fall seasons, and then averaged the output for the last month of experiment. The resulting zonal wind velocity (panel (c) in the Fig. 9.3) qualitatively resembles the wind distribution simulated in the previous experiment. However, it bears a closer resemblance to the observed zonal wind. The difference between the April-May and the October-November maximum wind in the simulated mid-latitude westerly jet in the Northern Hemisphere is weaker than in the previous experiment and closer to the observed. In addition in mid-latitudes of the Northern Hemisphere the simulated westerly zonal wind is weaker during the spring time than during the fall, in agreement with observations. The meridional mass stream function shown in panel (f) of the same figure, reveals three distinct cells in the Northern Hemisphere. The comparison of this figure with the observations (Fig. 9.3h) proves that the inclusion of the eddy-induced zonal forcing slightly improves the resulting meridional circulation. Though the simulated subtropical Northern Hemisphere cell is weaker than the observed, simulated and observed patterns of the meridional mass circulation are qualitatively very similar.

The only question that remains unresolved is: Does the spring-fall asymmetry in the eddy induced zonal forcing play a crucial role in determining the observed difference in the circulation during these transition periods? To address this question we ran a third model experiment similar to the one discussed above, except that the eddy induced zonal forcing was the same during the spring and the fall seasons. The simulated zonal wind velocity and mass stream function (shown in panels (b) and (e) respectively) exhibit only minor differences form the corresponing fields from the experiment that does not include eddy induced zonal forcing. Therefore, the seasonal

variability of the meridional circulation in the troposphere is partly caused by the seasonal variability of the eddy-induced zonal forcing, however, the cumulus heating variation plays the primary role in determining the structure of the meridional circulation and the zonal wind distribution.

In summary, our numerical experiments with the complete model lead to the following conclusions:

- The annual march in the upward mass flux in the region of the tropical tropopause is a manifestation of the seasonal variability in the meridional circulation in the lower stratosphere. This variability is dominated by the eddy induced zonal forcing in the stratosphere.
- The seasonal variability of the zonal wind in the upper troposphere is largely determined by the variation in cumulus heating.
- The cumulus heating also determines the main patterns of the mean meridional circulation in the troposphere.
- The eddy-induced zonal forcing partially controls the seasonal variability of the meridional circulation in the troposphere, especially in extratropics and high latitudes.

The experiments with the model reveal the relative role of the main physical mechanisms in maintaining the seasonal variability of the mean meridional circulation in the troposphere and lower stratosphere. The next and final chapter discusses the main results of our numerical experiments combined with the analysis of the observational data.

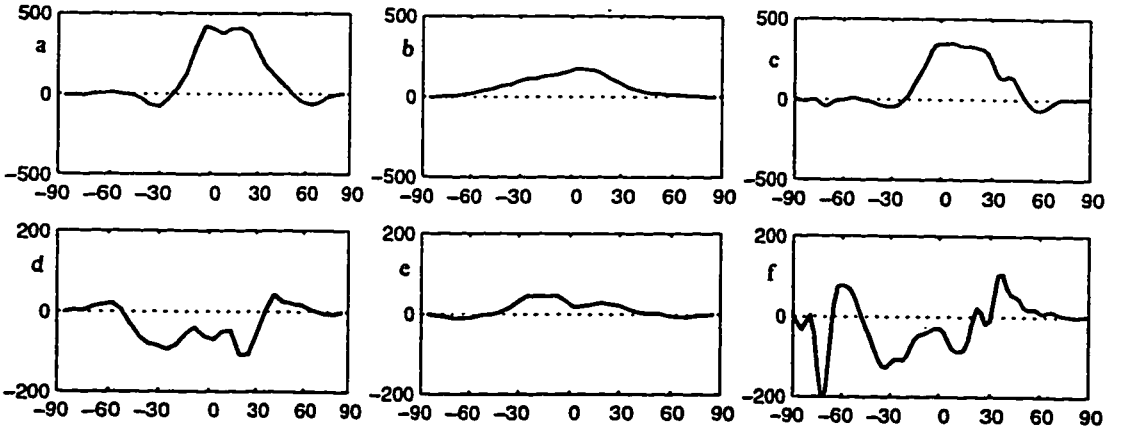

Figure 9.1: The simulated and observed mass streamfunction at the level of the tropical tropopause. (a) The simulated mass streamfunction for January, eddy zonal forcing included; (b) The simulated mass streamfunction for January, without eddy zonal forcing; (c) The mass streamfunction deduced from NCAR/NCEP reanalysis data; (d), (e) and (f) same as (a), (b) and (c) but for July.

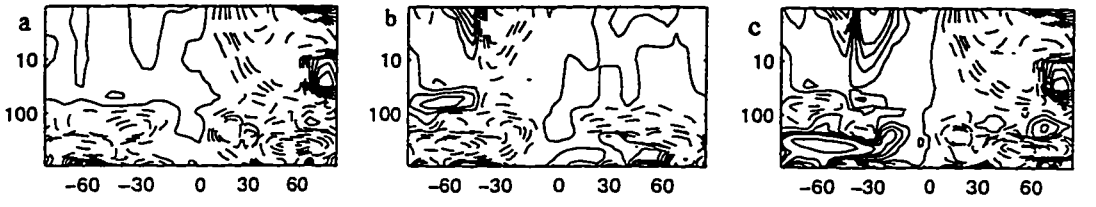

Figure 9.2: EP flux divergence in m/s/day for (a) January, contour interval 2m/s/day; (b) July; (c) Difference between January and July, contour interval 0.5 m/s/day

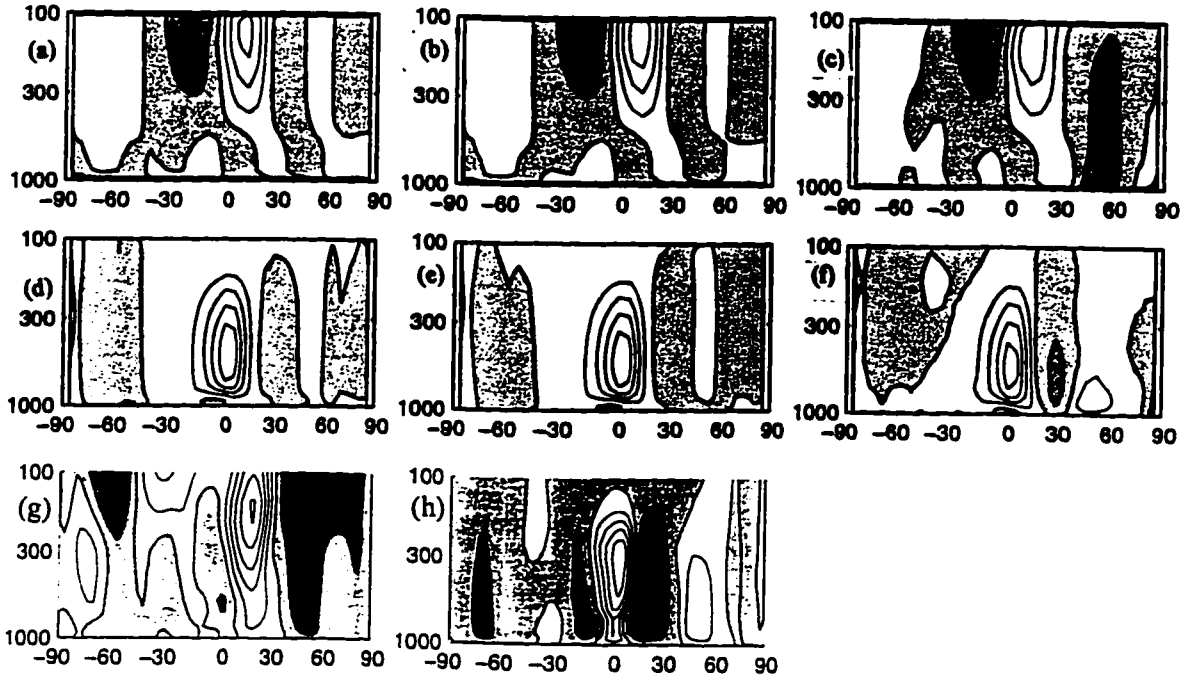

Figure 9.3: Simulated spring - fall difference in the zonal wind velocity; contour interval 2m/s, (a) zonal eddy forcing excluded, (b) zonal eddy forcing is included and is the same for both periods, (c) zonal eddy forcing is included and is different for these two periods, (g) observed from Fig. 3.13
Simulated spring - fall difference in the meridional mass streamfunction; contour interval 250 kg/s (d) zonal eddy forcing excluded, (e) zonal eddy forcing is included and is the same for both periods, (f) zonal eddy forcing is included and and is different for these two periods, (h) observed from Fig. 3.13

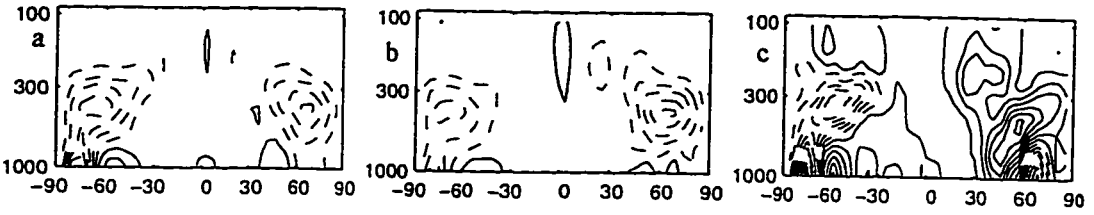

Figure 9.4: EP flux divergence in m/s/day for (a) NH spring, contour interval 2m/s/day; (b) same as (a) but for the NH fall; (c) spring-fall difference, contour interval 0.5 m/s/day

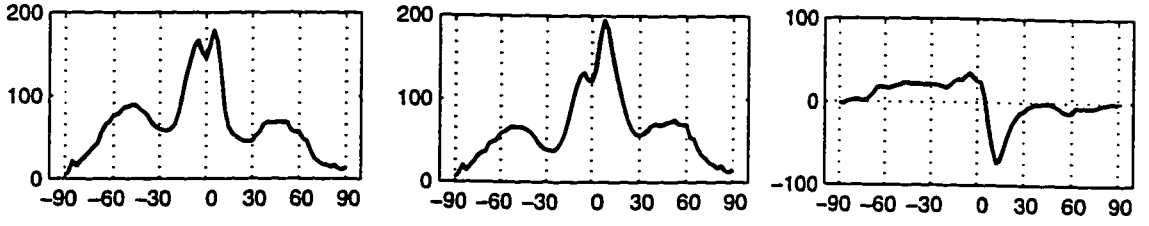

Figure 9.5: Same as Fig.9.4 but for the latitude sections of reanalyzed precipitation from Fig. 3.14

Chapter 10 Summary and Conclusions

10.1 The Principal Themes and the Research Strategy

The exchange between tropospheric and stratospheric chemical constituents has a major effect not only on the chemical structure of the atmosphere, but also on its dynamical and radiative balances. For this reason, the problem of STE has drawn much attention in scientific literature in recent years, and has been the primary focus of this research. This work investigated the physical mechanisms that determine the large-scale upwelling near the tropical tropopause, one of the principal components of the STE. These mechanisms, their interpretation, and mathematical modeling motivated the research strategy and the structure of this work. The initial discussion in Chapters 1 and 2 is a conceptual analysis of the tropical upwelling in the framework of the non-local control principle, and the mean meridional, thermally direct "Hadley" circulation, induced by the local external heating. Chapter 3 described the available observational data regarding the dynamics in the tropics on the seasonal time scales, and Chapter 4 presented our numerical model of the physical mechanisms responsible for tropical upwelling. The design and results of various experiments with the model were the focus of Chapters 5, 6 and 9. Chapter 5 dealt with the results of the model description of the meridional circulation in the stratosphere. Chapter 6 considered the thermally driven mean meridional circulations, in the troposphere obtained with the model. The mechanism of coupling between remotely-induced tropospheric mean meridional circulations and cumulus convection was presented in Chapter 7. Chapter 8 described the radiation code coupled with the dynamics which

was implemented in our model. The numerical experiments with the model containing all the above described physical mechanisms, and their results were discussed in Chapter 9.

The next section presents the main research outcomes that stem from the conceptual analysis of tropospheric upwelling, statistical analysis of the observational data, and the numerical simulation of the atmospheric dynamics in the region of the tropical tropopause.

10.2 Major Research Findings and Theoretical Contributions

Our research identified that the global-scale mean meridional circulations in the lower stratosphere, and the upward branch of the tropospheric Hadley circulation, which form two consistent parts of the dynamics in the region of the tropical tropopause, and should be considered together, rather than separately as in many previous studies (Chapters 3-6).

Our interpretation of the physical mechanisms driving the dynamics in the region of the tropical tropopause, can be sketched out as shown in Figure 10.1.

In this picture, the **meridional circulation in the tropical stratosphere as well as in the tropical troposphere is controlled by two main mechanisms**:

- Non-local extratropical wave-induced zonal forcing. Its influence has been studied within the framework of the "suction pump mechanism" concept *(Holton et al., 1995)*;

Local radiative and cumulus (in the troposphere) heating. Its action has been investigated within the framework of the zonally symmetric theory *(Schneider, 1977; Held and Hou, 1980)*.

The **role of cumulus convection** in tropical troposphere can be also approached from two different perspectives:

- The **CISK approach** in which cumulus convection is specified as an external heat source.
- The **statistical equilibrium theory** in which the convection changes the vertical temperature distribution and, thus, the buoyancy. In effect, the large-scale ascent "feels" an effective, positive static stability that, under typical conditions, is about an order of magnitude less than the dry static stability.

This work suggests that the second approach provides a better interpretation of the role of cumulus convection in maintaining of the tropospheric Hadley cell, and that it can be described within the framework of the non-local control theory.

Once the main components of the physical mechanism of the tropical upwelling were identified, we were able to examine their comparative contribution to mass transport between troposphere and stratosphere. This study included analysis of empirical data, and numerical simulation of the upwelling with our 2D model.

As regards data analysis, the major outcomes are as follows:

An analysis of monthly mean, zonally averaged temperatures from the lower-stratospheric MSU-4 channel shows that on the monthly time scale, there is **nearly complete compensation between temperature changes in the tropics and in the extratropics**. For the annual cycle, the MSU-4 data show a similar compensation

between temperatures in the tropics and those in high latitudes, with only a small residual variation in the global mean. The tropics are the coldest in January and the warmest in July, compensating for the warmer wintertime temperatures in the Northern Hemisphere compared to those in the Southern Hemisphere. These out-of-phase temperature variations between the tropics and extratropics are interpreted as the signature of an annual cycle in the strength of the wave-driven, Lagrangian mean meridional circulation. These results are consistent with the results of *Rosenlof [1995]* who studied the zonally averaged transport of mass in the stratosphere.

The **analysis of the NCAR/NCEP data** revealed that the **circulation pattern in the tropics in the lower stratosphere is dominated by the Northern Hemisphere meridional cell, which is in phase with the zonal eddy forcing**. The meridional circulation in the lower stratosphere cannot be explained just by the radiative heating, but rather by the combined effect of radiative heating and eddy forcing.

A similar analysis for the **tropospheric zonal circulation** documented the annual march of the meridional mass stream function in the upper troposphere. The Hadley circulation consists of a weak summer hemisphere cell and a strong cell in the winter hemisphere. At each period of time, the circulation can be considered as a superposition of two elements: a circulation caused by the oceanic ITCZ and a circulation caused by the monsoons diabatic heating.

The main outcome of this work is the development of a two-dimensional zonally averaged non-linear model of the physical mechanisms affecting the dynamics in the region of the tropical tropopause, and results obtained from numerical experiments with the model. The model represents an elaboration and,

in a sense, a combination of available 2D models that have been developed and used for studies of the meridional circulation separately in the troposphere *(Held and Hou, 1980)* and stratosphere *(Dunkerton, 1989)*.

The main characteristics of our model are as follows:

- The governing equations are in the TEM form, i.e. they describe the residual meridional circulation. This circulation is assumed to be a sufficient indicator of mass transport, and thus may be used as a measure of STE.
- The model is nonlinear, and therefore provides a more realistic description of the dynamical processes. As was noted in 2.3, nonlinear effects are crucial in the tropical regions.
- The model is specified in log-pressure coordinates, which offers the following advantages:
    - we have equally fine resolution in the troposphere and stratosphere (in comparison with sigma coordinates);
    - we can omit setting additional a priori boundary conditions at the tropopause which can influence model response (in comparison with a hybrid sigma - log-pressure vertical coordinates).
- The model is spectral in horizontal direction. This property:
    - does not bring in large numerical viscosity;
    - allows us to omit boundary conditions at the poles;
    - allows for efficient calculations of the horizontal derivatives.
- The static stability varies with both height and latitude. Due to this feature, the model better simulates the variability of observations, and allows for coupling between cumulus convection and large-scale dynamics.

- The cumulus convection is parameterized with Betts-Miller scheme which was designed to directly represent the quasi-equilibrium state established by convection.
- The radiative code developed by *Olaguer at al [1992]*, which is both sufficiently comprehensive and accurate in the region of the tropical tropopause, was implemented into the model. Thus, the feedback mechanism between the dynamics, radiation and cumulus convection was taken into the consideration.

Experimentation with the model led to numerous qualitative results

The most important results of the numerical simulation can be grouped as follows:

- Comparison of the relative contributions of non-local eddy-induced forcing, and local radiative heating in the stratosphere:
    - the relative role of these two factors is determined by the ratio of intrinsic dissipation parameters (dynamical dissipation time scale/radiative dissipation time scale);
    - for typical values of dissipation parameters in the stratosphere , local diabatic heating is not significant as a determinant of the meridional circulation. Experiments with varying diabatic heating showed no or little the model response;
    - eddy-induced forcing located as far as 40° - 60° from the equator, could significantly influence the meridional circulation in tropics, as was shown by the experiments with seasonally varying forcing in various ranges of central latitude and width of the forcing distribution.
- Comparison of the relative contributions of non-local eddy-induced forcing, and

local heating in the troposphere:

- remote eddy-induced forcing located in middle and high latitudes in the troposphere, influences the mean meridional (Hadley) circulation in the tropical region;
- this circulation has a stronger and more pronounced winter cell (consistent with observations);
- the simulated Hadley circulation is weaker than the observed. The strength of the circulation increases when it is supplemented by cumulus convection in a way described by the statistical-equilibrium theory.
- The difference between the spring and fall transition periods can be explained by the combined effect of the seasonal variability of the cumulus heating and the eddy-induced zonal forcing.

- Comparison of the relative contributions of non-local eddy-induced forcing, and local heating in the region of the tropical tropopause:
  - the radiative heating/cooling in the stratosphere and radiative heating/cooling combined with the cumulus heating in the troposphere produce, at 100 mb level a mean meridional circulation which differs substantially from the observed;
  - inclusion of the eddy induced zonal forcing in the stratosphere greatly improves the simulation results, the circulation in the region of the tropical tropopause in this case closely resembles the observed;
  - the eddy-induced zonal forcing in the troposphere does not alter the 100 mb mass stream function.

All these results adress the main question of our research: "What physical mechanisms determine the seasonal variability of the mass flux in the region of the tropical tropopause". By conceptual analysis of the dynamics at the region of the tropical tropopause, statistical examination of the circulation, and the experiments with a specially constructed dynamical model, we demonstrated the importance of the eddy-induced zonal forcing in maintaining the seasonally varying meridional circulation.

10.3 Future Research

The results summarized above serve as the basis for further research, focusing on the sensitivity of the large-scale zonally averaged circulation in the whole atmosphere, and in the region of the tropical tropopause particularly, to the various physical mechanisms discussed in this work.

This research could evolve in several directions. The immediate tasks include:

- further experiments with the 2D nonlinear model;
- objective analysis of zonally averaged meteorological variables.

As regards the first task, the experiments with the 2D nonlinear model should include the **realistic continuous time dependencies of the diabatic heating and the eddy-induced zonal forcing.**

In the discussion at the SPARC STE workshop in June 1995 *McIntyre* pointed out that the "sideways" control into the tropics by forcing with a period of around 360 days and located at the extratropics, does not completely determine the tropical upwelling in the lower stratosphere. The large scale upwelling in the tropics has a time-mean component, which apparently can be induced only by a mechanical zonal

forcing, located in the tropics (*Holton, personal communication*). Thus, another interesting question to address would be the extent of zonal forcing into the tropics necessary to produce realistic tropical upwelling in the nonlinear model.

As concerns the second task, the study focused so far on the last 13 years of observations, which were available through the NCAR/NCEP reanalysis project. In the nearest future, data for additional years will be available. This will provide not only for a more precise analysis of the seasonal variability in the zonally averaged circulation (similar to the one in Chapter 3), but also for new studies of the **interannual variability** in the meridional circulation, and its connection with the **ENSO** and **QBO** phenomena.

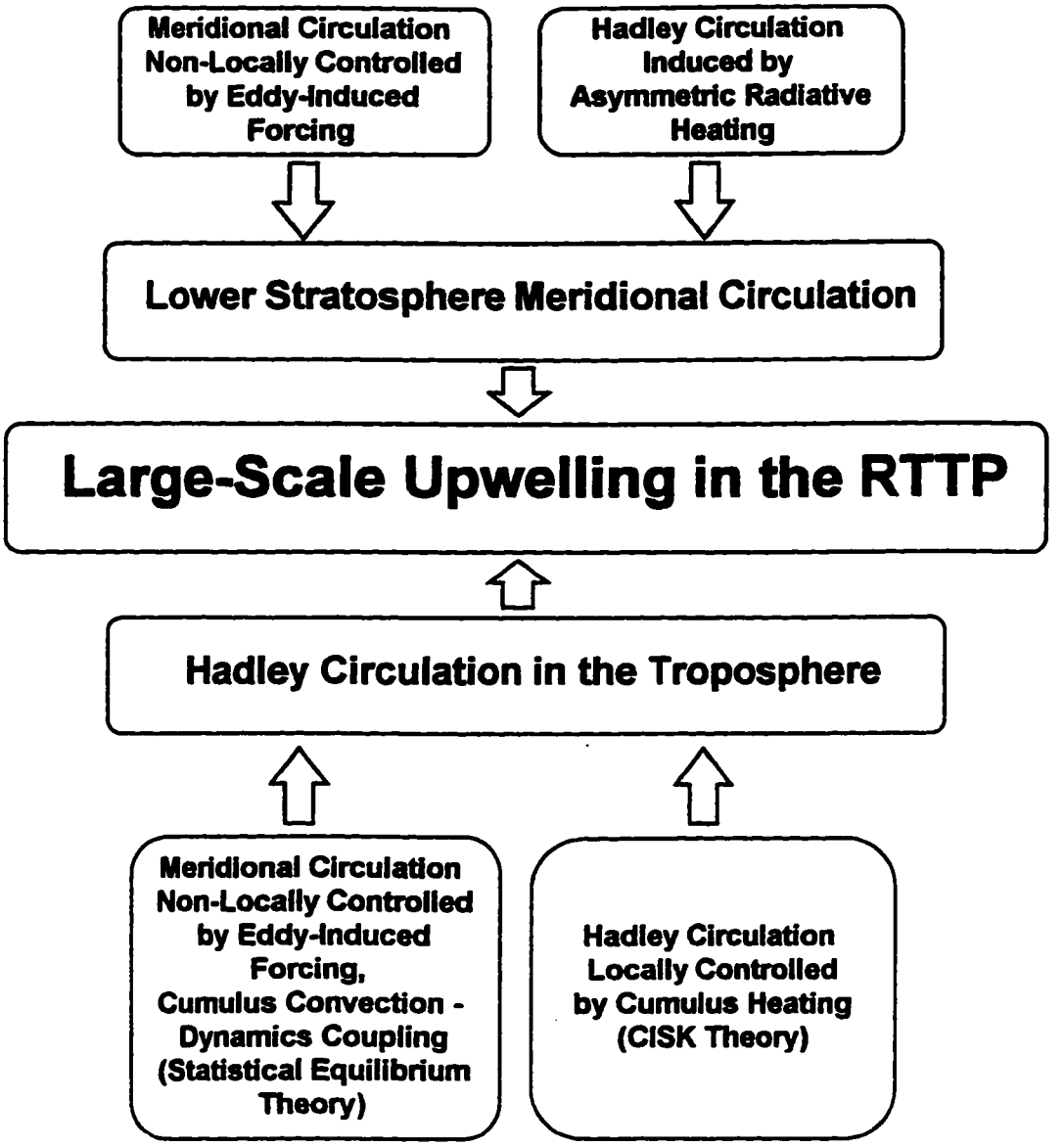

Figure 10.1: Interpretation of the mechanism of the large-scale upwelling in the region of the tropical tropopause

Bibliography:

Andrews, D.G., J. R. Holton., C. B. Leovy, Middle Atmospheric Dynamics, 489, 1987

Andrews, D.G. and M.E. McIntyre, Generalized Eliasen-Palm and Charney-Drazin theorem for waves on axisymmetric mean flows in compressible atmospheres., J. Atmos. Sci.,35, 175-185, 1978

Andrews, D.G. and M.E. McIntyre, An exact theory of nonlinear waves on a Lagrangian-mean flow, J. Fluid Mech., 89, 609-646, 1978b

Arakawa, A., and W. H. Shubert, Interaction of a cumulus cloud ensemble with the large-scale environment, PartI., J.Atmos. Sci., 31, 674-701, 1974

Betts, A.K., Saturation point analysis of moist convective overturning., J. Atmos. Sci., 39, 1484-1505, 1982

Betts, A. K., A new convective adjustment scheme . Part I: Observational and theoretical basis. Quart. J. Meteorol. Soc., 112, 677-691, 1986

Betts, A. K., and M.J. Miller, A new convective adjustment scheme. Part II: Single column tests using GATE wave, BOMEX, ATEX and arctic air-mass data sets. Quart. J. Roy. Meteor. Soc., 112, 693-709, 1986

Bolton, D., The computation of equivalent potential temperature, Mon. Wea. Rev., 108, 1046-1053, 1980

Bourke,W., An efficient, one-level, primitive-equations spectral model., Mon. Wea. Rev.,100, 683-689, 1972

Brewer, A.M., Evidence for a world circulation provided by the measurements of helium and water vapor distribution in the stratosphere, Quart. J. Roy. Meteor. Soc., 75, 351-363, 1949

Charney, J.G., and A. Eliassen, On the growth of the hurricane depression., J. Atmos. Sci., 21, 68-75, 1964

Danielsen, E F., Stratospheric-tropospheric exchange based upon radioactivity, ozone, and potential vorticity, J. Atmos. Sci., 25, 502-518, 1968

Dickinson, R. E., Analytical model for zonal winds in the tropics. I. Details of the model and simulation of gross features of the zonal mean troposphere., Mon. Wea. Rev., 99, 501-510, 1971a

Dickinson, R. E., Analytical model for zonal winds in the tropics. II. Variation of the tropospheric mean structure with season and differences between hemispheres, Mon. Wea. Rev., 99, 511-523, 1971b

Dobson, G. M., Origin and distribution of the polyatomic molecules in the atmosphere, Proc. R. Soc. London, Ser. A , 236, 187-193, 1956

Dunkerton, T. J., On the mean meridional mass motions of the stratosphere and mesosphere, J. Atmos. Sci., 35, 2324-2333, 1978

Dunkerton, T. J., On the inertial stability of the equatorial middle atmosphere., J. Atmos. Sci., 38, 2354-2364, 1981

Dunkerton, T. J., Nonlinear Hadley circulation driven by asymmetric differential heating, J. Atmos. Sci.,46, 955-974, 1989

Dunkerton, T. J., Body force circulations in a compressible atmosphere: key concepts., Pure and Appl. Geophys., 130, 243-262, 1989b

Dunkerton, T. J., Nonlinear propagation of zonal winds in an atmosphere with Newtonian cooling and equatorial wavedriving, J. Atmos., Sci., 48, 236-263, 1991.

Edmon, H. J., B.J. Hoskins, and M.E. McIntyre, Eliasen-Palm cross sections for the troposphere, J. Atmos. Sci., 37, 2600-2616.

Eliassen, A., Slow thermally or frictionally controlled meridional circulation in a circular vortex, Astrophys. Norvegica, 5(2), 19-60, 1951

Emanuel, K. A., A scheme for representing cumulus convection in large-scale models., J. Atmos. Sci., 48, 2313-2335, 1991

Emanuel, K. A., Neelin, J.D. and Bretherton, C.S., On large-scale circulation in convecting atmospheres, Quart. J. Roy. Meteor. Soc., 120, 1111-1143, 1994

Fels, S. B., A parameterization of scale-dependent radiative damping rates in the middle atmosphere., J. Atmos. Sci., 39, 1141-1152, 1982

Fels, S. B., Radiative-dynamic interactions in the middle atmosphere, Adv. Geophys., 28A, 277-300, 1985

Ferrel, W. An essay on the winds and the currents of the ocean. Nashville J. Medicine and Surgery, 11, 287-301, 1856

Fleming, E. L., Lim G.H., and J. M. Wallace, Difference between the Spring and Autumn Circulation of the Norther Hemisphere, J, Atmos. Sci., 44, 1266-1286, 1987

Garcia, R. R., On the mean meridional circulation of the middle atmosphere, J. Atmos. Sci., 44, 3599-3609, 1987

Garcia, R. R., and B. A. Boville, "Downward control" of the mean meridional circulation and temperature distribution of the polar winter stratosphere., J. Atmos. Sci., 51, 2238-2245, 1994

Gordon, C. T. and W. F. Stern, A description of the GFDL Global Spectral Model, Mon. Wea. Rev., 110, 625-644, 1982

Hadley, G. Concerning the cause of the general trade winds., Phil. Trans., 29, 58-62, 1735

Haynes, P.H. and McIntyre, M.E., On the conservation and impermeability theorems for potential vorticity, J. Atmos. Sci., 47, 2021-2031, 1990

Haynes, P.H., Marks, C.J., McIntyre, M.E., Shepherd, T. G., Shine, K.P., On the downward control of extratropical diabatic circulations by eddy-induced mean zonal forces, J. Atmos. Sci., 48., 651-678, 1991

Held, I.M. and Hou, A.Y., Nonlinear axially symmetric circulations in a nearly inviscid atmosphere, J. Atmos. Sci., 37, 515-533, 1980

Hide, R., Dynamics of the atmospheres of the major planets with an appendix on the viscous boundary layer at the rigid bounding surface of an electrically-conducting rotating fluid in the presence of a magnetic field., J. Atmos. Sci., 26, 841-853, 1969

Hoerling, M. P., T. K. Schaack and A. J. Lenzen, A global analysis of stratospheric-tropospheric exchange during northern winter,
Mon. Wea. Rev., 121,162-172, 1993

Holton J. R., An Introduction to Dynamic Meteorology, New York: Academic Press, 1979

Holton, J. R., Meridional distribution of stratospheric trace constituents, J. Atmos. Sci., 43, 1238-1242, 1986

Holton, J. R., On the global exchange of mass between the stratosphere and the troposphere, J. Atmos. Sci., 47, 392-395, 1990

Holton, J. R., P. H. Haynes, M. E. McIntyre, A.R. Douglass, R. B. Rood and L. Pfister, Stratosphere-troposphere exchange , Reviews of Geophysics, 1995

Holton, J. R., and W. Wehrbein A semi-spectral numerical model for the large scale stratospheric circulation., Dep. of Atmospheric Sciences, Univ. of Washington, 1979

Hoskins, B. J., M.E. McIntyre, and A.W. Robertson, On the use and significance of isentropic potential vorticity maps, Quart. J. Roy. Meteorol. Soc., 111, 877-946, 1985

Kritz, M.A., S. W. Rosner, E. F. Danielsen, and H. B. Selkirk, 1991: Air mass origins and troposphere-to-stratosphere exchange associated with mid-latitude cyclogenesis and tropopause folding inferred from Be measurements. J. Geophys. Res., 96, 17405-17414, 1991

Levy II, H., Mahlman J.D., Moxim, W. J., A stratospheric source of reactive nitrogen in the unpolluted troposphere, Geophys. Res. Lett., 7, 441-444, 1980.

Lindzen, R. S., and A. Y. Hou, Hadley circulations for zonally averaged heating centered off the equator., J. Atmos. Sci., 45, 2416-2427, 1988

Lindzen, R. S., Dynamics in Atmospheric Physics, Cambridge Univ. press, 1990

McIntyre, M.E., Dynamics and tracer transport in the middle atmosphere: An overview of some recent developments. , Transport Processes in the Middle Atmosphere, edited by G. Visconti and R. R. Garcia, 267-296, D. Reidel, Hingham, Mass

Mitchell, T. P., and J. M. Wallace, The Annual Cycle in Equatorial Convection and Sea Surface Temperature., J. of Climate, 5, 1140-1156, 1992

Murgatroyd, R. J., and F. Singleton, Possible meridional circulation in the stratosphere and mesosphere, Q. J. R. Meteorol. Soc., 87, 125-135, 1961.

Mote, P. W., J. R. Holton and B.A. Boville, Characteristics of stratosphere-troposphere exchange in a general circulation model, J. Geophys. Res., 16, 815-829, 1994.

Neelin, J. D., I. M. Held, and K. H. Cook, Evaporation-wind feedback and low-frequency variability in the tropical atmosphere. J. Atmos. Sci., 44, 2341-2348, 1987

Newell, R.E., J.W. Kidson, D. G. Vincent, and G, J. Boer, The General Circulation of the Tropical Atmosphere and Interactions with Extratropical Latitudes, Vol.1.

Cambridge, MA: M.I.T. press, 1972

Oort, A., H., Global Atmospheric Circulation Statistics., U.S. Department of Commerce, National Oceanic and Atmospheric Administration, 180 pp, 1983

Oort, A. H., and E.M. Rasmusson On the annual variation of the monthly mean meridional circulation. Mon. Wea. Rev., 98, 423 -442, 1970

Oort, A. H., and J. J. Yienger, Observed Interannual Variability in the Hadley Circulation and Its Connection to ENSO, J. of Climate, 9, 2751-2767, 1996

Pfeffer, R. L., A study of eddy-induced fluctuations of the zonal-mean wind using conventional and transformed Eulerian diagnostics., J. Atmos. Sci., 49, 1036-1050, 1992

Panetta, R. L. Zonals Jets in Wide Baroclinically Unstable Regions: Persistence and Scale Selection, J. Atmos. Sci., 50, 2073 - 2106, 1993

Philips, N. A., Energy transformations and meridional circulations associated with simple baroclinic waves in a two-level, quasi-geostrophic model., Tellus, 4, 3273-3286, 1954

Plumb, R.A., Zonally symmetric Hough modes and meridional circulations in the middle atmosphere, J. Atmos. Sci., 39, 983-991, 1982.

Plumb, R.A., and A. Y. Hou, The response of a zonally symmetric atmosphere to subtropical thermal forcing: threshold behavior.,
J. Atmos. Sci., 49, 1790-1799, 1992

Ramaswamy, V., M.D. Schwarzkopf and K.P. Shine, Radiative forcing of climate from halocarbon-induced global stratospheric ozone loss,
Nature, 355, 810-812, 1992

Randel, W. J., Global atmospheric circulation statistics, 1000-1 mb,
NCAR technical note,1992

Reed, R. J., and Danielsen, Fronts in the vicinity of the tropopause., Arch. Meteor Geophys. Bioklim., 11, 1-17, 1959

Reed, R. J.. and C.L. Vlcek, The annual temperature variation in the lower tropical stratosphere, J. Atmos. Sci., 26, 163-167, 1969.

Reid, G. C., and K. S. Gage, On the annual variation in height of the tropical tropopause., J. Atmos. Sci., 38, 1928-1938, 1981

Reiter, E. R., M.E. Glasser, and J. D. Malman, The role of the tropopause in stratospheric-tropospheric exchange processes.,
Pure Appl. Geophys., 12, 183-221, 1969

Reiter, E. R., Stratospheric-tropospheric exchange processes, Rev. Geophys Space Phys., 13, 459-474, 1975

Rosenlof, K. H., Mass transport in the stratosphere examined using the Transformed Eulerian-Mean residual circulation., Ph.D thesis, 1994

Rosenlof, K. H.,The seasonal cycle of the residual mean meridional circulation in the stratosphere, J. Geophys. Res., 100, 5173-5191, 1995

Rosenlof, K. H. and J.R. Holton, Estimates of the stratospheric residual circulation using the downward control principle, . J. Geophys. Res., 98, 10, 465-479, 1993

Satoh, M., M. Shiobara, and M. Takahashi, A role of Hadley circulations and baroclinic waves on the global angular momentum budget: a comparison between symmetric and asymmetric calculations, Tellus 1994

Shiotani, M., 1992, Annual quasi-biennial, and El Nino-Southern Oscillation (ENSO) time scale variations in equatorial total ozone,
J. Geophys. Res., 97, 7625-7633, 1992

Schneider, E. K. Axially symmetric steady-state models of the basic state for instability and climate studies Part II: Nonlinear calculations,
J. Atmos. Sci., 34, 280-297, 1977.

Schneider, E. K., Response of the annual and zonal mean winds and temperatures to variations in the heat and momentum sources.,
J.Atmos. Sci., 41, 1093-1115, 1984

Seager,R., S. E. Zebiak Convective interaction with dynamics in a linear equation model, J. Atmos. Sci., 51, 1307-1331, 1994

Solomon, S., J. T. Kiehl, R. R. Garcia and W. L. Grose, Tracer transport by the adiabatic circulation deduced from satellite observations, J. Atmos. Sci., 43, 1603-1617, 1986

Spencer, R.W., and J.R. Christy, Precision lower stratospheric temperature monitoring with the MSU: Technique, validation, and results 1979-1991. J. Climate, 6, 1194-1204, 1993

Spencer, R. W., J.R. Christy and N. C. Grody, Global atmospheric temperature monitoring with satellite microwave measurements: Method and results 1979-84., J. Climate, 3, 1111-1128, 1990

Tung, K. K., On the two-dimensional transport of stratospheric trace gases in isentropic coordinates, J. Atmos. Sci., 39, 2330-2355, 1982.

Wie, M.-Y., A new formulation of the exchange of mass and trace constituents between the stratosphere and troposphere, J.Atmos. Sci, 44, 3079-3086, 1987

Williams, G.P. and J.L. Hollowary, Range and unity of planetary circulations, Nature, London, 297 (5864), 295-299, 1982

Williams, G.P., The dynamics range of global circulation., Climate Dynamics,

2, 205-260, 3, 45-84, 1988

WMO Numerical methods used in atmospheric models, GARP publication series, 17,1979

WMO, Atmospheric Ozone 1985, WMO, No. 20, World Meteorological Organization, Geneva, Switzerland, 1986

WMO, Scientific Assessment of Ozone Depletion: 1994, WMO, No. 37, World Meteorological Organization, Geneva, Switzerland, 1995

Xu, K.-M., and K.A. Emanuel, Is the tropical atmosphere conditionally unstable?, Mon., Wea. Rev., 117, 1471-1479, 1989

Yang, H., Tung K.K., and E. P. Olaguer, Nongeostrophic theory of zonally averaged circulation, Part II: Eliassem_Palm flux divergence and isentropic mixing coefficient. J. Atmos. Sci., 47, 215-241, 1990

Yang, H., E. P. Olaguer, and K. K. Tung, Simulation of the present day chemical composition of the stratosphere using a coupled 2D model in isentropic coordinates. J. Atmos. Sci., 48, 442-471, 1991

Yu Jin-Yi, and D.L. Hartmann, Zonal Flow Vacillation and Eddy Forcing in a Simple GCM of the Atmosphere, J.Atmos. Sci., 50, 3244-3259, 1993

Yulaeva, E., J.R. Holton and J.M. Wallace, On the cause of the annual cycle in the tropical lower stratospheric temperature, J.Atmos. Sci., 51, 169-174, 1994.

Vita

Elena Yulaeva

Date of Birth: June 9, 1964

Place of Birth: Kharkov, Ukraine

Education:

Ph.D. (Atmospheric Sciences), University of Washington, September 1991 - April 1997
Dissertation: *On the Mechanism of the Seasonally Varying Upwelling in the Region of the Tropical Tropopause*

Diploma (M.A.) in Physics, Moscow Physical-Technical Institute (Moscow, Russia), September 1982 - June 1988
Thesis: *The Dynamics of the Baroclinic Waves in the Atmosphere of Venus*